Universitat Autònoma de Barcelona

SYNTHESIS, KINETIC CONTROL AND PROPERTIES ENGINEERING OF CERIUM OXIDE NANOPARTICLES FOR BIOMEDICAL APPLICATIONS

Tetyana Yudina

DOCTORAL THESIS

SYNTHESIS, KINETIC CONTROL AND PROPERTIES ENGINEERING OF CERIUM OXIDE NANOPARTICLES FOR BIOMEDICAL APPLICATIONS

Tetyana Yudina

Director: Prof. Dr. Victor Puntes
Catalan Institute of Nanoscience and Nanotechnology (ICN2)
Universitat Autonoma de Barcelona (UAB)

Bellaterra 2016

Universitat Autònoma de Barcelona

Institut Català de Nanociència i Nanotecnologia

EXCELENCIA SEVERO OCHOA

Tesi Doctoral

Programa de Doctorat en Bioquímica, Biología Molecular i Biomedicina

" Synthesis, kinetic control and properties engineering of cerium oxide nanoparticles for biomedical applications "

Memòria presentada per aspirar al Grau de Doctor per ***Tetyana Yudina***

Director i supervisor: ***Víctor F. Puntes*** *Tutor:* ***Jaume Farrés Vicén***

Institut Català de Nanociència i Nanotecnología (ICN2)

Universitat Autònoma de Barcelona (UAB)

Facultat de Biociències

Departament de Bioquímica i Biología Molecular

Bellaterra, 2016

TABLE OF CONTENTS

ABSTRACT

The current Doctoral Thesis is the fruit of collaboration between the Catalan Institute of Nanoscience and Nanotechnology (ICN2) and the Hospital Clinic of Barcelona, involved in the project *"Marató TV3 2012",* with the objective to apply Cerium oxide nanoparticles (CeO_2 NPs or nanoceria) as a new therapeutic tool for tissue regeneration in liver diseases.

CeO_2NPs is a fascinating inorganic material with many applications and more to come. What makes nanoceria very appealing is its high capacity to buffer electrons from an oxidant/reducing environment due to the unfilled 4f electronic structure. This is due to its easy ability of being oxidized and reduced, followed by the capture or release of oxygen or reactive oxygen species (ROS and free radicals as OH·). As a result, nanoceria behaves as a natural *electron sponge*. Note that ROS disbalance takes place in an enormous number of human diseases. Also, the overproduction of ROS is critical in neurodegeneration. Despite the appealing redox catalytic capacity of CeO_2 NPs, an important controversy upon biological effects of CeO_2 has been numerously reported. During this Thesis, the existent methods of nanoceria preparation have been analyzed in detail, as well as the quality of the obtained products and the toxicological aspects of both (the processes and the products).

The current research work has been focused in overtaking the existent problematics of the nanoceria toxicity (due to aggregation of NPs, toxic surfactant or solvent, or contamination with endotoxin) and designing suitable solutions, in order to take full advantage of the antioxidant CeO_2NPs properties in biomedical research and applications.

ACKNOWLEDGEMENTS

As it is a good tradition, I would like to acknowledge the help and knowledge that I received from people, who have surrounded me during the three years of Thesis research.

First of all, I would like to thank my supervisor, Prof. Dr. Víctor Puntes, for providing me with the opportunity to explore the fascinating field of nanomedicine, in a stimulating and friendly environment; for his teaching, guiding and encouragement.

When it comes to the rest of the members of the Inorganic Nanoparticles Group, I would like to thank my colleague Dr. Eudald Casals, for sharing his knowledges on Cerium oxide and guiding me during the first months of investigation. Also, to Dr. Neus G. Bastús for her advisory support regarding the data analysis and discussions.

Regarding the collaboration with the researchers from the Hospital Clinic de Barcelona, with the members of la Marató TV3 project, I would like to thank: Dr. Wladimiro Jiménez, Dr. Manuel Morales-Ruiz, Dr. Guillermo Fernández-Varo, Denise Oró, Dr. Altamira Arce-Cerezo and Jordi Ribera Sabaté, among others.

I would like to thank Prof. Arben Merkoçi Hyca, Prof. Daniel Maspoch Comamala and Prof. Julia Lorenzo Rivera for being part of the annual follow-up Committee of this Thesis work, and to the tutor of the Thesis, Prof. Jaume Farrés Vicén.

Also, I would like to acknowledge Prof. Jordi Arbiól and Dr. Belén Ballesteros for their advisory support in issues related to Electron Microscope Imaging.

I am grateful to all of the colleagues who shared the moments of everyday work with me: Javier Patarroyo, Jordi Piella Bagaria, Martí Busquets Fité, Florind Merkoçi Xelo, Lorenzo Russo and Ariadna Peral Guillamón.

At last but not least, I would like to give a special thanks to my parents for their unconditional love and encouragement: Спасибо за то, что вы есть!

CHAPTER 1

RESEARCH OBJECTIVES

INTRODUCTION

The current Doctoral Thesis is the fruit of collaboration between the Catalan Institute of Nanoscience and Nanotechnology (ICN2) and the Hospital Clinic of Barcelona, involved in the project *"Marató TV3 2012",* with the objective to apply Cerium oxide nanoparticles (CeO_2 NPs) as a new therapeutic tool for tissue regeneration in liver diseases. The following Introductory Chapter gives a general overview of the main issues of investigation of this work. More detailed information and the correspondent bibliographic references can be found in the following Chapters.

Cerium oxide nanoparticles (CeO_2NPs or nanoceria) are a fascinating inorganic material with many applications and more to come. Besides being a rather chemically inert ceramic, its fluorite-like structure and the unfilled 4f electronic structure, confer it a variety of relevant properties when it reaches the nanoscale, making nanoceria one of the most interesting NPs in industry and, more recently, in biomedical research. What makes nanoceria very appealing is its high capacity to buffer electrons from an oxidant/reducing environment. This is due to its easy ability of being oxidized and reduced, followed by the capture or release of oxygen or reactive oxygen species (ROS and free radicals as OH·). As a result, nanoceria behaves as a natural *electron sponge*.

For decades, regarding the ROS scavenging capacity of CeO_2 NPs, they have been widely used in industrial processes where the redox reactions involved. More recently, the use of nanoceria to control the population of free radicals in biological environments has emerged, since the controlled redox reactions are crucial in the metabolism of living organisms. In healthy conditions, the physiological intracellular redox balance is carefully maintained by the activity of specific enzymes such as

superoxide dismutase (SOD), catalase and glutathione (GSH), through balanced generation and elimination of

endogenous ROS. However, during an environmental or intracellular stress, the cell may no longer maintain redox homeostasis correctly, which triggers significant damage of cellular integrity by inducing chronic inflammation, lipid peroxidation, damage to DNA and oxidation-sensitive proteins, metabolic flux disruption and apoptosis.

Note that ROS disbalance takes place in an enormous number of human diseases, such as liver cirrhosis, cancer, diabetes mellitus, cardiovascular disease (CDV), age-related macular degeneration (AMD) and many others. Also, the overproduction of ROS is critical in neurodegeneration, including Alzheimer, Parkinson, Huntington, schizophrenia, between others. Therefore, two main function of cerium oxide NPs have raised from therapeutic point of view: to manage acute inflammation (ex. septic shock, ischemia) and to revert chronic inflammation (ex. liver cirrhosis).

Despite the appealing redox catalytic capacity of CeO_2 NPs, useful as a potential biomedical tool to decrease tissue inflammation and to recover redox homeostasis of inflamed tissue, an important controversy upon biological effects of CeO_2 has been numerously reported. During this Thesis we have analyzed in detail the existent methods of nanoceria preparation, the obtained products, as well as the toxicological aspects of both, the process and the product. Based on these findings, we questioned the quality of the used nanoparticles in the reported studies, seeing a direct correlation between the size and aggregation state of nanoceria and the consequent detrimental biological effects. What is clear is that there is a strong correlation between the cellular effects of the NPs and their engineering, including the preparation method, morphology (size, shape), surface composition, contaminants and aggregation state. The nanoparticle state is critical, and in order to take full advantage of the nanoceria, a consideration of the engineering of entire NP, including morphology and chemical environment is needed.

Regarding the reported aspects of nanoceria toxicity, the majority of biomedical studies explore the effects of CeO_2NPs, but using use commercial nanoparticles. The majority of commercial NPs are available in a powder state. By default, in biomedicine the NPs need to be redispersed in biological media, before their use *in-vivo* or *in-vitro*. However, such procedure leads to heterogeneous NP collections, including aggregates of thousands of nanometers that often cause cytotoxicity.

Moreover, it is crucial to use biocompatible surfactants and coatings for nanoparticles. This factor is not always taken into account and, as a result, an observed toxicity may be due not to the nanoparticles themselves, but to their detergent coating or organic nature of the solvent.

Finally, we put a special emphasis on another potential source of nanoceria toxicity, which is sample contamination with endotoxin. Endotoxin or lipopolysaccharide (LPS) is omnipresent bacterial contaminant. Regarding the fact that most of the NPs are prepared under non-sterile conditions, contamination with endotoxin may easily occur during NP synthesis or handling.

Consequently, for the hard task of performing precise work inside the biological machinery, a fine morphological control of CeO_2 nanoparticles and their aggregation state is mandatory, since it drives the reactivity, colloidal stability, interaction with proteins and bio distribution (pharmacokinetics) of the nanoparticles within the organism. The scheme below summarized the main “three B” fundamentals, crucial for a correct design of the nanoparticles for biomedical applications:

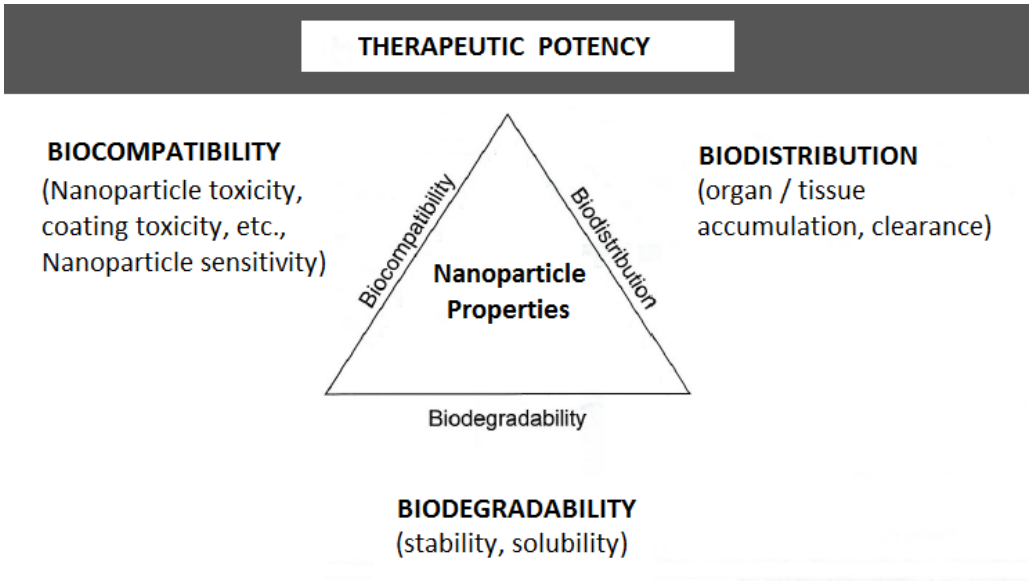

Scheme 1. Nanotechnological fundamentals that drive to biomedical applicability of the nanoparticles. *Scheme taken from the presentation of Stephan Stern at the Alliance for Nanotechnology in Cancer (NCI) conference.*

This Doctoral research has been focused in overtaking the mentioned problematics and offering suitable solutions, in order to take full advantage of the antioxidant CeO_2NPs properties in biomedical research and applications. In this collaborative project two aims have been pursued: (i) the optimization of CeO_2 NPs synthesis for biomedical applications and (ii) the evaluation of CeO_2 NPs as a therapeutic tool to improve hepatic fibrosis and liver regeneration.

Thus, the current work has been focused on the study of physicochemical and biochemical properties of CeO_2 NPs, to optimize the preparation methods and the product in an environmentally-friendly and biocompatible way (Chapter 2, Annex 2). The optimization of the NPs size and monodispersity (Chapter 2); evaluation of the antioxidant activity (Chapter 3) were also performed. Finally, the *in-vivo* biodistribution study of CeO_2 NPs, as well as their effects on inflammatory and fibrogenic mediators were evaluated at molecular and cellular level, demonstrating that administration of CeO_2 NPs could be of therapeutic value in liver diseases (Annex 3).

CHAPTER 2

Synthesis and characterization of CeO_2 NPs.

Design of optimized CeO_2 NPs for biomedical applications, based on current attainments, limitations and challenges.

INTRODUCTION

During the last decades, a hot-topic branch of material sciences, known as nanoscience or nanotechnology, has been tightly linked to the field of biomedicine. Numerous types of the particles that offer high variety of interesting properties at the nanoscale, have found their protagonist role in biological systems (e.g. drug delivery, imaging of tumors or presenting antigens) [75]. Some of such NPs are: antioxidant cerium oxide (CeO_2) that treats inflammation [1]; photocatalytic and antibacterial titanium oxide (TiO_2) that coat biomedical devices [2]; as well as bactericidal silver (Ag) [3], between many others.

Nowadays, some of nanomaterials are already well understood and easily manipulated at small and large scales. Nevertheless, there are some of nanoparticles, whose unique and useful properties are accompanied with incomprehensible behavior, which is a current topic of intense study (e.g. mechanisms of growth or aggregation). As a result, when nanoscience has crossed the door of biomedicine, such exotic nanomaterials have brought to biomedical scenario some of the pending and unresolved aspects of their surface physicochemistry, that usually result in biotoxicity.

As introduced in Chapter 1, one of such materials is nanometric cerium oxide. What makes nanoceria very appealing is its high capacity to buffer electrons from an oxidant/reducing environment, which is due to its easy ability of being oxidized and reduced, followed by the capture or release of oxygen or reactive oxygen species (ROS, as OH·) [41].

The Scheme 1 summarizes the main parameters of the optimally designed nanoparticles for biomedical applications.

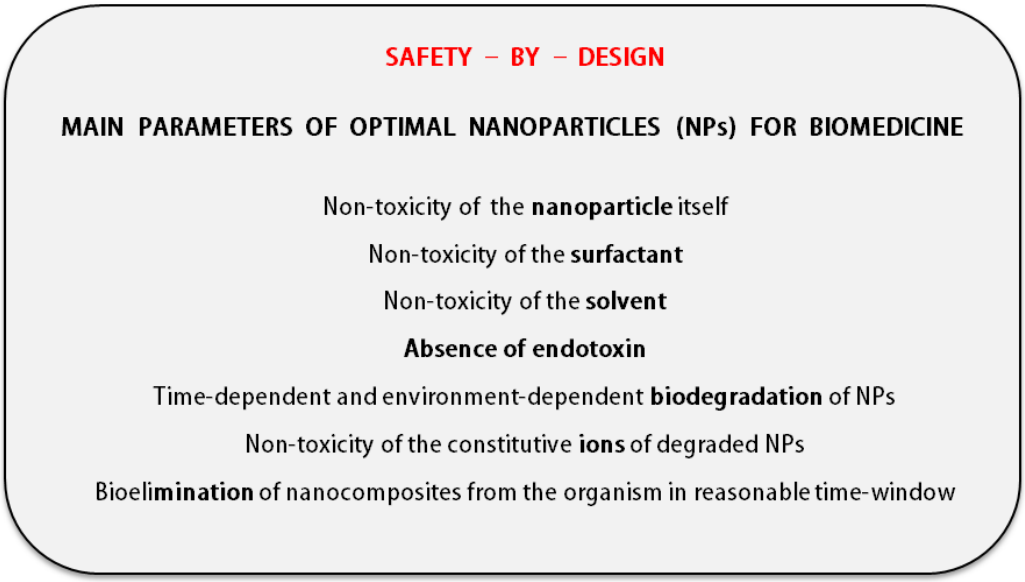

Scheme 1. *Safety-by design requirements for the maximally biocompatible NPs.*

The safety-by-design consists in taking into account health and safety risks during design development. The concept supports the view that along with quality, program and cost, safety is determined during the design stage. This implies to develop nanomaterials with a good knowledge regarding their full lifetime: from the moment of the NPs synthesis, their *in-vitro/in-vivo* administration and a therapeutic effect; to a non-toxic elimination from the biological system within reasonable time-window, and a friendly interaction with the environment during their storage, manipulation and discarding).

Note that in the *in-vitro* applications as smaller the NPs the better, due to a higher surface-to-volume ratio, *ergo* higher reactivity at the nanoscale). In contrast, the *in-vivo* administration of NPs is accompanied with more restrictive demand regarding their size. Thus, during a natural *in-vivo* biodistribution of NPs, those with a final hydrodynamic diameter below 5.5 - 6 nm, will run through the renal (glomerular)

filtration barrier, followed by a rapid and efficient urinary excretion from the body. For instance, a study of Frangioni, J. F. et al. reported elimination of quantum dots (QDs) from the body, in a matter of minutes, due to their small size [38]. Considering these biological size restrictions, the term of an "*optimal size"* of CeO_2 for biomedicine has emerged throughout this work. Thus, from now on, the optimally-sized nanoceria will be referred to nanoparticles with an average diameter from of 5 – 6 nm to around 20nm, since this size range accomplish three main biomedical requirements: (1) high surface reactivity (*ergo*, antioxidant capacity), (2) minimal renal elimination of CeO2NPs (due to the size over the glomerular filter barrier), (3) minimal long-term accumulation in the liver (due to the size below 20 nm).

In this Chapter, the existent methods of synthesis that produce, apparently small-sized CeO_2NPs, are analyzed in detail. The main parameters of reactions, the obtained products and the problematics of their usability in biomedicine are discussed. To conclude the Chapter, several potential solutions, such as an optimization of nanoceria preparation, biocompatible coating, monodispersity and purity, are suggested and supported with experimental data. In particular, the designed protocol of optimally-sized nanoceria is described. The designed NPs are small sized, highly catalytic, prepared in aqueous phase, free of endotoxin and monodispersed (free of aggregates). To offer maximally suitable (optimal) size, not only for *in-vitro* but also *in-vivo* applications (to avoid renal clearance), we describe two possibilities of biocompatible coating of CeO_2 NPs that will slightly increase the hydrodynamic diameter of the NPs and limit their renal exclusion: one of the coatings is Polyvinylpyrrolidone (PVP) and the other, albumin protein (BSA).

1. THE EXISTENT METHODS OF CeO_2NPs SYNTHESIS OF OPTIMAL SIZE AND THEIR PROBLEMATICS FOR BIOMEDICINE

Up to now, different methods of synthesis have tried to offer new options for preparation of small-sized, *ergo* highly reactive CeO_2NPs. The most common are: thermal hydrolysis; sonochemical, mechanochemical and electrochemical methods; non-isothermal and wet chemical precipitation; hydrothermal and solvothermal processing; microemulsion and sol-gel. Table 1 (page 11) summarizes the main reagents, synthesis conditions and obtained product found in literature. The main parameters involved in these methods are analyzed next.

SYNTHESIS METHODS OF SMALL-SIZED CeO_2NPs	CERIUM SOURCE	REAGENTS, ADDITIVES	PHASE	TEMPERATURE PROCEDURES (ºC)	CHRYSTALLINE SIZE (nm)	PRODUCT SIZE (nm)	REF
Thermal hydrolysis	$(NH_4)_2Ce(NO_3)_6$	-	aqueous	5h hydrolysis at 150-240° Drying on air	6	agg	4
Sonochemical synthesis (ultrasound radiation)	$Ce(NO_3)_3$	AZO, TMAOH, TEAOH, TBAOH, washed by ethanol	aqueous	3h sonication at 80° Drying at vacuum	5.9 – 7	20, agg	5
Mechanochemical	$CeCl_3$	$ZnCl_2$, Na_2CO_3, NaOH, NaCl	powder	4h milling at 25 – 400° Calcination at 500°	10.2	5-40, agg	6
Electrochemical	$Ce(NO_3)_3$	$NaNO_3$	ceria films deposition on stainless steel	Deposition at 60°	5		7
Non-isothermal precipitation	$Ce(NO_3)_3$	ammonia	aqueous	1h nitrate stirring at 70° 24h synthesis at 0° Precipitate drying at 90°	10 – 12		8
Wet chemical precipitation	$Ce(NO_3)_3$	ammonia	aqueous	Precursor drying at 110° Calcination at 500°	4 – 5	agg	9
Hydrothermal	$CeCl_3$	citric acid, ammonia, methanol	aqueous	Reagents stirring at 50° Heating at 80° Ultrasonic agitation Liophilisation at -80°	5	agg	10
Microemulsion	$Ce(NO_3)_3$	DEAO, 1-octanol, H_2O_2, ammonia	organic	Precursor drying at 90° Calcination	3.9-11	69, agg	11
Sol-gel	$Ce(NO_3)_3$	TEA, ethanol	organic	Dissolution of ce(III) salt in TEA at 90° 2h convertion to gel at 270° Calcination of CeO_2 at 90°	6.5-13	84, agg	11
Solvothermal	$Ce(NO_3)_3$,	NaOH, NH4OH, PVP, CTAB, etc	non-aqueous	From 100 to 400°	2.5 – 800	2.5 – 800	12

Table 1. *List of the majority of synthesis methods of nanosized cerium oxide.*

1.1 Understanding of the chemistry of nanoceria formation

At the bottom of the listed syntheses lies a chemical transformation (oxidation) of *soluble Ce^{3+} precursor* into cerium oxide nanoparticles, composed of *unsoluble Ce^{4+}* and oxygen. In majority of methods, the precursor is some of cerium salt, such as nitrate or chloride. The formation of colloidal nanoparticles consists in a rapid dissolution of cerium salt within aqueous or organic phase, followed by its oxidation, through one of the next processes:

- Temperature-dependent oxidation of Ce^{3+} during calcination within a powder state;
- pH-dependent oxidation of Ce^{3+} in a liquid phase (in solution).

The correspondent chemical reactions are developed in the Scheme below.

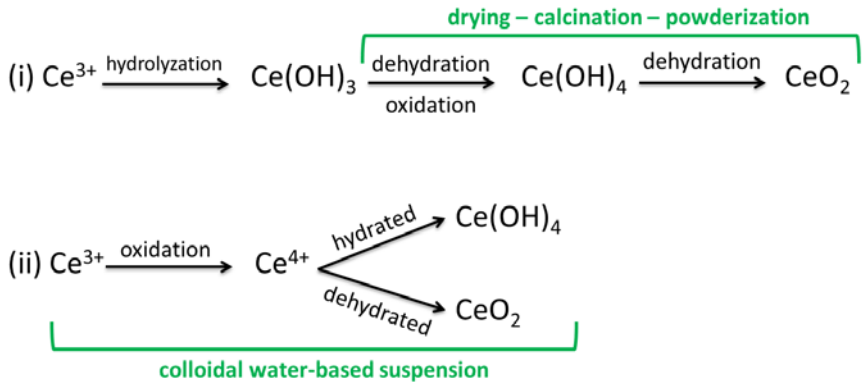

***Scheme 2. Chemical mechanisms of CeO_2NPs formation**: (i) thermal decomposition of Ce^{3+} to powdered CeO_2NPs within a dehydrated (powder) state. A calcination procedure is mandatory to oxidize the precursor and form the nanoparticles; (ii) pH-dependent oxidation of Ce^{3+} to colloidal CeO_2NPs within a liquid phase. A calcination procedure of already formed nanoparticles is optional.*

In the first case, (i), a calcination process is mandatory, since the NPs are formed in a process of drying. In the second case, (ii), a calcination procedure is optional: CeO_2NPs are formed in solution and remain colloidally dispersed after being synthesized.
Since a powderization of nanoceria is the most common step of commercially available and lab-made final product, this process is analyzed separately here:

1.2 Powdered nanoparticles and biotoxicity of the aggregates

In 1988, Matijevic E. et al. [13] extensively described the preparation of ceramic powders, metal oxide particles and colloidal particles by homogeneous precipitation (a process in which the precipitating agent, e.g. nanoparticles, is synthesized in the solution) based on forced hydrolysis.
The forced hydrolysis can be achieved by increase of pH of the solution, or by heating the solution (hydrothermal treatment). However, only a homogeneous precipitation achieved by hydrothermal treatment succeeds in controlling agglomerates morphology and their size distribution. On the contrary, a homogeneous precipitation achieved by increase of pH, drives to a hardly redispersible agglomerates in solution [13].
At first sight, a formation of NPs through a hydrothermal treatment (usually product drying or calcination), seems to be the preferred method of synthesis of small-sized and monodispersed nanoparticles. Despite this, this kind of product is unsuitable for biomedical applications, for the next reason: by default, to be used in biomedical research, the powdered nanoparticles are redispersed in aqueous-based solution, previous to their use in the *in-vitro* or *in-vivo* models. Usually, the nanopowders are redispersed in a cell culture medium, diluted to biocompatible concentrations and spread on the cells or injected to animals. Precisely, the step of the nanopowder redispersion drives to an important problematics: a formation of irreversible aggregates that might reach hundreds of nanometers in size. The main problematics of aggregation is the irreversibility of NPs bonding or collision. The following Scheme

(Egerton, T. A. et al., 2014), illustrates main types of the interactions between NPs. Weak interactions (agglomeration) are reversible flocculates of NPs that may be broken into primary particles, for instance by sonication procedure. On the contrary, when the interactions between NPs are strong (aggregation), a resultant morphology is irreversible; therefore the monodispersity of primary nanoparticles is inevitably lost. For that reason, the phenomenon of aggregation remained under study long after being discovered and is a topic of study until now.

Thus, in 1998, Djurucic B., et al. [14] underlined the need to engineer and optimize the nanopowder properties to suit particular applications. A decade later, the problematics of powder aggregates still remained under study. In 2008, Zhang Y., et al. [15] reported that neither ultrasound nor chemical dispersants were able to break up powder aggregates into primary monodispersed nanoparticles. Still in 2016, the aggregability of nanopowders during redispersion remains a challenge in the field of material sciences and biomedicine as well.

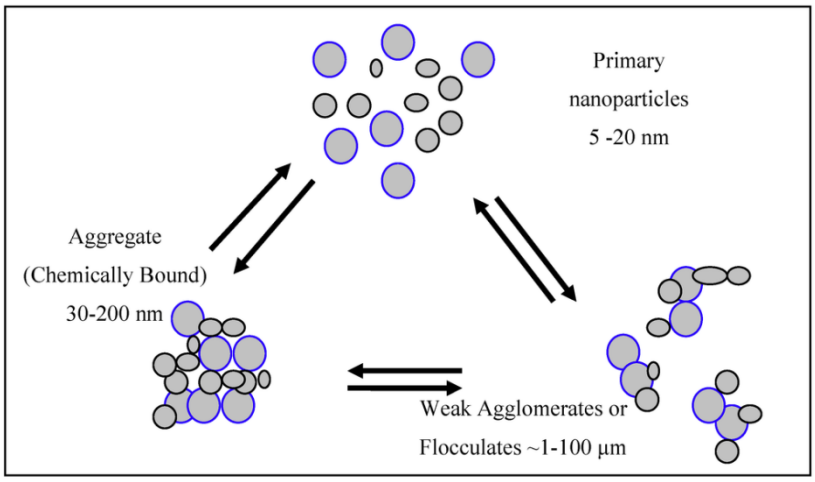

Scheme 3. Schematic illustration of the agglomeration and aggregation of NPs *(taken from Egerton, T. A. (2014). "UV-Absorption-The Primary Process in Photocatalysis and Some Practical Consequences." Molecules **19**(11): 18192-18214.*

Regarding the biological size-effects of nanoceria, the next contradictions have arisen: despite an attractive redox catalytic capacity of CeO_2 NPs, apparently useful as a

potential biomedical tool to decrease tissue inflammation and to recover redox homeostasis of inflamed tissue, an important controversy upon biological effects of CeO_2 have been abundantly reported. For instance, several biomedical studies reported nanoceria-dependent induction of cytotoxicity, oxidative-stress (OS), decrease of cellular viability, damage of cell membrane, lipid peroxidation and increase of ROS levels [16-19], suggesting pro-oxidant and pro-inflammatory nature of nanoceria in biological environments. In addition and contrarily to the suggested damaging nature of nanoceria, numerous biomedical studies have reported the beneficial effects of CeO_2NPs. Thus, Schubert et al. 2006 [20] and Niu et al. 2007 [21] reported CeO_2 NPs to be neuroprotective and cardio protective, respectively. While multiple *in-vitro* studies of the past decade reported non-toxicity [27-31, 33] and protection capacity of CeO_2NPs in cancer [22], endothelial wounds [23], retinal inflammation [24], and liver cirrhosis [25], among others.

What is clear is that there is a strong correlation between the cellular effects of the NPs and their engineering, including the preparation method, morphology (size, shape, surface composition, surface charge, contaminants) and aggregation state [26, 27-40]. In our previous work, Cafun et al. (2013) [41] highlighted the complexity, exceptional plasticity of the electronic structure of ceria at the nanoscale and a resulting ability to buffer electrons when its size is decreased down to 5nm. In the mentioned work, a catalytic activity of the CeO_2NPs was tested by monitoring the catalase mimetic activities *in operando* (during reaction). As a result, the 3 nm CeO_2NPs showed the highest chemical activity, while the 25 nm NPs did not show any detectable effects. Consequently, the size here is critical and in order to take full advantage of the nanoceria, a consideration of the engineering of entire NP, including morphology and chemical environment is needed. Based on these findings, we questioned the quality of the used nanoparticles in the majority of reported studies, seeing a direct correlation between the size and aggregation state of nanoceria and the consequent biological

effects. Thus, those who reported damaging nanoceria-induced effects have been working with polydisperse CeO_2NPs of above 20-30 nm, including aggregates that could reach hundreds of nanometers. In contrast, nanoceria was reported as non-cytotoxic and antioxidant when the diameter of used nanocrystals did not exceed 20-30 nm.
All in all indicates that large and polydisperse samples are not the preferred ones for medicine. In particular, a special attention should be paid to an avoidance of powderization of nanoparticles. Optimally, when intended for biomedicine, only stable colloidal nanoparticles should be considered.

However, the avoidance of nanopowders and a use of colloidal NPs are not that trivial, since aspects as aggregability, biocompatibility of the solvent and the surfactant, as well as a contamination of NP with bacterial endotoxin, still require a better understanding and optimization.

2. THE CLOSEST ENVIRONMENT OF COLLOIDAL CeO_2NPs (SURFACTANT AND SOLVENT) AND ITS BIOCOMPATIBILITY

As previously commented, during the last decades the use of colloidal NPs has been accompanied with adjacent limitations that are still to be overcome (e.g. undesired aggregation). Taking into account this phenomenon, certain modifications of the NP surface are usually applied in order to control the size and aggregation, but keeping the right functionality of NPs after being modified. For such purpose, a surfactant coating of NPs is used.

The reason of NPs coating comprises the fact that an ionic or non-ionic monolayer is formed on top of its surface. Such surface modification causes steric or electrostatic repulsions between adjacent NPs. Thus, the surface tension and surface attraction decrease, so they can move easily in solution (see scheme below).

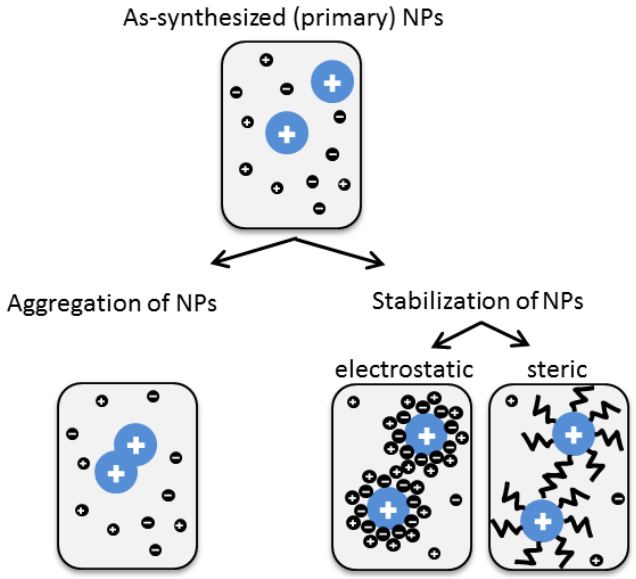

Scheme 4. Schematic illustration of the surface modification (stabilization) of colloidal NPs vs aggregation of non-stabilized NPs. *A natural aggregability of naked colloidal nanoparticles may be avoided by surface stabilization and correspondent colloidal or steric repulsions between adjacent nanoparticles.*

The efficiency of colloidal stability of coated nanoparticles directly depends on the type and concentration of the used surfactant. Until now, the most commonly used surfactants are detergents and hydrocarbon (organic) coatings, because of their efficacy, frequent availability in chemical laboratories and a good stability in solution (e.g. BDAC, CTAB, DMABs) [42]. However, the relatively recent biomedical applications of NPs do require biocompatibility of the surfactant as well. Note that a detergent coating of NPs may be not relevant in industry, however, it is a highly important factor and a potential source of side effects in biomedicine.

For instance, CTAB surfactant is able to induce severe cellular damage and immune response. Thus, small-sized and monodispersed CTAB-coated CeO_2NPs, are excellent for industrial use, but would be highly cytotoxic *in-vitro* and *in-vivo,* due to a detergent nature of CTAB [73].

Therefore, regarding the attractive use of nanoceria in biomedicine, it is crucial to use biocompatible coating of nanoparticles only (i.e. PEG, PVP, silica, etc). Until now, this factor has not always been taken into account and, as a result, the observed and reported toxicity of nanoceria could be not due to the nanoparticles itself, but to their non-biocompatible coating.

Besides, biocompatibility is mandatory in case of the solvent, in which the colloidal NPs are dispersed. For instance, when the non-toxic NPs are coated with a biocompatible surfactant, but dispersed in organic solvent, any sample of similar composition may induce damaging cellular and immunologic responses, instead of therapeutic ones, due to the solvent itself. Between the existent receipts of nanoceria synthesis, a great percentage includes an organic phase as a solvent. But as previously commented, the NPs destined for biomedicine need to be small-sized. This fact makes it difficult to remove them from organic phase into an aqueous solution, previous to biological

administration, due to difficulties in purification NPs smaller than 25nm. A better option is to synthesize NPs in aqueous phase from the very beginning.

In addition it is a plus to chose a non-toxic precipitation agent as well, when the preparing the NPs in liquid phase. Several precedents of nanoceria synthesis in aqueous media report a use of HMT [74] as surfactant and precipitating agent, which is toxic, weakly mutagenic and may produce hydrolytic release of formaldehyde in aqueous media. In this Thesis work, we chose a non-toxic ammonium salt (TMAOH), to avoid similar consequences.

2.1 The advantage of PVP coating of CeO_2NPs

To avoid use of toxic surfactants, biocompatible molecules have been analyzed to design optimal coating of nanoceria. For instance, a water-soluble polymer, known as Polyvinylpyrrolidone (PVP), with a molecular weight of 10-20kDa is highly biocompatible and has been massively used to increase the oncotic pressure in cases of bleeding. This fact plays in favor of the use of PVP as a suitable coating of colloidal nanoceria. Moreover, PVP displays long-term stability in aqueous solution, that is an additional plus for further storage of NPs. Note that PVP with a molecular weight over 10-20 kDa tend to accumulate in the body and become toxic.

Numerous precedents underline the benefits of PVP coating of NPs in order to increase the monodispersity and protect them from aggregation. Thus, a recent review of Koczkur M. K. et al. [48], underlined the usability of PVP in synthesis of nanoparticles as a surface stabilizer, growth modifier, nanoparticle dispersant, and reducing agent that can affect nanoparticle growth and morphology by providing solubility in diverse solvents, selective surface stabilization and even access to kinetically controlled growth conditions. One of the precedents, where PVP used as a surfactant, was the work of Phokha S. et al. [43], focused on a study cerium oxide properties. The correspondent hydrothermal method of synthesis included high temperature treatments of the

samples, as autoclaving at 200°, product drying at 80° and sample annealing at 400º; giving place to a powder of 200 nm sized monodispersed nanospheres. Another precedent of PVP-coated nanoceria synthesis, the work of Girija D., et al. [45], reported another way to produce nanoceria in a size range from 5 to 600 nm (10-20nm by XRD and 500-600 nm by SEM), that were finally dried at 100°. The work of Chitsaza A., et al. [46], underlined the beneficial effects of PVP coating of nanoceria, regarding the better morphology and lower agglomeration of the product. The reported synthesis method consisted in a powder preparation by a co-precipitation method. However, the obtained 8 nm sized- and weakly aggregated nanoceria was also calcined at 600°. Wang, F. X., et al. [47], also reported a use of PVP as a stabilizer of monodispersed 50-60 nm nanoceria, prepared by a solvothermal route and dried in vacuum previous to storage.

The mentioned precedents, among others, do underline the advantage of PVP coating regarding the monodispersity of resultant nanoparticles. However, in many of these cases, the nanoparticles are finally calcined. Consequently, during a calcination procedure, the PVP is completely destroyed and the previously analyzed problematics of nanopowder aggregability is maintained. In this Thesis work, we take advantage of PVP coating in one of the methods of nanoceria preparation and in order to increase the monodispersity of highly concentrated NPs. However, the calcination procedure is completely avoided, keeping the NPs in colloidal state.

2.2 The challenge of BSA coating of CeO_2 NPs

To produce even more biocompatible NPs, a challenge of protein coating of NPs *during the synthesis* was considered in this research. It is experimentally easy to coat the synthesized nanoparticles with BSA or other proteins, after the synthesis. Such coating is widely known as formation of protein corona. Protein corona does affect the surface charge of NPs, but if the synthesis solution contains aggregates or agglomerations of

NPs, a protein corona will coat the whole aggregate, not each particle per separate. What is a real challenge in case of nanoceria synthesis, is to use BSA as a surfactant from the very beginning of the synthesis reaction. And the challenge comprises the fact that proteins are too delicate to be used in chemical reactions without losing their integrity and functionality.

Proteins comprise an extremely heterogeneous class of biological macromolecules. They are often unstable when not in their native environments, that can vary considerably among cell compartments and extracellular fluids. In certain buffer conditions, proteins can lose activity as a result of aggregation, denaturation and conformational changes. Optimal conditions for storage are different to each protein; however, some general guidelines for storage and stability of purified proteins are reported in literature. For instance, diluted protein solutions (< 1mg/ml) are more susceptible to inactivation. Thus, it is common to purify BSA at this concentration and store at ≤ 4ºC in simple buffers and in clean, autoclaved glassware of polypropylene [49-55].

Considering these pecularities, an attractive challenge of synthesis of BSA-coated CeO_2NPs is confronted to additional problematics of the proteins sensitivity. For that reason, in this Doctoral research, one option (protocol of synthesis) of BSA-coated NPs was designed and remains under study for further optimizations.

2.3 Other functionalizations of CeO_2 NPs

In previous sections 2.1 and 2.2, the NPs coating has been analyzed regarding the aspect of monodispersity of colloidal NPs and avoidance of aggregation. On the other hand, another interesting issue of nanoceria coating is the functionalization of its surface. Unlike the previously commented topics and their problematics, the functionalization of CeO_2 NPs does decorate the primary nanoparticle with additional properties. Thus, despite the intrinsic properties of CeO_2NPs (catalytic, optical,

antioxidant), diverse functionalizations of its surface have been numerously tested and described in literature, with the objective to enhance the properties of nanoceria or to supply it with additional ones, for industrial and biomedical applications. For instance, Swanand P. et al. described the derivatization of nanoceria surface with human carbonic anhydrase II inhibitors and fluorophores, as a potential drug delivery device and fluorescent tracking of nanoparticles[59]. Similarly, Yang L. K. et al. tested radiolabeled cerium oxide for *in-vivo* studies of biodistribution[56]. In 2010, Asati A. tested the conjugation of nanoceria with polyacrylic acid (PNC), aminated polyacrylic acid (ANC), or dextran (DNC) and the following surface-charge-dependent cell localization and toxicity, related to cancer treatment[57]. While Shah V. studied the anti-bacterial activity of dextran-coated CeO_2NPs[58]. Also, PEG (polyethylene glycol) coated CeO_2NPs were targeted to an amyloid-beta antigen of Alzheimer´s disease for the studies of neurodegeneration[60]. While Alpaslan E. et al. engineered the surface of nanoceria with dextran to observe its activity in the presence bone cancer cells[61].

RESULTS AND DISCUSSIONS

1. CHARACTERIZATION OF THE DESIGNED CeO2 NPs

1.1 UV-vis absorption of CeO_2NPs

The prepared non-coated CeO_2NPs exhibit a characteristic absorption peak at 298 nm in the UV-visible spectrum [62], (Figure 1, red line). The UV absorption spectrum of cerium precursor (cerium nitrate salt) was used as a control, previous to NPs formation. Cerium compounds normally absorb near 300 nm, the formation of the NPs results in a modest blue shift and a significant broadening of the peak.

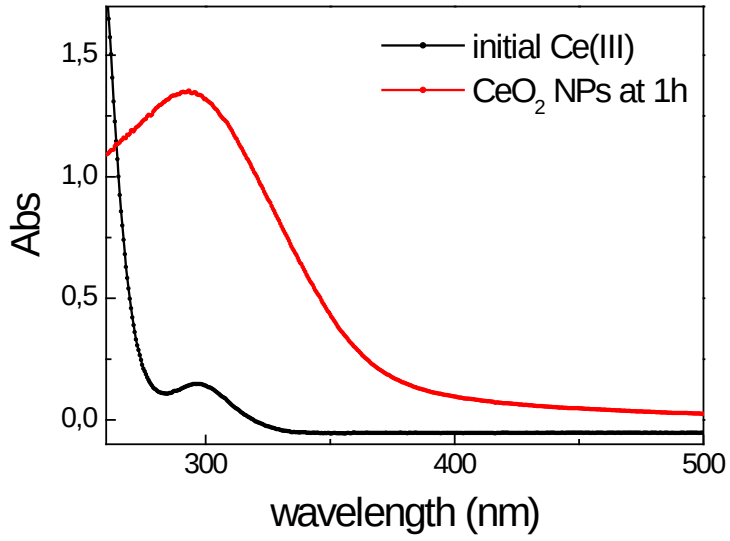

Figure 1. UV-visible spectra of non-coated colloidal CeO_2NPs. *(Black line): UV-visible spectrum of initial cerium precursor, showing an intense peak at low wavelength (below*

260), correspondent to an aqueous solution of cerium nitrate salt; (Red line): as-synthesized non-coated CeO_2NPs at 1h of reaction.

1.2 Electron Microscopy characterization CeO_2NPs

To minutely examine the quality of produced CeO_2NPs, in terms of morphology, size, aggregation state and chemical composition (purity), the samples were analyzed by high resolution electron microscopy (HR-TEM, STEM-HAADF, EELS). A few representative images of as-synthesized surfactant-free nanoparticles of CeO_2 are displayed in Figure 2. The size distribution was computer analyzed by Image J software, displaying a particle size of 5.2 ± 1.9 nm. The atomic planes of single-crystalline nanoparticles may be seen in Figure 2 (a, d). The homogeneity and monodispersity degree of nanoceria are inspected at high and low magnifications. Figures 2 (b) and (c) confirm a good monodispersity and homogeneous size distribution of the particles, using STEM-HAADF and HR-TEM modes, respectively. The profile of chemical composition of the samples was analyzed by EELS mode, displaying absolute purity of the samples (Figure 2, f). In addition, a Fourier Transformation (FFT) of a typical single crystalline CeO_2 NP (Figure 2, e) indicates the correspondent atomic planes, confirming a fluorite-like electronic structure.

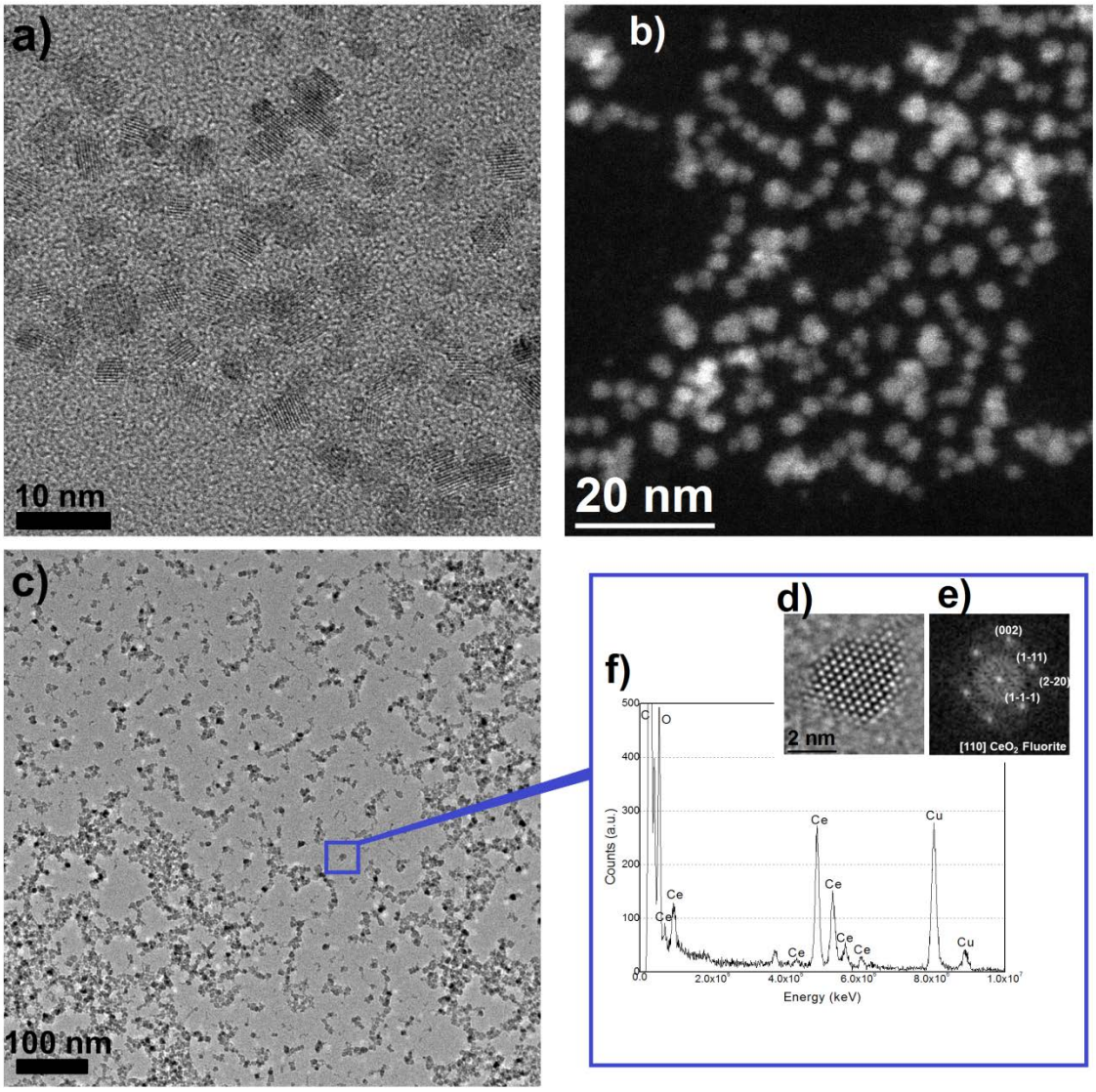

Figure 2. Characterization of CeO_2NPs by transmission electron microscopy (TEM).
a) high resolution TEM micrograph (HR-TEM) at high (400.000X) magnification, revealing the atomic planes of single-crystalline nanoparticles; b) High Angle Annular Dark Field (STEM-HAADF) image; c) HR-TEM image at low magnification (71.000Xcheck); d) atomic resolution HR-TEM image of one single CeO_2NP, showing spherical morphology and the correspondent atomic planes; e) FFT digital diffractogram calculated from the particle shown in (d); f) EELS map of the chemical composition of as synthesized CeO_2NP.

1.3 X-ray spectroscopy (XRD) characterization CeO_2NPs

The structural and compositional characterization, phase identification and size of CeO_2NPs were analyzed by X-ray Diffraction (XRD). The XRD pattern of as-synthesized and surfactant-free CeO_2NPs is displayed in Figure 3. The XRD pattern was scanned from 20 to 80 degrees and the XRD profile confirmed the monocrystalline nature of CeO_2NPs. The characteristic diffraction peaks were observed at 2θ = 28.51°, 33.12°, 47.44°, 56.30°, 58.88°, 69.36°, 76.75°, 79.02°, 88.35° and 95.34° correlated to (111), (200), (220), (311), (222), (400), (331), (402), (422), (333) crystal planes, respectively.

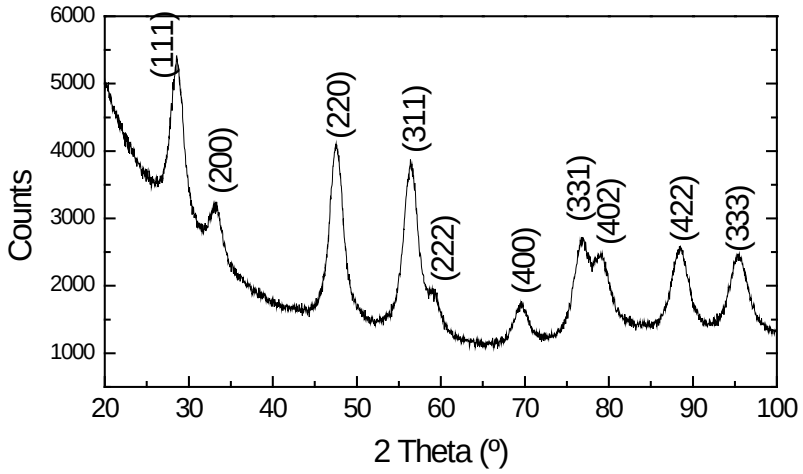

Figure 3. XRD pattern of 5nm CeO_2 nanoparticles. *All of the reflection peaks are in agreement in position and intensity with the database standard (JCPDS 34-0394) of the face-centered cubic CeO_2 crystal with the fluorite structure. The absence of additional diffraction peaks confirms the monocrystalline nature and purity of the samples.*

An experimental comparison of the XRD profile of designed NPs with other types of nanoceria is displayed in Figure 4. The correspondent CeO_2NPs of different size and purity consisted of commercial nanopowder (Figure 4, a) and laboratory-prepared NPs (Figure 4, b-e). The pattern of the designed surfactant-free nanoparticles is represented in Figure 4 (e), whose average size diameter determined by the Scherer equation is of

4.2 nm. Note that the XRD technique is a good tool to corroborate the compositional purity of the samples, as well as the correspondent crystalline size (the additional diffraction peaks of the impurities are represented in Figure 4 (c) and labeled with asterisks). However, the performed comparison put evidence in the fact that the X-ray technique gives limited information about the material. For instance, sample (a) corresponds to a highly aggregated nanopowder, while the sample (c) is performed with biologically toxic HMT reagent. With this brief example, we underline the importance of the nanoparticles characterization by as much techniques as possible, in order to conclude whether the material is suitable or not for biological administration. In case of the designed NPs, a high purity and a small crystalline size are confirmed (e).

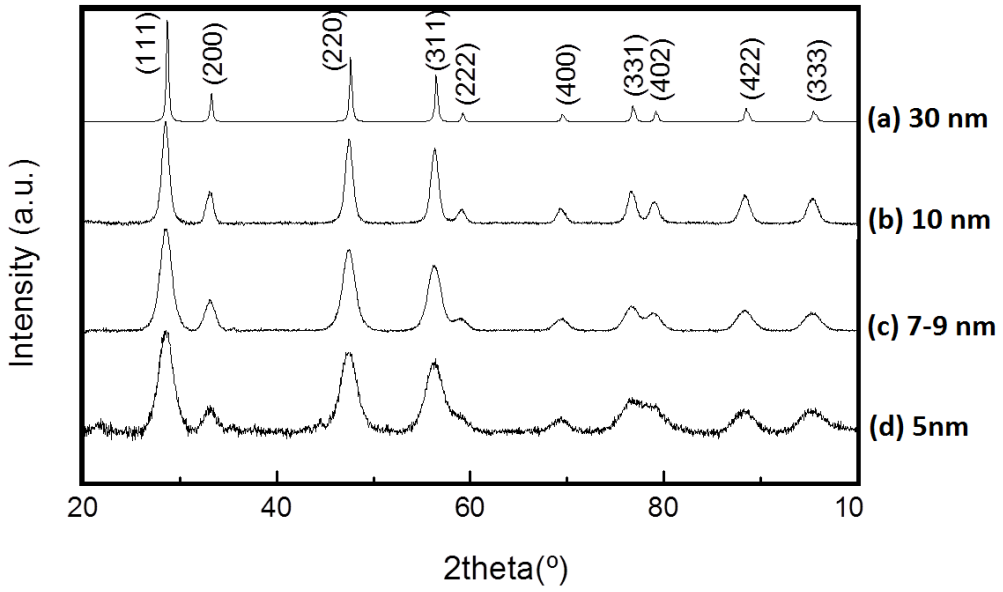

Figure 4. XRD pattern of differently-sized and differently-prepared CeO_2 NPs. *The correspondent CeO_2NPs of different size and purity consist of commercial nanopowder (a) and laboratory-prepared NPs (Figure 4, b-d). The pattern of the designed surfactant-free nanoparticles is represented in Figure 4 (c and d).*

2. MONITORING OF THE CeO_2 NPs SYNTHESIS KINETICS

2.1 pH monitoring

As described in the experimental section (2.1.2), the designed synthesis is carried out between cerium nitrate salt and ammonium salt in aqueous phase at room temperature (see the reaction below). The used TMAOH reagent is a quaternary ammonium salt, non-toxic at used concentrations, which in aqueous solution is decomposed in hydroxide ions (OH^-) and tetramethylammonium (TMA^+). While the hydroxide ions play essential role in favoring the oxidation of cerium precursor, the large counter-ion of (TMA^+) acts as a stabilizer of the formed NPs, providing them with certain colloidal stability by electrostatic repulsion. A final product is a hydrated cerium oxide

$$Ce^{3+} + OH^- \leftrightarrow Ce(OH)_{4\ (s)} \leftrightarrow CeO_{2\,(s)} + H_2O + H_3O^+$$

During the cerium precursor oxidation, hydroxide ions are transformed into water. We take advantage of the consequent protons generation in solution during the reaction to monitor the pH variations and have an idea about the kinetics of the synthesis. As displayed in Figure 5, the initial pH value of 12.2 rapidly decreased to final pH 4.8 within approximately 2h of reaction and remained invariable onwards. Such pH decay indirectly put evidence on the hydroxyl consumption and oxidation of cerium precursor.

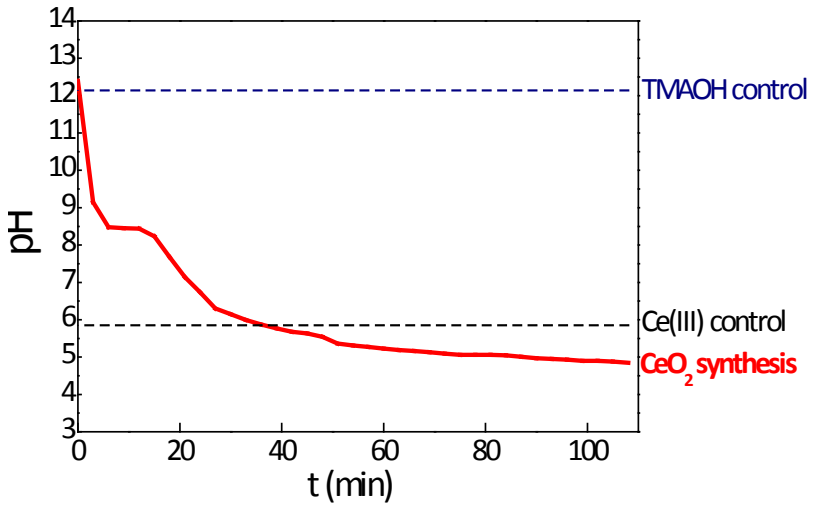

Figure 5. pH monitoring during the designed synthesis of CeO_2NPs. *The pH measurements of the reagents (in a separate way) are used as controls and represented with dot lines: TMAOH control (blue line), cerium precursor control (black line). The red line corresponds to a decay of pH in a solution of synthesis of CeO_2NPs during the first 2h of reaction and is maintained invariable onwards.*

2.2 XRD spectra monitoring

To visualize the possible changes in the crystalline structure and purity of the forming NPs during the first 2h of reaction, series of XRD spectra were measured. The Figure 6 displays the X-ray diffraction pattern of the samples, taken at 5, 15, 30, 40, 80, 100 and 135 minutes of synthesis. A gradual increase in the Intensity of the diffraction peaks is observed over time, which corroborate a formation of crystalline particles in solution and, consequently, an increase of the CeO_2NPs concentration over time. The Scherer equation of the first sample (at 5 min of reaction) and the last one (135 min) indicates an average crystalline size of around 6 nm. Consequently, initial nuclei of nanoceria are rapidly formed and do not grow over time.

According to Scherer equations, FWMH $_{5min}$ ≈ FWMH $_{135min}$, therefore, the only thing that happens in solution is a formation of more NPs with time.

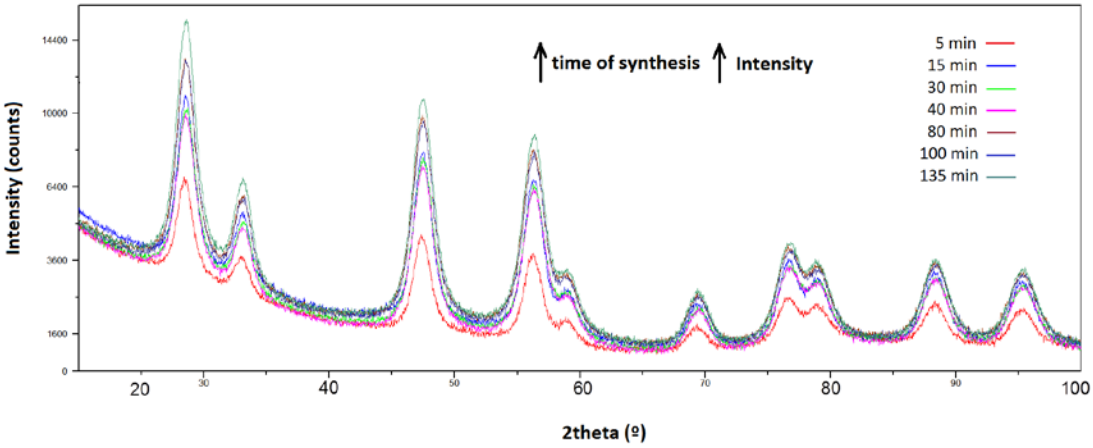

Figure 6. XRD monitoring during the designed synthesis of CeO_2NPs. *Samples were taken at 5, 15, 30, 40, 80, 100 and 135 minutes of synthesis. All of the reflection peaks are in agreement with the database standard (JCPDS 34-0394) of the face-centered cubic CeO_2 crystal with the fluorite structure. The absence of additional diffraction peaks confirms the monocrystalline nature and purity of the samples.*

3. The surface charge and Isoelectric Point of CeO_2NPs

It is well established that an oxide or a hydroxide suspended in aqueous environment can acquire its surface charge by adsorbing H^+ or OH^- ions [76]. The OH groups, present on the surface of a wet oxide can undergo acid-base dissociation, as weak acids or bases do when interacting with water molecules [77, 78]. Thus, in alkaline solutions the oxide surfaces are negatively charged or anionic, while in acidic solution they are positively charged or cationic. This data coincides with the fact that the designed surfactant-free CeO_2 NPs present cationic surface charge (+41.5 ±1.4 mV) at acidic pH (e.g. pH 4.8) and are negatively or anionically charged (-42.1 ±1.4mV) at alkaline pH (e.g. pH 12).

The pH at which the surface is electrically neutral (the solid has no net charge) is defined as the Isoelectric Point (PI) or Point of Zero Charge (PZC). It reflects the

chemical composition of the solid and the electrolyte in which it is immersed [63]. Since the PI is an important element of characterization, the knowledge of the PI of the material of interest facilitates a choice of a surfactant for a specific purpose. Besides, it facilitates as well the optimization of the manipulation and storage of the nanoparticles after the synthesis. According to literature, the PI is a complex parameter since its value depends on several variables: the chemical and physical structure and composition of the NP surface [65]; the impurities of the NP surface (structural, anionic and cationic) [63]; the hydration grade of the NP surface; the method of sample preparation and of PI determination [65, 67]. Interestingly, the PI of CeO_2 reported in literature is between values of 6 and 11.2 (Table 1).

PI (CeO_2NPs)	6	6,75	7,3	7,6	7,92	8,01	8,6
Reference	69	63	70	66	72	67	72

Table 1. Isoelectric points of CeO_2NPs reported in literature and the correspondent bibliographic references.

To delve into the existent differences of the PI values of nanoceria, next considerations must be taken into account. According to an extensive review of George A. Parks (1965), structural and adsorbed anionic impurities of the NP surface are able to cause PI shift to more acid values, while adsorbed cationic impurities to the NP surface shift PI to more basic values [63]. Also, the majority of discrepancies regarding the PI values reported in literature are due to purity of materials and the design of titration experiment [64]. Therefore, it is crucial to be critical in order to consider as valid one PI value or another for a material of interest. According to Petro N. Sh. et al. (1990), for the same type of NPs, the smaller the NP, more amount of H_2O and OH present directly on its surface, due to its higher surface-to-volume ratio. In another words, as smaller the nanoparticle, higher its hydration rate and amount of OH on its surface, therefore higher is its PI value [66].

On that base, considering the fact that the NPs, designed in this work are of a very small size, the hydration rate and consequent PI were expected to be quite high (alkaline). To corroborate such postulations and characterize the PI value, a titration of as-synthesized CeO_2 nanoparticles was performed. Effectively, the PI was 9.5 (Figure 7).

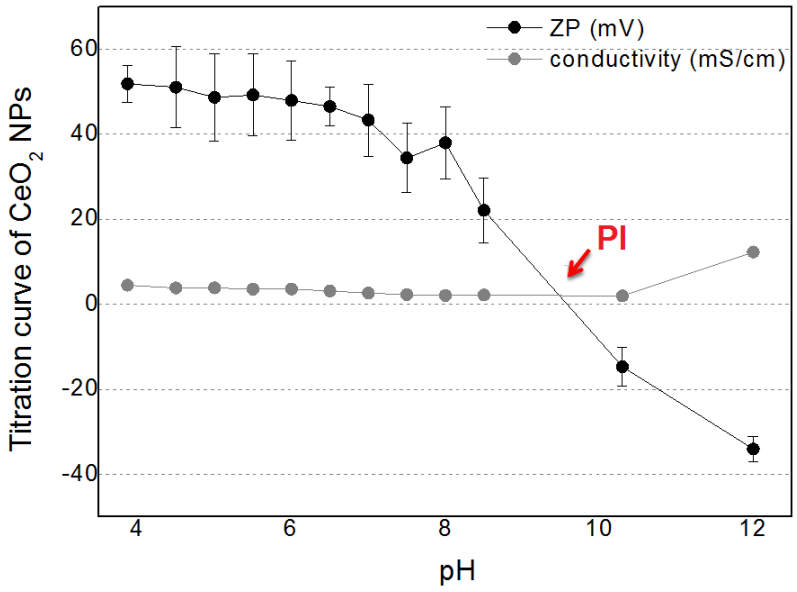

Figure 7. Titration curve of CeO_2NPs *(pH-dependent surface charge, Zeta Potential, of as-synthesized CeO_2NPs). The point of zero charge of CeO_2NPs is at pH = 9.5.*

It is well known, that when the nanoparticles are dispersed in a solution with a pH near to their point of zero charge, the colloidal stability of the NP is compromised. Such environment is thermodynamically unfavorable and the nanoparticles tend to aggregate in a rapid and often irreversible way, in order to decrease their surface energy.

As commented in Chapter 2, aggregated, as well as big-sized nanoparticles are highly undesirable for biomedical applications, due to cellular toxicity of aggregates. Therefore, the fact that the PI of the designed nanoceria is far from physiological pH (which oscillates between 7.2 and 7.4) indicates that naked (non-coated) nanoceria will

not tend to aggregate under physiological conditions due to this parameter, which is a good advantage in order to use them for biological applications.

4. DESIGNING OF THE OPTIMAL CeO_2NPs SYNTHESIS CONDITIONS

All of the previously described results correspond to the *optimal synthesis conditions* that have been chosen after a set of experiments, in which different parameters were tested and the obtained products analyzed. A chemical reaction of preparation of colloidal nanoparticles is a complex system where numerous parameters are involved. In the outlined process of synthesis by wet precipitation method, the most important factors are the type of the chemical reagents and their proportions; the pH of the solution; the reaction temperature and the agitation rate. Only controlling the largest number of parameters makes it possible to refine the product criteria such as size and aggregation. For this purpose each of the parameters must be studied in detail. Following the above considerations we have been studying one parameter while maintaining fixed all the others. As was observed, some of them are more critical than others.

First, physical factors such as the reaction temperature and agitation rate. Syntheses performed at 50° and 100° led to a fast and irreversible aggregation of nanoparticles. In this research work the synthesis at room temperature was selected as the optimum to produce nanoparticles under environmentally friendly conditions. In the case of agitation of the corresponding solutions was observed that the lower is the agitation rate, the greatest is the degree of aggregation of nanoparticles. For instance, in a volume of 100 ml, a minimal sufficient agitation was of 500 rpm, which was selected as optimal one and was kept invariable onwards.

Better controls of the reaction kinetics come from the variations of chemical parameters (the reagents). An ammonium salt TMAOH is the source of hydroxyls ([OH-]) in solution and this is a critical requirement for the oxidation of precursor. For this reason five reactions were carried out by adding different amount of TMAOH in each.

Surprisingly, a very clear evidence of the UV-vis spectra profiles indicated which condition is the optimal one. These results are discussed in detail next.

The optical study with ultraviolet-visible spectroscopy (UV-vis) was carried out to corroborate the particles formation [62] and to monitor the reaction kinetics upon different amounts of [OH-]. Despite the unspecificity of UV light absorption at short spectra wavelengths, it resulted in a good technique to monitor the progress and evolution of the reaction (but not to characterize materials). Aliquots were taken at time zero, 40min, 60min, 90 min; 7h and 48h of synthesis (Figure 8). Figure 8 (a) is a negative control that corresponds to cerium precursor in its non-oxidized state, before the synthesis of NPs started. Note that a negative control is displayed in all of the figures (b-f) and represents a lack of nanoparticles in solution. Also, figures (b-f) display the UV-vis absorption profile of the correspondent reactions.

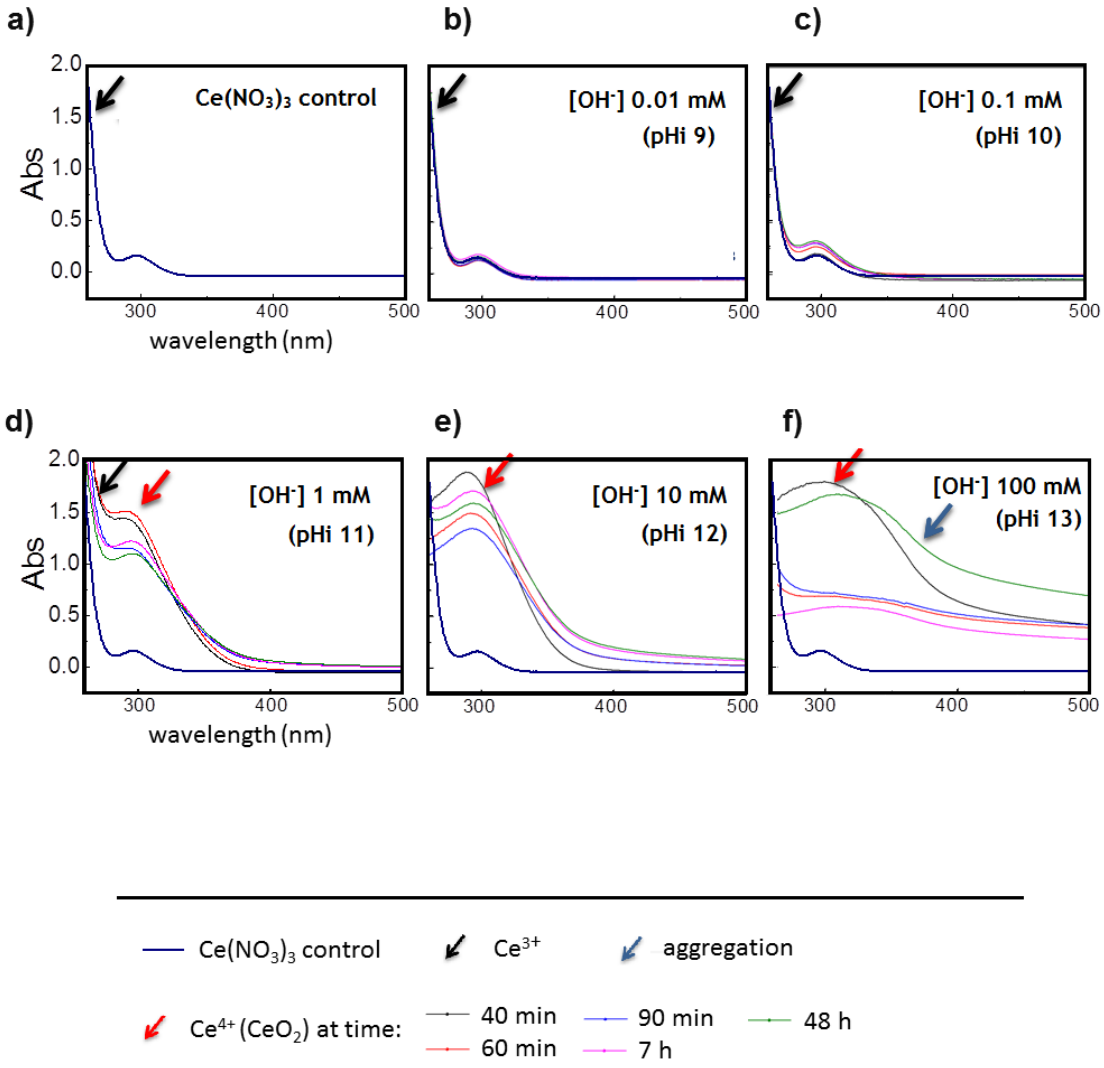

Figure 8. UV-vis spectroscopy characterization of CeO2 synthesis upon different initial pH conditions. (a) *the control spectra of initial 10mM cerium (III) precursor, previous to the addition of TMAOH.* ***(b)*** *Synthesis at initial pH of 9 (at 0.01mM concentration of TMAOH). The UV-vis spectra highly coincides with the cerium precursor spectra showed in (a), suggesting no NPs formation in this conditions.* ***(c)*** *Synthesis at initial pH of 10 (at 0.1mM concentration of TMAOH). Similarly to the (b), no significant formation of CeO_2NPs is detected.* ***(d)*** *Synthesis at initial pH of 11 (at 1mM concentration of TMAOH). The red arrow points a characteristic peak of Ce^{4+} at 298nm suggesting formation of CeO_2NPs by partial (incomplete) oxidation of precursor [62]. The black arrow points the non-oxidized cerium precursor, similar to (a).* ***(e)*** *Synthesis at initial pH of 12 (at 10mM concentration of TMAOH). Similarly to (d), the red arrow points the*

pronounced absorption peak of Ce^{4+} at 298 nm approximately, indicating formation of CeO_2NPs. Unlike figures (a-d), in figure (e) no cerium precursor peak is observed (no black arrow), suggesting a complete oxidation of cerium precursor in this synthesis conditions. ***(f)*** *Synthesis at initial pH of 13 (at 100mM concentration of TMAOH). The red arrow points a peak of Ce^{4+} corroborating the formation of NPs. The blue arrow points the enhanced absorption peaks that suggest aggregation of the formed nanoparticles in such highly alkaline conditions.*

Additional measurements of the pH monitoring of the same reactions (Figure 9 i) are accompanied with the size distribution of the formed NPs (Figure 9 ii). In reactions at 0.01 and 0.1 mM of [OH-], the pH evolved into a final pH of 6-7 (Figure 9i, b). Inspite the modest pH evolution (ergo modest [OH-] consumption), no NPs were observed by HR-TEM microscopy. This data indicates that these concentrations of [OH-] (0.01 and 0.1 mM) were not enough to oxidize cerium precursor and form NPs. This data is in accordance with Figure 8 (b) and (c), where no Ce^{4+} peak was observed, suggesting no NPs formation either.

In contrast, when the synthesis was performed at 1 and 10 mM concentration of [OH-], the pH of both solutions evolved into a final pH of 4.8 (Figure 9i, d) and the HR-TEM microscopy imaging corroborated formation of NPs. This data is in accordance with a pronounced absorption peak at UV-vis spectra (Figure 8 d and e) that suggested NPs formation. The size distribution of the formed NPs was determined by Image J software, counting at least 150 NPs per image. As displayed in Figure 9ii, the NPs at 1 mM of initial [OH-], were around 5 nm in diameter (4.2 ± 0.97 nm). In contrast, the NPs formed at initial 10 mM of [OH-], were of 5.2 ± 1.9 nm at 24h of synthesis and grew in size up to 7-9 nm (7.13 ±2.7 nm) within 48h of synthesis. The analytical ICP-MS analysis of these samples indicated that in case of 1 mM of initial [OH-], the reaction yield was of 5% that corresponds to a formation of NPs at final concentration of 0.1mg/ml (Figure 12, synthesis at pH 11). On the contrary, the reaction yield of the synthesis at 10 mM of

initial [OH-] was of 85%, that corresponds to a formation of highly concentrated nanoparticles at 1 mg/ml concentration (Figure 10, synthesis at pH 12).

Summarizing, at 1 mM concentration of [OH-], less NPs were formed and the size of these NPs remained invariable (around 5 nm). In contrast, at 10 mM concentration of [OH-], a big amount of NPs were formed in solution (highly concentrated) and the size of the NPs evolved from around 5 nm to approximately 7-9 nm within 48h of synthesis. The next Results section analyzes the reasons of such NPs growth. Note that the highly concentrated NPs tend to agglomerate and aggregate in solution within short periods of time. That is why the PVP coating of the NPs was proposed as alternative synthesis method; in order to avoid aggregation of highly concentrated nanoparticles.

At last, the synthesis reaction at initial [OH-] concertation of 100 mM did not display any evolution of the pH, due to an excess of alkali (Figure 9i (a)). However, these reaction conditions led to the formation of big aggregates, composed of small-sized nanoparticles (Figure 9ii). This data is in accordance with the enhancement of the absorption peak of the UV-vis spectra in Figure 8 f. The correspondent fast and irreversible aggregation of the small-sized nanoparticles is a result of an excessive ionic strength in solution.

Based on these results, the reaction conditions at initial [OH-] of 0.01 and 0.1 mM were discarded due to a lack of NPs formation. Also, the reaction condition at [OH-] 100 mM was discarded due to the rapid aggregation of the formed nanoparticles. While the reaction conditions at [OH-] concentration of 1 and 10 mM were selected as valid, in order to form small-sized nanoparticles at room temperature.

i)

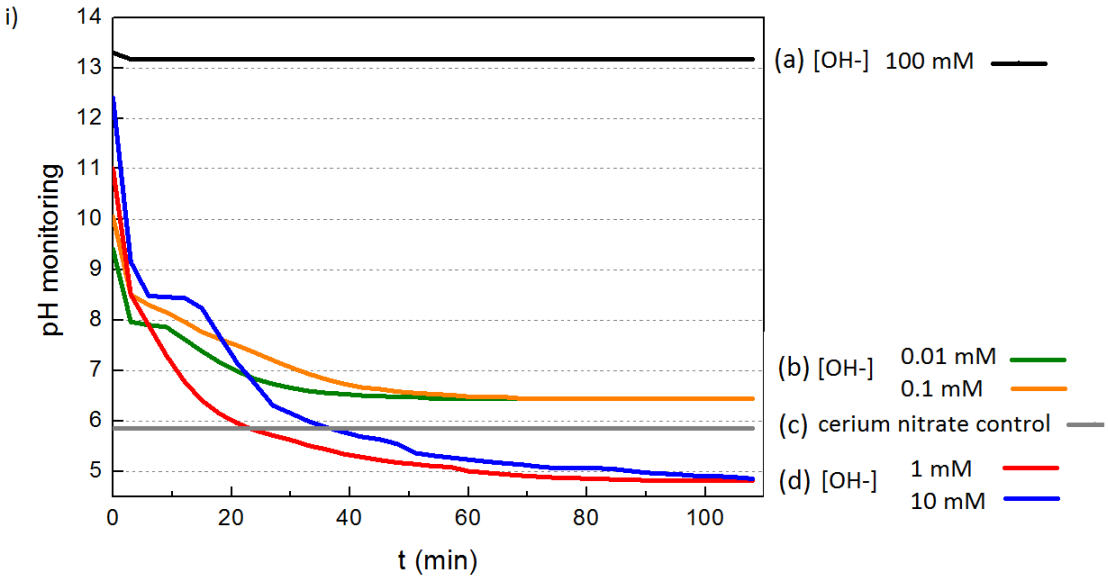

ii)

[OH-] mM	0,01	0,1	1	10	100
Average NP size at t=100 min	-	-	4,4 ± 1,1 nm	5,2 ± 1,9 nm	4,5 ± 1,3 nm (agg.)
Average NP size at t=48h	-	-	4.2 ± 0.97 nm	7,13 ± 2,7 nm	4,4 ± 0,9 nm (agg.)

Figure 9. Monitoring of the NP size and the pH evolution, in reactions of CeO2 synthesis upon different initial amount of TMAOH (hydroxyl [OH-] ions). *(i) Size distribution of NPs formed in the reactions performed at initial [OH-] concentration of 0.01, 0.1, 1, 10 and 100 mM. The samples were taken at 100 min and 48 h of the syntheses and analyzed by HR-TEM at 400.000X magnification. The size distribution was computer analyzed by Image J software. (ii) pH monitoring of the reactions at different [OH-] concentration. The grey lines corresponds to control of cerium precursor ($Ce(NO_3)_3$ ct). The lines in (i) correspond to a pH decay of reactions at initial pH of 9 and 10, indicating partial consumption of the hydroxyl source. The lines in (ii) correspond to a pH decay of reactions at initial pH of 11 and 12, indicating a greater consumption of the hydroxyls, while the black like in (iii) corresponds to a synthesis at initial pH of 13 and shows no variations in pH levels. The data in (iii) corroborates an excessively high alkaline media in the respective synthesis reaction.*

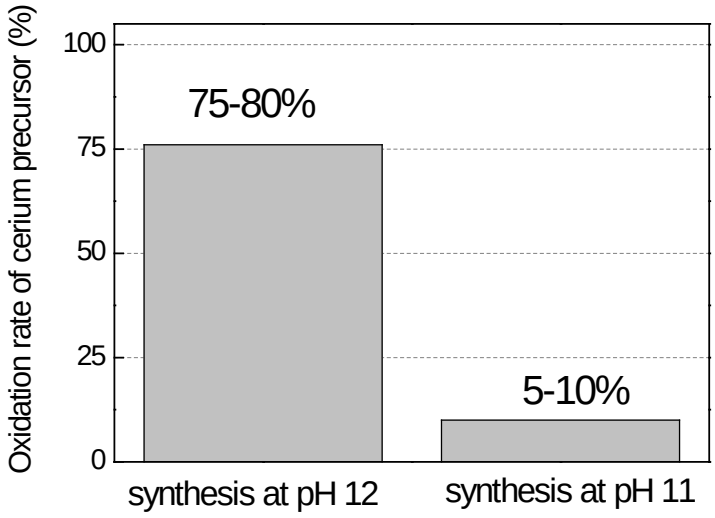

Figure 10. ICP-MS analytical determination of the reaction yield in synthesis ar initial pH of 11 and 12 (at 10 and 1 mM of [OH-] concentration, respectively). *The initial amount of cerium precursor was normalized to 100%. The correspondent oxidation rate of precursor showed to be more efficient in reaction at pH 12 (75-80% yield).*

5. MORPHOLOGICAL TIME-EVOLUTION OF CeO_2NPs

For a better understanding of the nanoceria nature, a long-term study without literary precedents was performed. For that aim, the samples of CeO_2NPs were stored during two years and a half, being systematically characterized by HR-TEM to follow their morphological and compositional evolution.

Throughout this study we observed that single nanoparticles of cerium oxide exhibit a clear tendency to be cemented (sintered) via oriented attachment (Figure 11, red brackets). This behavior strongly depends on the NPs concentration, since diluted NPs (prepared at 5% yield synthesis and 0.1 mg/ml concentration) sinterized later than concentrated ones (prepared at 80% yield synthesis and 1 mg/ml concentration). Such differences arise from the fact that the probability to collide between single NPs is lower in diluted solution than in a concentrated one. Besides, the electron microscopy characterization of the samples at high magnification (400.000X at HR-TEM), revealed a formation of the "peanut-like" transition morphology of NPs. Over time, the transition peanut-like nanostructures showed a tendency to eventually achieve the most energetically favorable spherical shape of 7,13 ± 2,7 nm in diameter, probably achieved through local atomic reorientation.

On the other hand, at larger time of storage (e.g. one-year-aged nanoceria, stored at room temperature), the NPs exhibited morphological changes that consisted in natural tendency to end up in a stamp-like morphology (Figure 11 blue brackets). For geometrical reasons that we observe, it cannot be explained only by oriented attachment, so some recrystallization might also occur.

Moreover, another and inevitable phenomenon of surfactant-free CeO_2NPs was partial aggregation within the same sample, explained by a tendency of small-sized NPs to achieve more thermodynamically stable states (Figure 11 d).

A more detailed schematic overview of the morphological time-evolution of nanoceria is represented in Figure 12.

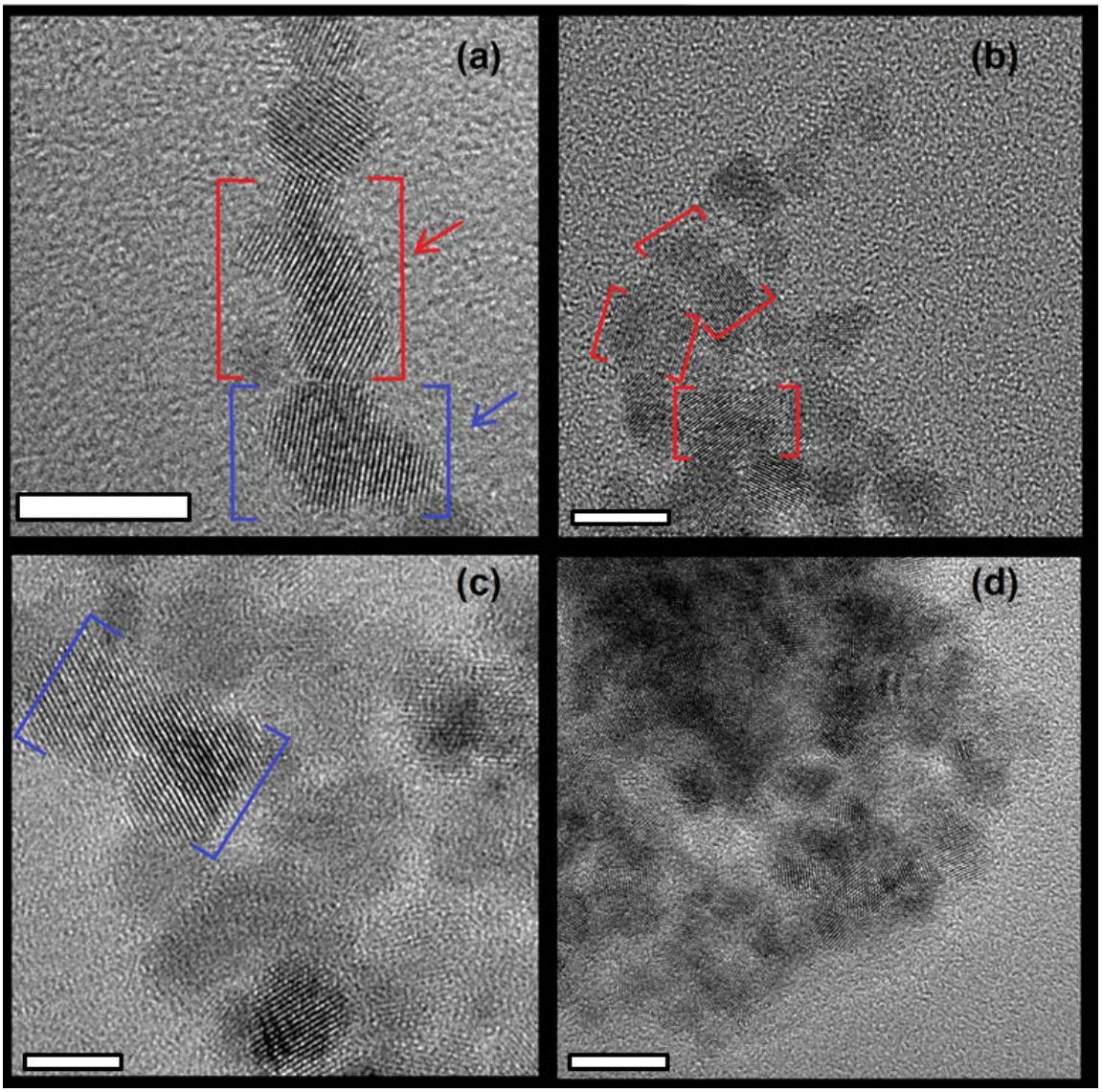

Figure 11. HR-TEM micrographs of the morphological time-evolution of nanoceria. *Red brackets in (a) and (b) show sintering (oriented attachment) between single nanoparticles. Blue brackets in (a) and (c) show stamp-like morphology of CeO_2NPs that appears at larger times of storage (e.g. one year and a half). The image in (d) is a typical aggregate of small-sized NPs, located in the same sample. The correspondent scale bars are of 10 nm length.*

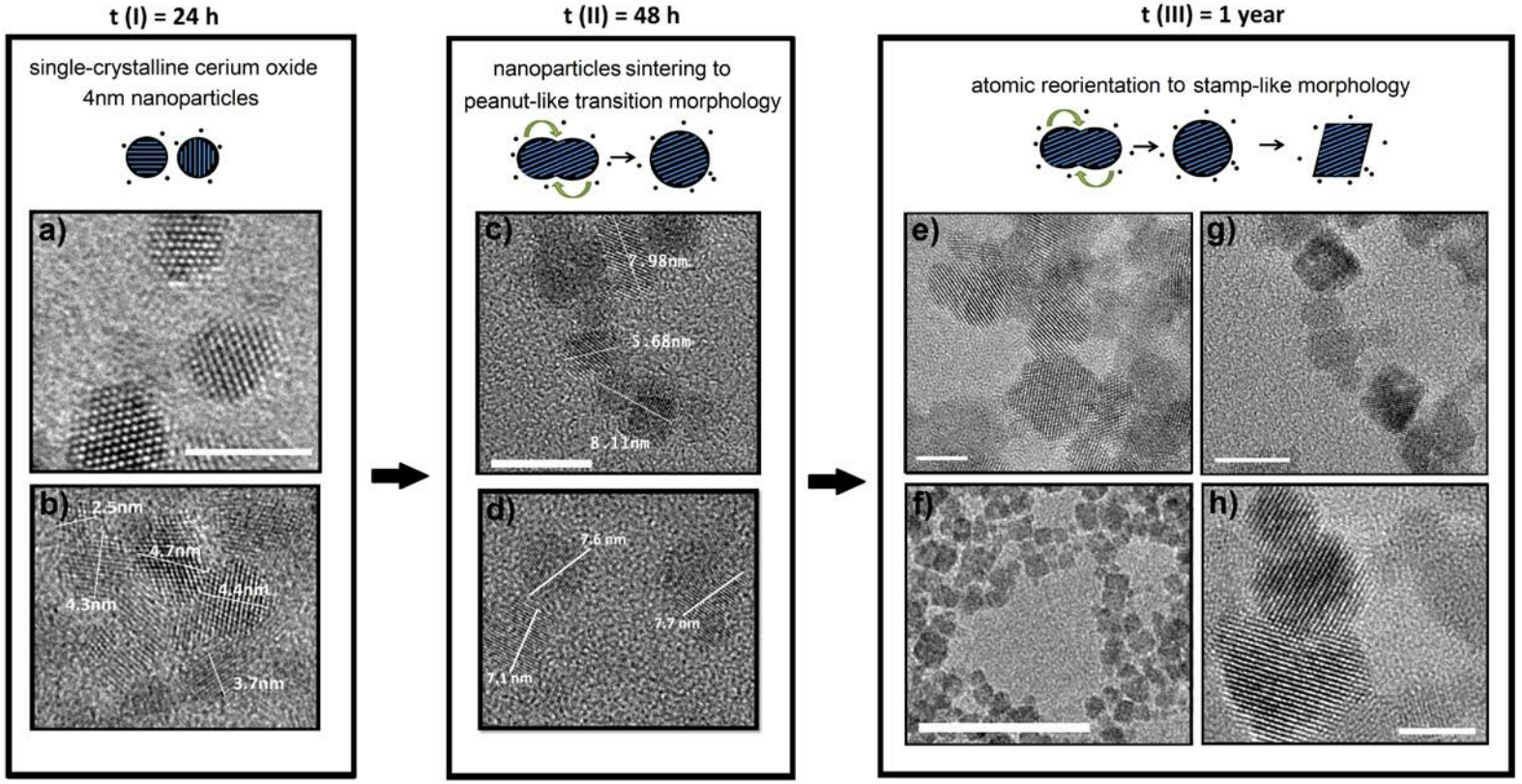

Figure 12. HR-TEM micrographs and a schematic overview of the morphological time-evolution of nanoceria. *The given scheme corresponds to CeO_2NPs of the R4 synthesis reaction (initial pH of 12, final pH of 4.8). t (I): CeO_2NPs at 24h of synthesis. The high resolution micrographs (HR-TEM) in (a) and (b) show spherical morphology of single-crystalline nanoparticles with average diameter of 4.5 nm. t(II): CeO_2NPs at 48h of synthesis. HR-TEM images (c) and (d) reveal the oriented attachment sintering between single nanoparticles, achieving single-crystalline peanut-like transition morphology. The average diameter of sintered structures is* 7,13 ± 2,7 nm*. t(III): CeO_2NPs at larger times (up to one year) after synthesis. HR-TEM images e) – h) show the tendency of CeO_2NPs to reorient atoms in order to obtain stamp-like structures. The correspondent scale bars are: a) 5nm, c) 10nm, e) 5nm, f) 50nm, g) 10nm, h) 5nm.*

Similar intermediate or *transition* morphologies were reported in 2002, where Pacholski et al. [82] illustrated by HR-TEM images the formation of pearl-chain-like aggregates during the ZnO nanoparticles growth by oriented attachment. Also, an examination of such behavior as oriented attachment was discussed by Alivisatos A. P [77] and Horst Weller [82], among others, supporting the experimental observations with speculations about the rising potential applications of similar materials. According to Weller, oxide nanoparticles are very favorable for oriented attachment (e.g. ZnO, CeO2), nevertheless similar phenomena was reported as well for materials as PbS [79], Pt3Fe [80], Cu [81], among others.

Unfortunately a precise mechanism of the nanoparticles growth remains as a challenge and in 2012, the volume 336 of the Science magazine was dedicated to nanoparticles attachment phenomena with correspondent speculations on the growth mechanism, and applications. As was claimed by H-G.Liao et al. [83], an understanding of the mechanism of one-dimensional colloidal nanocrystal growth, using nanoparticles as building blocks, provides a link between the world of single molecules and hierarchical nanostructures, and paves the way to rational design of nanomaterials with controlled properties.

As previously discussed in this Chapter, the designed NPs with PVP or BSA coating are the optimal ones for biomedicine, since such surface coating provides an optimal size of the nanoparticles and avoids the described surface evolution, due to repulsion between NPs. However, the obtained data about the surface evolution of the surfactant-free is an additional knowledge that serves as a platform for further research. For instance, a development of the synthesis receipts of cerium oxide nanorods or nanobelts is a rising branch of study with potential applications of such catalytic nanoplatforms.

Another possibility of the surface changes of nanoceria is its dissolution into constitutive ions under certain conditions of the NPs environment. It is an attractive property for biomedicine and is detaily discussed in Chapter 4.

BIBLIOGRAPHY

[1] Hirst, S. M., A. S. Karakoti, et al. (2009). "Anti-inflammatory Properties of Cerium Oxide Nanoparticles." Small **5**(24): 2848-2856.

[2] Visai, L., L. De Nardo, et al. (2011). "Titanium oxide antibacterial surfaces in biomedical devices." International Journal of Artificial Organs **34**(9): 929-946.

[3] Dal Lago, V., L. F. de Oliveira, et al. (2011). "Size-selective silver nanoparticles: future of biomedical devices with enhanced bactericidal properties." Journal of Materials Chemistry **21**(33): 12267-12273.

[4] Hirano, M., Y. Fukuda, et al. (2000). "Preparation and spherical agglomeration of crystalline cerium(IV) oxide nanoparticles by thermal hydrolysis." Journal of the American Ceramic Society 83(5): 1287-1289.

[5] Yin, L. X., Y. Q. Wang, et al. (2002). "Sonochemical synthesis of cerium oxide nanoparticles - Effect of additives and quantum size effect." Journal of Colloid and Interface Science 246(1): 78-84.

[6] Tsyzuki, T., Robinson, J. S., McCormick, P. G (2002). "UV-shelding ceramic nanoparticles synthesised by mechanochemical processing". Journal of Australian Ceramic Society 38(1): 15-19.

[7] Lair, V., A. Ringuede, et al. (2008). "Synthesis and characterization of cerium oxide by electrochemical methods." Physica Status Solidi C - Current Topics in Solid State Physics, Vol 5, No 11 2008 **5**(11): 3492-3495.

[8] Khadse, V. R., S. Thakur, et al. (2014). "Humidity-sensing studies of cerium oxide nanoparticles synthesizedby non-isothermal precipitation." Sensors and Actuators B-Chemical **203**: 229-238.

[9] Renuka, N. K. (2012). "Structural characteristics of quantum-size ceria nano particles synthesized via simple ammonia precipitation." Journal of Alloys and Compounds 513: 230-235.

[10] Masui, T., H. Hirai, et al. (2002). "Synthesis of cerium oxide nanoparticles by hydrothermal crystallization with citric acid." Journal of Materials Science Letters 21(6): 489-491.

[11] Balavi, H., S. Samadanian-Isfahani, et al. (2013). "Preparation and optimization of CeO2 nanoparticles and its application in photocatalytic degradation of Reactive Orange 16 dye." Powder Technology 249: 549-555.

[12] Walton, R. I. (2011). "Solvothermal synthesis of cerium oxides." Progress in Crystal Growth and Characterization of Materials 57(4): 93-108.

[13] Matijevic, E., (1987). "Colloidal science in ceramic powders preparation". High Tech Ceramics, ed. P.Vincenzini. Elsevier, pp. 441-458.

[14] Djuricic, B. and S. Pickering (1999). "Nanostructured cerium oxide: Preparation and properties of weakly-agglomerated powders." Journal of the European Ceramic Society **19**(11): 1925-1934.

[15] Zhang, Y., Y. S. Chen, et al. (2008). "Stability of commercial metal oxide nanoparticles in water." Water Research **42**(8-9): 2204-2212.

[16] Lin, W.S., et al., Toxicity of cerium oxide nanoparticles in human lung cancer cells. International Journal of Toxicology, 2006. 25(6): p. 451-457.

[17] Fang, X.H., et al., Stresses exerted by ZnO, CeO2 and anatase TiO2 nanoparticles on the Nitrosomonas europaea. Journal of Colloid and Interface Science, 2010. 348(2): p. 329-334.

[18] Lin, W. S., Y. W. Huang, et al. (2006). "Toxicity of cerium oxide nanoparticles in human lung cancer cells." International Journal of Toxicology 25(6): 451-457.

[19] Park B, Martin P, Harris C, et al. Initial in vitro screening approach to investigate the potential health and environmental hazards of Envirox^{TM} – a nanoparticulate cerium oxide diesel fuel additive. Particle and Fibre Toxicology. 2007;4:12. doi:10.1186/1743-8977-4-12.

[20] Schubert, D., R. Dargusch, et al. (2006). "Cerium and yttrium oxide nanoparticles are neuroprotective." Biochemical and Biophysical Research Communications 342(1): 86-91.

[21] Niu, J. L., A. Azfer, et al. (2007). "Cardioprotective effects of cerium oxide nanoparticles in a transgenic murine model of cardiomyopathy." Cardiovascular Research 73(3): 549-559.

[22] Giri, S., et al., Nanoceria: A Rare-Earth Nanoparticle as a Novel Anti-Angiogenic Therapeutic Agent in Ovarian Cancer. Plos One, 2013. 8(1).

[23] Chigurupati, S., et al., Effects of cerium oxide nanoparticles on the growth of keratinocytes, fibroblasts and vascular endothelial cells in cutaneous wound healing. Biomaterials, 2013. 34(9): p. 2194-2201.

[24] Kyosseva, S.V., et al., Nanoceria inhibit expression of genes associated with inflammation and angiogenesis in the retina of Vldlr null mice. Experimental Eye Research, 2013. 116: p. 63-74.

[25] Oró, D., Yudina, T., et al.. (2016). "Cerium oxide nanoparticles reduce steatosis, portal hypertension and display antiinflammatory properties in rats with liver fibrosis." J Hepatol. 64(3):691-8.

[26] Buzea, C., Pacheco, II, et al. (2007). "Nanomaterials and nanoparticles: sources and toxicity." Biointerphases 2(4): MR17-71.

[27] Oostingh, G. J., E. Casals, et al. (2011). "Problems and challenges in the development and validation of human cell-based assays to determine nanoparticle-induced immunomodulatory effects." Particle and Fibre Toxicology 8.

[28] Pfaller, T., V. Puntes, et al. (2009). "In vitro investigation of immunomodulatory effects caused by engineered inorganic nanoparticles - the impact of experimental design and cell choice." Nanotoxicology 3(1): 46-59.

[29] Sperling, R. A., E. Casals, et al. (2009). "Inorganic Engineered Nanoparticles and Their Impact on the Immune Response." Current Drug Metabolism 10(8): 895-904.

[30] Garcia, A., R. Espinosa, et al. (2011). "Acute toxicity of cerium oxide, titanium oxide and iron oxide nanoparticles using standardized tests." Desalination 269(1-3): 136-141.

[31] Schlinkert, P., E. Casals, et al. (2015). "The oxidative potential of differently charged silver and gold nanoparticles on three human lung epithelial cell types." Journal of Nanobiotechnology 13.

[32] Barrena, R., E. Casals, et al. (2009). "Evaluation of the ecotoxicity of model nanoparticles." Chemosphere 75(7): 850-857.

[33] Casals, E., E. Gonzalez, et al. (2012). "Reactivity of inorganic nanoparticles in biological environments: insights into nanotoxicity mechanisms." Journal of Physics D-Applied Physics 45(44).

[34] Goy-Lopez, S., J. Juarez, et al. (2012). "Physicochemical Characteristics of Protein-NP Bioconjugates: The Role of Particle Curvature and Solution Conditions on Human Serum Albumin Conformation and Fibrillogenesis Inhibition." Langmuir 28(24): 9113-9126.

[35] Piella, J., N. G. Bastus, et al. (2013). "Characterizing Nanoparticles Reactivity: Structure-Photocatalytic Activity Relationship." Nanosafe 2012: International Conferences on Safe Production and Use of Nanomaterials 429.

[36] Casals, E., T. Pfaller, et al. (2011). "Hardening of the Nanoparticle-Protein Corona in Metal (Au, Ag) and Oxide (Fe3O4, CoO, and CeO2) Nanoparticles." Small 7(24): 3479-3486.

[37] Dowding, J.M., et al., Cellular Interaction and Toxicity Depend on Physicochemical Properties and Surface Modification of Redox-Active Nanomaterials. Acs Nano, 2013. 7(6): p. 4855-4868.

[38] Choi, H. S., W. Liu, et al. (2007). "Renal clearance of quantum dots." Nature Biotechnology 25(10): 1165-1170.

[39] Kosmulski, M. (2002). "The pH-dependent surface charging and the points of zero charge." Journal of Colloid and Interface Science 253(1): 77-87.

[40] Puntes, V. (2015). "Design and pharmacokinetical aspects for the use of inorganic nanoparticles in radiomedicine". Br J Radiol; 88: 20150210.

[41] Cafun, J.D., et al., Absence of Ce^{3+} sites in chemically active colloidal ceria nanoparticles. ACS Nano, 2013. 7(12): p. 10726-32.

[42] Gu, H. and M. D. Soucek (2007). "Preparation and characterization of monodisperse cerium oxide nanoparticles in hydrocarbon solvents." Chemistry of Materials **19**(5): 1103-1110.

[43] Phokha, S., S. Pinitsoontorn, et al. (2012). "Synthesis, characterization, and magnetic properties of monodisperse CeO_2 nanospheres prepared by PVP-assisted hydrothermal method." Nanoscale Research Letters **7**.

[44] Merrifield, R. C., Z. W. Wang, et al. (2013). "Synthesis and Characterization of Polyvinylpyrrolidone Coated Cerium Oxide Nanoparticles." Environmental Science & Technology **47**(21): 12426-12433.

[45] Girija, D., et. al (2011). "Cerium oxide nanoparticles - a green, reusable, and highly efficient heterogeneous catalyst for the synthesis of Polyhydroquinolines under solvent-free conditions". Scholars Research Library **3** (3):373-382

[46] Chitsaz, A., M. Jalilpour, et al. (2013). "Effects of PVP and CTAB surfactants on the morphology of cerium oxide nanoparticles synthesized via co-precipitation method." International Journal of Materials Research **104**(5): 511-514.

[47] Wang, F. X., Z. F. Wang, et al. (2010). "Fabrication of mono-dispersed cerium oxide nanopowders via mixed solvothermal route." Journal of Rare Earths **28**: 139-143.

[48] Koczkur, K. M., S. Mourdikoudis, et al. (2015). "Polyvinylpyrrolidone (PVP) in nanoparticle synthesis." Dalton Transactions **44**(41): 17883-17905.

[49] Marsalek, R. (2014). "Adsorption of bovine serum albumin on CeO_2"International Journal of Chemical, Nuclear, Materials and Metallurgical Engineering Vol8, No: 12

[50] Barone, G., S. Capasso, et al. (1995). "Thermal denaturation of bovine serum albumin and its oligomers and derivatives pH dependence." Journal of Thermal Analysis **45**(6): 1255-1264.

[51] Giancola, C., C. DeSena, et al. (1997). "DSC studies on bovine serum albumin denaturation - Effects of ionic strength and SDS concentration." International Journal of Biological Macromolecules **20**(3): 193-204.

[52] Vlasova, I. M. and A. M. Saletsky (2009). "Study of the Denaturation of Human Serum Albumin by Sodium Dodecyl Sulfate Using the Intrinsic Fluorescence of Albumin." Journal of Applied Spectroscopy **76**(4): 536-541.

[53] Masuelli, M., A. (2013) Study of sovine serum albumin solubility in aqueous solutions by intrinsic viscosity measurements." Advanced Physical Chemistry Volume 2013
Michnik, A., K. Michalik, et al. (2005). "Stability of bovine serum albumin at different pH." Journal of Thermal Analysis and Calorimetry **80**(2): 399-406.

[54] Barone, G., C. Giancola, et al. (1992). "Dsc Studies on the Denaturation and Aggregation of Serum Albumins." Thermochimica Acta **199**: 197-205.

[55] Xu, Y., K. A. Linares, et al. (2004). "pH dependent change in the optical properties of surface modified gold nanoparticles using bovine serum albumin." Nsti Nanotech 2004, Vol 1, Technical Proceedings: 15-18.

[56] Yang, L. K., G. Sundaresan, et al. (2013). "Intrinsically radiolabeled multifunctional cerium oxide nanoparticles for in vivo studies." Journal of Materials Chemistry B **1**(10): 1421-1431.

[57] Asati, A., S. Santra, et al. (2010). "Surface-Charge-Dependent Cell Localization and Cytotoxicity of Cerium Oxide Nanoparticles." ACS Nano **4**(9): 5321-5331.

[58] Shah, V., S. Shah, et al. (2012). "Antibacterial Activity of Polymer Coated Cerium Oxide Nanoparticles." Plos One **7**(10).

[59] Patil, S., S. Reshetnikov, et al. (2007). "Surface-derivatized nanoceria with human carbonic anhydrase II inhibitors and fluorophores: A potential drug delivery device." Journal of Physical Chemistry C **111**(24): 8437-8442.

[60] Patent number US 8,877,207 B2

[61] Asati, A. R. and J. M. Perez (2008). "BIOL 125-Unique pH-dependent free radical scavenging activity of dextran coated cerium oxide nanoparticles." Abstracts of Papers of the American Chemical Society **236**.

[62] Greenhaus, H. L., A. M. Feibush, et al. (1957). "Ultraviolet Spectrophotometric Determination of Cerium(Iii)." Analytical Chemistry **29**(10): 1531-1534.

[63] George A. Parks, et al. (1965). "The isoelectric points of solid oxides, solid hydroxides, and aqueous hydroxo complex systems." Chem. Rev. 65 (2): 177–198.

[64] Kosmulski M., et al. (2002). "The pH-dependent surface charging and the points of zero charge." J. Colloid Interface Sci. 253, 77-87.

[65] De Faria L. A., et al. "The point of zero charge of oxide surfaces: an intensive property to separate electronic from geometric factors."

[66] Petro N. Sh., et al. (1990). "On the behaviour of hydrous ceria as an ion exchanger: surface properties, structural features, capacity and apparent pH values." Colloids and Surfaces, 49: 211-218.
5 Yoon R. H., et al. (1978). "Predicting points of zero charge of oxides and hydroxides." J. Colloid Interface Sci. Vol. 70, No. 3.

[67] De Faria L. A., et al. (1994). "The point of zero charge of CeO_2." J. Colloid Interface Sci. 167, 352-357.

[68] Trasatti S. (1990). "Surface chemistry of oxides and electrocatalysis." Conference paper.

[69] Antonova, A. A., O. V. Zhilina, et al. (2001). "Synthesis and some properties of cerium dioxide hydrosols." Colloid Journal 63(6): 662-667.

[70] Ocana, M. (2002). "Preparation and properties of uniform praseodymium-doped ceria colloidal particles." Colloid and Polymer Science 280(3): 274-281.

[71] Hirano, M., Y. Fukuda, et al. (2000). "Preparation and spherical agglomeration of crystalline cerium(IV) oxide nanoparticles by thermal hydrolysis." Journal of the American Ceramic Society 83(5): 1287-1289.

[72] Nabavi, M., O. Spalla, et al. (1993). "Surface-Chemistry of Nanometric Ceria Particles in Aqueous Dispersions." Journal of Colloid and Interface Science **160**(2): 459-471.

[73] Wu, Z. H., J. Zhang, et al. (2002). "Structure and chemical transformation in cerium oxide nanoparticles coated by surfactant cetyltrimethylammonium bromide (CTAB): An x-ray absorption spectroscopic study." Journal of Physical Chemistry B **106**(18): 4569-4577.

[74] Zhang, F., Q. Jin, et al. (2004). "Ceria nanoparticles: Size, size distribution, and shape." Journal of Applied Physics **95**(8): 4319-4326.

[75] Sahu, T., S. S. Bisht, et al. (2013). "Nanoceria: Synthesis and Biomedical Applications." Current Nanoscience **9**(5): 588-593.

[76] Yoon R. H., et al. (1978). "Predicting points of zero charge of oxides and hydroxides." J. Colloid Interface Sci. Vol. 70, No. 3.

[77] De Faria L. A., et al. "The point of zero charge of oxide surfaces: an intensive property to separate electronic from geometric factors."

[78] Trasatti S. (1990). "Surface chemistry of oxides and electrocatalysis." Conference paper.

[79] Schliehe, C., B. H. Juarez, et al. (2010). "Ultrathin PbS Sheets by Two-Dimensional Oriented Attachment." Science **329**(5991): 550-553.

[80] Liao, H. G., L. K. Cui, et al. (2012). "Real-Time Imaging of Pt3Fe Nanorod Growth in Solution." Science **336**(6084): 1011-1014.

[81] Shen, S. L., J. Zhuang, et al. (2009). "Size Effects in the Oriented-Attachment Growth Process: The Case of Cu Nanoseeds." Inorganic Chemistry **48**(12): 5117-5128.

[82] Pacholski, C., A. Kornowski, et al. (2002). "Self-assembly of ZnO: From nanodots, to nanorods." Angewandte Chemie-International Edition **41**(7): 1188-+.

[83] Liao, H. G., K. Y. Niu, et al. (2013). "Observation of growth of metal nanoparticles." Chemical Communications **49**(100): 11720-11727.

CHAPTER 3

ANTIOXIDANT ACTIVITY OF CeO_2 NPs

INTRODUCTION

1. REACTIVE OXYGEN SPECIES (ROS) AND THE ELECTRON SPONGE NATURE OF CeO_2 NPs

Controlled redox reactions are crucial in the metabolism of living organisms, since they are used to generate most of their energy for living. In physiological conditions, partial reduction of oxygen produces by-products known as Reactive Oxygen Species (ROS) that include superoxide radical (O^{2-}), peroxide (O_2^{2-}) and the hydroxyl radical ($OH^{\cdot}$) (Figure 1). ROS are present in cells, tissues and fluids, and have important roles in cell signaling, homeostasis, genomic stability and immune defense. In case of bacterial infection, the cell uses an increased ROS production as a natural defensive antimicrobial mechanism [6, 17].

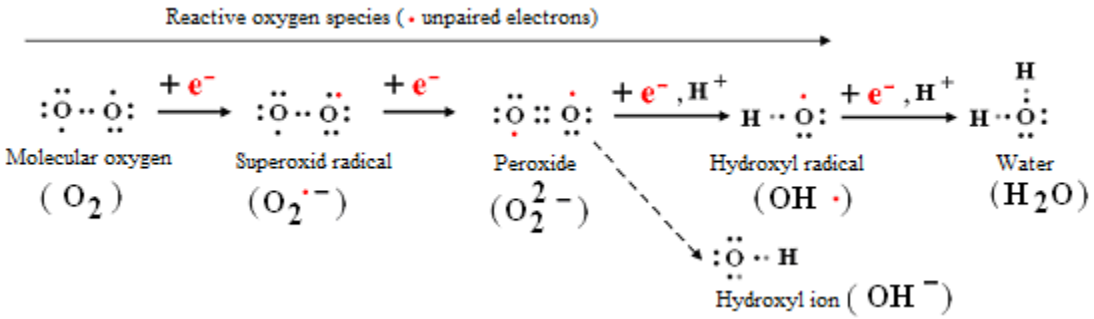

Figure 1. Generation of reactive oxygen species. *Molecular oxygen (O_2) is very reactive from thermodynamic standpoint. Its single electrons (red dots) cannot react rapidly with already paired electrons (black dots) in the covalent bond of organic molecules that are abundant in living cells. Instead, molecular oxygen can rapidly react with single unpaired electrons and as a consequence, it is harmless to these organic molecules. Scheme taken from Cristiana, F. et al. (2012).*

Normally, the intracellular redox balance, known as homeostasis, is maintained through generation and elimination of ROS by the activity of specific enzymes as superoxide dismutase (SOD), catalase and glutathione (GSH) (Figure 2 a). In contrast, during an environmental or intracellular stress, the cell may no longer maintain redox balance correctly, so the levels of ROS are dramatically increased. The heightened levels of ROS can damage significantly cellular integrity by inducing chronic inflammation, lipid peroxidation, DNA damage, damage of oxidation sensitive proteins, or even trigger cell death (apoptosis) by a metabolic flux disruption (Figure 2 b).

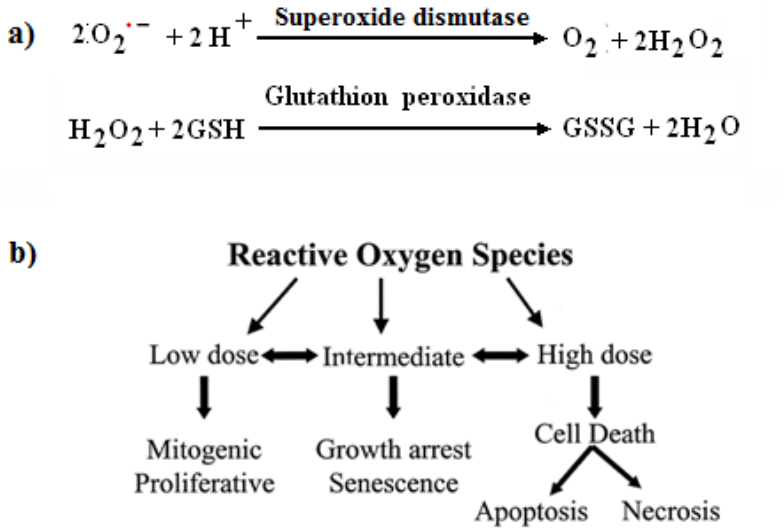

Figure 2 . Dose-dependent ROS homeostasis. *(a) Superoxide dismutase and Glutathione activity. (b) Cell response under ROS attack. Scheme taken from Cristiana, F. et al. (2012).*

What makes nanoceria very appealing is its high capacity to buffer electrons from an oxidant/reducing environment. This is due to its easy ability of being oxidized and reduced, followed by the capture or release of oxygen or reactive oxygen species (ROS, as OH·). As a result, nanoceria behaves as a natural *electron sponge* [1].

For decades, regarding the ROS scavenging capacity of CeO_2NPs, they have been widely used in those industrial processes where redox reactions are involved. For instance, in

the petrochemical industry; as a catalyst in exhaust converters; as diesel fuel additive; as a catalytic supplier of oxygen for combustion of hydrocarbons; as well as converter of toxic CO and NO_x emissions into non-toxic forms [3]; and a converter of non-biodegradable organic pollutants into biodegradable forms in wastewater treatment [4]. Besides, CeO_2NPs are used in treatments of industrial wastes such as leachate oxidation by heterogeneous Fenton-like processes [5]; as well as a fluid cracking catalyst in petroleum refineries; as glass polishing powder; as UV absorbent; as component of the mesoporous inorganic filters for water purification; and many others.

More recently, the use of CeO_2NPs to control the population of free radicals in biological systems has emerged. Note that ROS disbalance takes place in enormous number of human diseases, such as liver cirrhosis [2], cancer [7, 8], diabetes mellitus [9], cardiovascular disease (CDV) [10], age-related macular degeneration (AMD) [11], ophthalmology [12] and many others. Also, the overproduction of ROS is critical in neurodegeneration, including Alzheimer, Parkinson, Huntington, Schizophrenia, among others [13-16]. Therefore, two main function of cerium oxide NPs have raised from therapeutic point of view:

(i) to manage acute inflammation;

(ii) to revert chronic inflammation.

As displayed in Figure 2, hydrogen peroxide is a reactive metabolic product that is a key regulator in a number of oxidative-stress-related states. For this reason, it can be used as a reagent to analyze the antioxidant capacity of CeO_2NPs. In this work, a specific dye of hydrogen peroxide was employed during the correspondent assays of the nanoceria activity. The *Materials and methods section* of this Chapter summarizes the main reasons for having chosen a cell-free method of measurements and the Results show the size, concentration and surface coating of CeO_2NPs affect their reactivity in terms of hydrogen peroxide degradation.

RESULTS AND DISCUSSIONS

1. Size- and coating-dependent activity of CeO_2NPs

As previously mentioned, hydrogen peroxide (H_2O_2) is a reactive metabolic product that is a key regulator in a number of oxidative-stress-related states. For this reason, it has been used as a main component to evaluate the antioxidant capacity of CeO_2NPs in this study. Note that the selection of appropriate method for such evaluations is crucial, in order to obtain reliable data without artifacts or interferences. Therefore, the antioxidant capacity of nanoceria was evaluated under cell-free environment in aqueous solution. The advantage of performing catalytic reactions under cell-free conditions is that nothing, but the reagents of interest, are added to the samples. Consequently, neither cellular nor chemical interferents might mask or alter the measurements of surface reactivity of the nanoparticles. In the present study, H_2O_2 was fluorescently-labeled in aqueous solution by a highly specific Europium-Tetracycline dye (EuTc). For more detailed information, consult the Materials and methods section of Chapter 3. The effects of the NPs size, coating and concentration were evaluated.

At first place, four types of CeO_2NPs were compared between them: commercial CeO_2 nanopowder of 25 nm in diameter, the designed PVP-coated NPs of 5 nm in diameter, the designed and surfactant-free NPs of 5nm in diameter, and the surfactant-free NPs of a mixed size distribution (approximately from 6 to 12nm). The initial fluorescence of dye-labeled peroxide was normalized to 1 (Figure 1). The NPs were equaled to a number of NPs per sample and the reaction between the NPs and the labeled peroxide

was carried out for 20 min. According to data, the smaller the nanoparticles, more pronounced is the fluorescence decay, therefore more degradation of peroxide, is observed (Figure 1 d). Tecnically, as more available is the NPs surface (naked or surfactant-free), the better its antioxidant capacity is (Figure 1 c and d). However, surfactant-free small-sized nanoceria aggregates in a rapid and irreversible way. That makes the PVP-coated NPs more suitable for further applications. Note that commercial NPs of 25 nm are naked but hardly degrade the peroxide (Figure 1 a). This data corroborates the fact that the antioxidant activity of cerium oxide is size-dependent: as smalle the NP, higher its surface-to-volume ratio and, consequently, higher its reactivity (comparison between Figure 1 a and d).

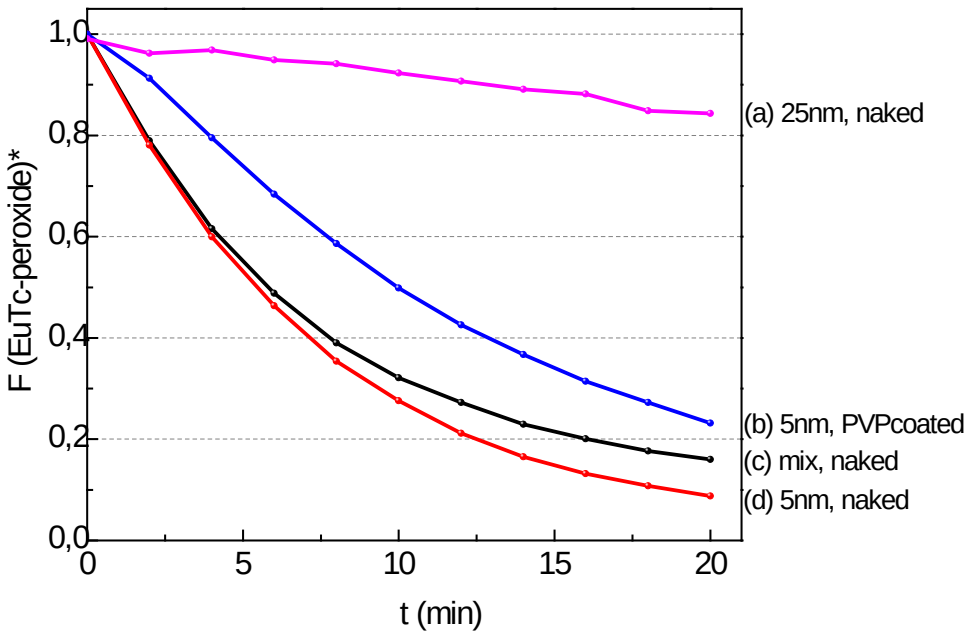

Figure 1. Size-dependent and surfactant-dependent reactivity of CeO_2NPs. *Curves of CeO_2NPs antioxidant effect on fluorescently-labeled hydrogen peroxide (EuTc-H_2O_2 complex*). (a) Commercial 25-nm-sized CeO_2NPs; (b) PVP-coated 5-nm-sized CeO_2NPs; c) surfactant-free mix of CeO_2NPs (mix of sizes from 6 to dozens of nm); (d) surfactant-free 5-nm-sized CeO_2NPs. In cell-free environment, as bigger the diameter of CeO_2NPs,*

lower their antioxidant capacity, which is displayed by an inefficient decay of fluorescence (F) versus time (t). The PVP coating slightly decreases the NPs reactivity.

In order to evaluate the reactivity of naked (surfactant-free) 5-nm-sized CeO_2NPs at longer times, as well as to check the effect of protein coating of the NPs (protein corona) on their long-term reactivity, the NPs were incubated for 25 months in cell culture medium (CCM, DMEM) supplemented with serum proteins (FBS). As a control, CCM not supplemented with serum was employed. Two years later after the incubation, the reactivity of the NPs was measured. The NPs were purified from the CCM and subjected to the previously commented EuTc-peroxide assay (Figure 2). Apparently, under serum-free conditions (Figure 2 a), the NPs have lost their reactivity with time, probably due to their dissolution and/or partial aggregation in CCM. In contrast, when the NPs surface is coated with protein corona (serum proteins), their reactivity is maintained 25 months after the incubation (Figure 2 b). This data suggests that protein corona might act as a partial surface stabilizer, that keep the NP activity.

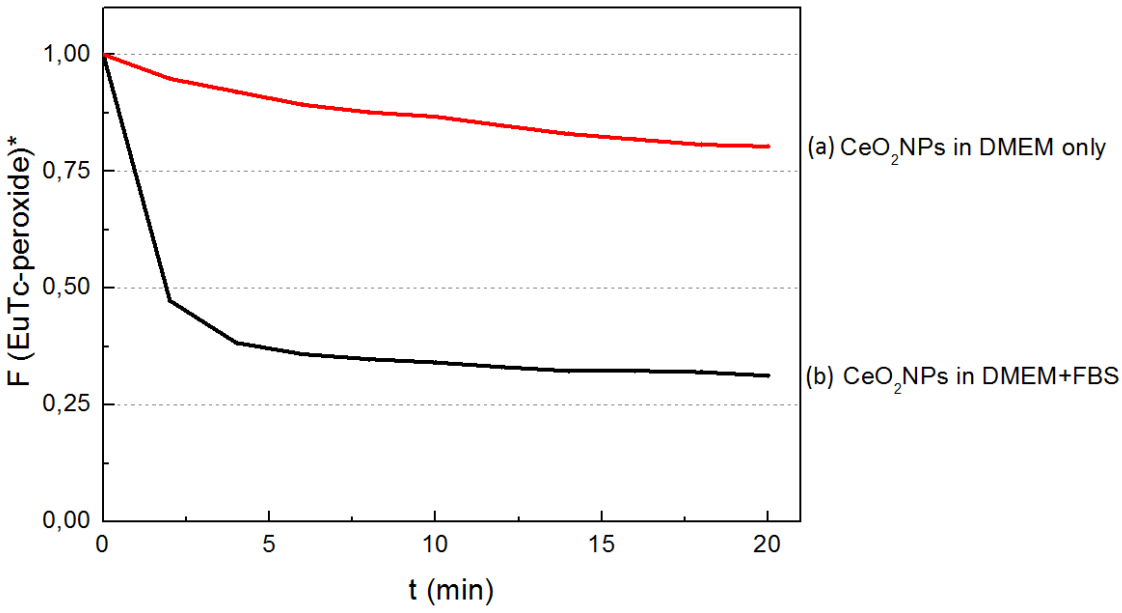

Figure 2. Time- and protein coating-dependent activity of 5nm CeO_2NPs in cell culture medium (CCM). *Curves of CeO_2NPs antioxidant effect on fluorescently-labeled peroxide*

(EuTc-H_2O_2 complex). CeO_2NPs of 5nm were incubated for 25 months (two years) in CCM (DMEM) without serum (a) and CCM supplemented with serum (DMEM+FBS). Proportion of NPs to CCM was 1:10. In serum-free conditions (a), the NPs lose their reactivity with time, probably due to their dissolution and/or partial aggregation in CCM. Thus, the degradation of the labeled peroxide complex is minimal (low fluorescence decay vs reaction time). In CCM with serum (b) the NPs surface is recovered by serum proteins, ergo protein corona is formed. In these conditions the NPs reactivity is maintained 25 months after the incubation (high fluorescence decay vs reaction time corresponds to efficient degradation of labeled peroxide by the NPs).*

Interestingly, at the nanoscale, even the very small differences in size of CeO_2NPs are reflected in their antioxidant capacity, as displayed in the following Figure 3. Similarly to previous experiments, fluorescently labeled peroxide was incubated for 20 min with highly concentrated CeO_2NPs of 5nm in size (Figure 3 c) and 7-9nm in size (Figure 3 d). The same number of NPs was employed and same antioxidant capacity was detected (similar decay of fluorescence vs reaction time), due to an excess of NPs in solution. In contrast, when diluted, the smallest NPs displayed higher reactivity (Figure 3 b) in comparison of the bigger ones (Figure 3 a). The comparison between NPs of such a small differences in size put in evidence how critical is the NP size regarding heir antioxidant activity.

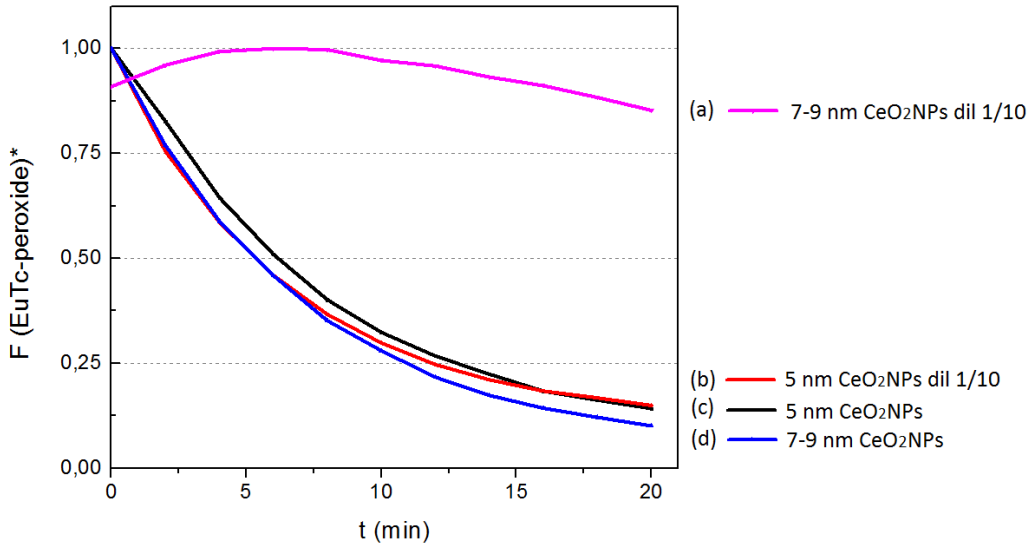

Figure 3. Comparison of the size-dependent activity between 5nm vs 7-9nm CeO_2NPs. *Curves of CeO_2NPs antioxidant effect on fluorescently-labeled peroxide (EuTc-H_2O_2 complex*). Highly concentrated NPs showed similar reactivity independently of the size, due to an excess of NPs in solution. When the amount of NPs was brought to a limit (diluted), the smallest NPs showed high capacity to degrade labeled peroxide (b), while the bigger ones showed a significant decrease in their reactivity (a).*

2. Concentration-dependent activity of CeO_2NPs and the hormetic (dose-response) effect

In catalysis, it is well known that as higher the concentration of nanoparticles, more effect is observed. To corroborate this fact, the same cell-free experiment of the antioxidant activity of CeO_2NPs at different concentrations was measured and, effectively, the degradation of fluorescently-labeled hydrogen peroxide was higher when the concentration of NPs was increased (Figure 4).

However, it is important to take into account that under *in-vivo* and *in-vitro* environment, the concentration of drugs and nanoparticles is a delicate factor that presents certain limitations. In particular, a dose-response effect, known as hormesis,

may occur [18,19]. This phenomenon comprises the fact that the dose of drugs (or nanoparticles) can be elevated to a certain limit (to the highest bio-compatible dose) and, when the maximal concentration is overtaken, the drug or therapeutic nanoparticles such as antioxidant cerium oxide, become toxic for the cells (*in-vitro*) and tissues/organs (*in-vivo*). The hormetic dose-response of CeO_2NPs in hepatic cells is currently under study at one of the collaborative research group of the Hospital Clinic of Barcelona, lead by Morales-Ruiz, M. et al.

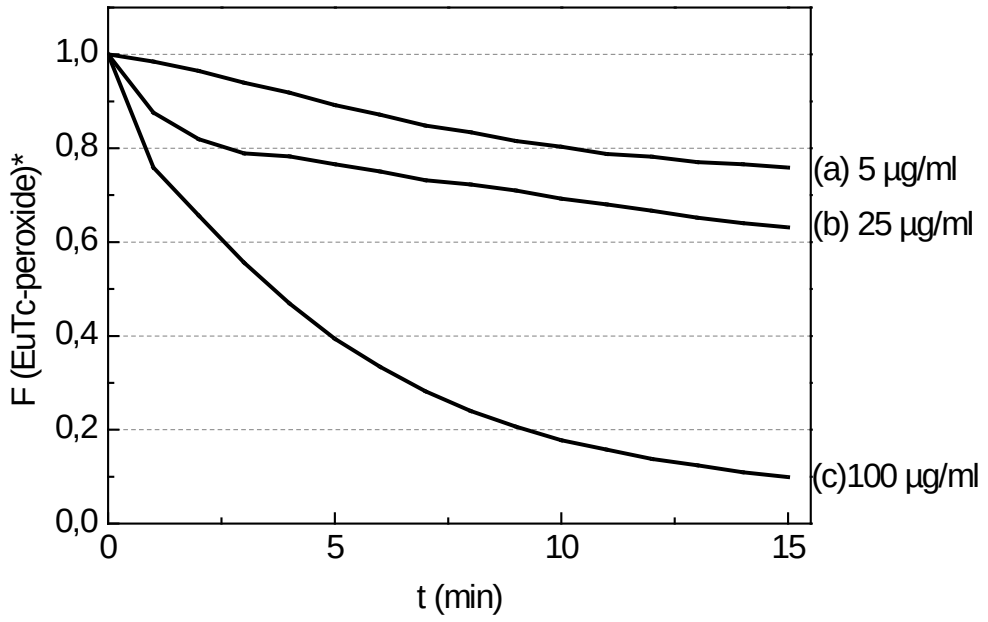

Figure 4. Concentration-dependent activity of 5nm CeO_2NPs. Curves of CeO_2NPs antioxidant effect on fluorescently-labeled peroxide (EuTc-H_2O_2 complex*). *In cell-free environment, as higher the concentration of CeO_2NPs, higher its antioxidant capacity, which is displayed by a faster decay of fluorescently labeled peroxide (F) versus time (t). Thus, NPs at 100 µg/ml concentration are more active than NPs at 25 µg/ml, and at only 5 µg/ml.*

BIBLIOGRAPHY

[1] Cafun, J.D., et al., Absence of ce(3+) sites in chemically active colloidal ceria nanoparticles. ACS Nano, 2013. 7(12): p. 10726-32.

[2] Oró, D., Yudina, T., Fernández-Varo, G., Casals, E., Reichenbach, V., Casals, G., González de la Presa, B., Sandalinas, S., Carvajal, S., Puntes, V., Jiménez, W., Cerium oxide nanoparticles reduce steatosis, portal hypertension and display antiinflammatory properties in rats with liver fibrosis, Journal of Hepatology (2015)

[3] Sajith, V., C.B. Sobhan, and G.P. Peterson, Experimental Investigations on the Effects of Cerium Oxide Nanoparticle Fuel Additives on Biodiesel. Advances in Mechanical Engineering, 2010.

[4] Garcia, A., L. Delgado, et al. (2012). "Effect of cerium dioxide, titanium dioxide, silver, and gold nanoparticles on the activity of microbial communities intended in wastewater treatment." Journal of Hazardous Materials 199: 64-72.

[5] Aneggi, E., et al., Potential of Ceria-Based Catalysts for the Oxidation of Landfill Leachate by Heterogeneous Fenton Process. International Journal of Photoenergy, 2012.

[6] Fang, F. C. (2011). "Antimicrobial Actions of Reactive Oxygen Species." Mbio 2(5).

[7] Schumacker, P.T., Reactive oxygen species in cancer cells: Live by the sword, die by the sword. Cancer Cell, 2006. 10(3): p. 175-176.

[8] Wason, M.S. and J.H. Zhao, Cerium oxide nanoparticles: potential applications for cancer and other diseases. American Journal of Translational Research, 2013. 5(2): p. 126-131.

[9] Giacco, F. and M. Brownlee, Oxidative Stress and Diabetic Complications. Circulation Research, 2010. 107(9): p. 1058-1070.

[10] Griendling, K.K. and G.A. FitzGerald, Oxidative stress and cardiovascular injury - Part I: Basic mechanisms and in vivo monitoring of ROS. Circulation, 2003. 108(16): p. 1912-1916.

[11] Winkler, B.S., et al., Oxidative damage and age-related macular degeneration. Molecular Vision, 1999. 5(24-35).

[12] Chen, J.P., et al., Rare earth nanoparticles prevent retinal degeneration induced by intracellular peroxides. Nature Nanotechnology, 2006. 1(2): p. 142-150.

[13] Ciofani, G., et al., Effects of Cerium Oxide Nanoparticles on PC12 Neuronal-Like Cells: Proliferation, Differentiation, and Dopamine Secretion. Pharmaceutical Research, 2013. 30(8): p. 2133-2145.

[14] Park, E.J., et al., Induction of Inflammatory Responses in Mice Treated with Cerium Oxide Nanoparticles by Intratracheal Instillation. Journal of Health Science, 2010. 56(4): p. 387-396.

[15] Nagy, K. and I. Dekany, Preparation of nanosize cerium oxide particles in W/O microemulsions. Colloids and Surfaces a-Physicochemical and Engineering Aspects, 2009. 345(1-3): p. 31-40.

[16] Popa-Wagner, A., et al., ROS and brain diseases: the good, the bad, and the ugly. Oxid Med Cell Longev, 2013. 2013: p. 963520.

[17] Meyer, J. J. (1994). "The Validity of Thoracolumbar Paraspinal Scanning Emg as a Diagnostic-Test - an Examination of the Current Literature." Journal of Manipulative and Physiological Therapeutics **17**(8): 539-551.

[18] Iavicoli, I., L. Fontana, et al. (2014). "Hormetic dose-responses in nanotechnology studies." Science of the Total Environment **487**: 361-374.

[19] Iavicoli, I., E. J. Calabrese, et al. (2010). "Exposure to Nanoparticles and Hormesis." Dose-Response **8**(4): 501-517.

CHAPTER 4

IN-VIVO BIODISTRIBUTION AND SURFACE CHEMISTRY OF CeO_2 NPs

INTRODUCTION

In Chapter 2, the importance of the NPs quality is analyzed from the viewpoint of the synthesis reaction, where the safety-by-design requirements are discussed (Scheme 1, Chapter 2). In Chapter 4, a broader vision is given to the fate of the NPs, from the moment of being introduced to the body to its elimination. In particular, the aspects of ADME are considered (ADME: A – administration, D – distribution, M – metabolization, E – excretion).

1. BIODISTRIBUTION OF INORGANIC NANOPARTICLES

There are several ways of the nanoparticles administration to animal models (e.g. intravenous, intraperitoneal). Whatever the route of administration is, the introduced NPs immediately undergo *pharmacokinetics* processes (Figure 1). For instance, when the NPs are injected intravenously, they are brought into the bloodstream, where they interact with serum proteins, mainly albumin. As a result, a protein corona (PC) is formed on the NP surface [1]. In contrast, when the injecion is intraperitoneal, the NPs are drained from the lymph to the lymph nodes and only after that, to the bloodstream.

Note that formation of PC directly depends on the presence of surfactant coating on the NP surface, as well as on the type of surfactant. Thus, naked (or surfactant-free) NPs tend to interact with plasma proteins in a greater degree than coated Nps. These interactions with proteins lead to certain changes of the surface chemistry of the NP, such as surface charge and hydrodynamic diameter.

After the PC formation, the NPs are spread into tissues and organs from the bloodstream. According to De Jong et al. (2008), the consequent organ distribution of

Gold (AuNPs) is size-dependent, where the smaller NPs spread into more organs than the larger ones [12]. Taking into account that the particular properties of AuNPs have converted it into a nanomaterial of reference, similar behavior regarding the size-dependent biodistribution would be expected in case of the rest of nanoparticles as well. A model of the "smart oxygen-dependent behavior" of nanoceria is hypothesized in the Results section of this Chapter and further corroborated by a complex study of the *in-vivo* biodistribution of CeO_2NPs within 32 rats.

During the biodistribution process, the metabolization of nanoparticles majorly occurs inside the liver. However it has been reported that it can start earlier, within the gastrointestinal tract in case of the ingested NPs [2]. At last, the elimination of NPs from the organism takes place via the kidney (urine) or bile (feces), as long as no bioaccumulation occurs.

At any stage of the pharmacokinetics process, the nanocomposite-induced toxicity may arise if some of the compounds of a nanocomposite is not controlled or understood from (bio) chemical point of view. Note that a term of *nanocomposite* is referred to a complex suspension, composed of colloidal nanoparticles, the solvent and the surfactant (optional). Any of these elements may result in a potential source of toxicity or pathological biodistribution and bioaccumulation of nanoparticles. The Chapter 2 is partially focused on the major problematics of these toxicity sources. However, in the current Chapter, another important perspective of the nanoparticle-induced problematics is analyzed next and is related to a dissolution and bioelimination of NPs within time.

Within different types of toxicological effects, there are hematological, organ and immune toxicity (Figure 1). Such problems may arise from the long-term retention of NPs in the organs, their interactions with enzymes, damage to organelles (in particular mitochondria) or dissolution of NPs into toxic ions. Thus, contrarily to undesirable accumulation of NPs in tissues or fluids, their insufficient adsorption and diffusion into

other tissues of interest may also occur. Both factors can compromise the therapeutic activity of the NPs, reducing their efficiency. Besides, in those cases where NPs could cross biological barriers such as the blood–brain or placental barrier (both with permeability limit around 500 Da ≈ 1.05 – 1.3 nm), neurotoxicity or reproductive toxicity has to be also studied.

The following Figure 1 summarizes the main stages of the NP fate inside the organism and lists possible toxicities associated to each of these steps.

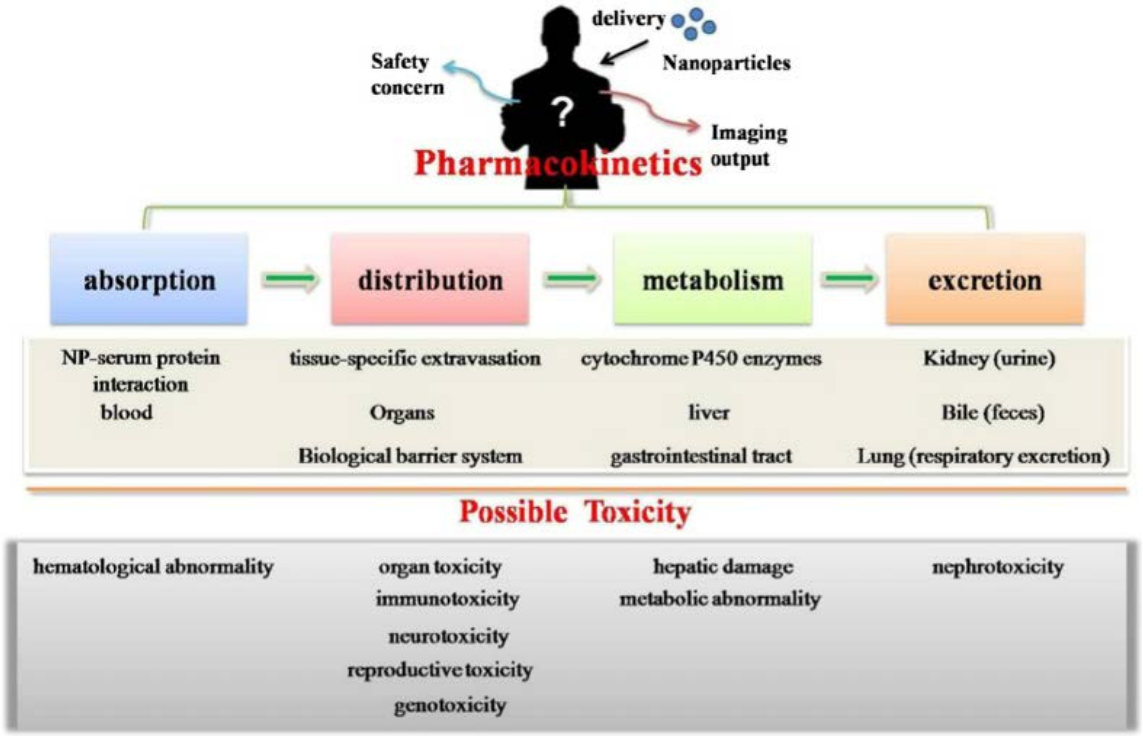

Figure 1. An illustrative scheme for the pharmacokinetics of extraneous nanoparticles in vivo and possible toxicities that may arise. *Scheme taken from Li, J. X., X. L. Chang, et al. (2014)* [2].

The following Figure 2 gives complementary information, illustrating the main routes of administration, distribution and elimination of the nanoparticles.

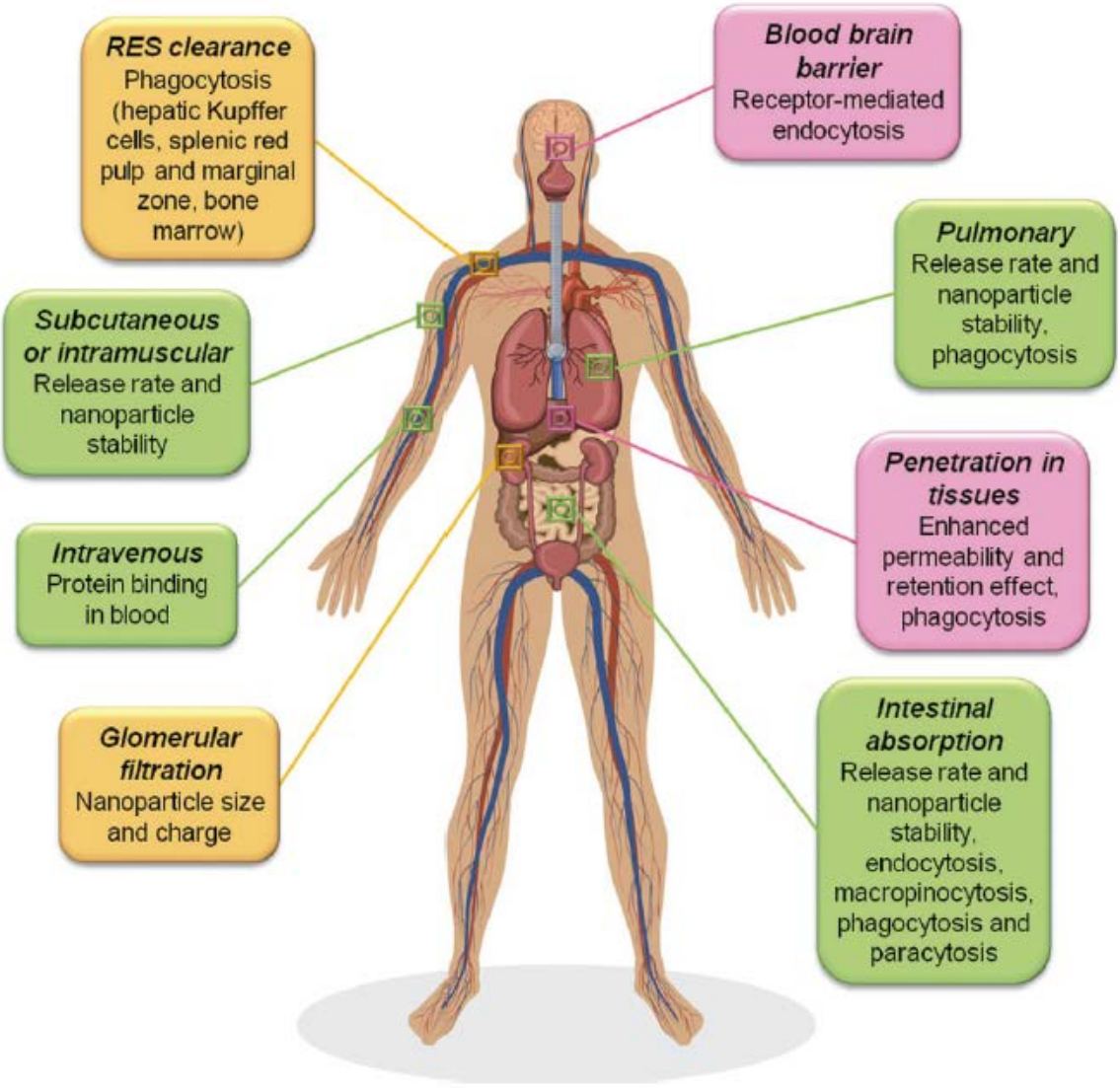

Figure 2. A selection of issues relating to the administration (green boxes), distribution (pink boxes) and elimination (orange boxes) of nanomedicines. *RES, reticuloendothelial system. Scheme taken from Moss, D. M. and M. Siccardi (2014)* [3].

2. THE IMPORTANCE OF THE NPs DISSOLUTION IN PHYSIOLOGICAL ENVIRONMENT AND TOXICITY OF THE GENERATED IONS

Optimally, any design of NPs intended for biomedical applications should be accompanied with the knowledge about the full life cycle of this material. Otherwise, a lack of understanding of these details might result in a loss of the NP quality and its therapeutic effect within the body or a cell culture.

As visualized in Figures 1 and 2, one of the main requirements of the nanodrugs is their elimination from the body after having reached the therapeutic target and have acted on it. To this day, little is known about the pharmacokinetics of nanoparticles. Thus, fundamental studies of the NP characteristics and surface chemistry would significantly clarify certain doubts, regarding the biopersistence of NPs under physiological conditions, previous to their administration.

From the viewpoint of biodistribution, the nanoparticles dissolution into constituent ions is a desirable surface property, able to facilitate the nanodrug removal from the organism. Yet, there are certain exceptions related to those nanoparticles that dissolve into ions that are highly toxic to humans and animals. For instance, cadmium selenide nanoparticles (CdSeNPs) possess interesting properties to be used in the *in-vivo* imaging and diagnostics [4-6]. Nevertheless, while Se is an essential micronutrient in low amounts, the Cd ions are highly toxic to humans by causing renal, hepatic and neurologic toxicity [4, 7, 8]. Similar problematics was reported in case of silver nanoparticles (AgNPs), whose dissolution in silver ions is considered one of the main factors of potential toxicity of AgNPs in biological systems [9, 10].

Fortunately, the dissolution of CeO_2NPs under physiological conditions is not that dramatic. In distant 1947, Burkes S. et al. reported on the bacteriostatic activity of cerium nitrate [16]. Similarly, the bactericidal effects of cerium compounds (including Ce^{3+}

ions) had been recognized near the end of the nineteenth century by Drossbach (1897). According to Garner J. P. et al (2005) cerium nitrate displays beneficial effects in burns [15], while Silva-Dias A. et al. (2015) reported on its antifungal activity *in-vitro* and prevention of biofilm formation *in-vivo* [14]. The mentioned precedents, among many others, indicate that the dissolution of CeO_2NPs into Ce^{3+} ions would not bring additional toxicity problematics under physiological conditions.

From the standpoint of chemical composition, in proximity to the NP surface the dissolved ions are in chemical equilibrium with the NPs. According to the law of Le Chatelier, those factors that can reduce the concentration of these ions from the surface of NP will shift this equilibrium towards nanoparticle dissolution. Accordingly, the colloidal stability of nanoparticles (or degree of dissolution) will always depend on the environment in which they are dispersed.

3. THE EFFECTS OF TISSUE/ORGAN OXYGENATION IN THE CHEMISTRY OF THE NANOPARTICLE SURFACE

As known, a pathological oxygenation and inflammation are two intertwined processes that involve molecular cross-talk between each other. There is a tight biochemical link between hyperoxia and liver inflammation. Hyperoxia generally induces apoptosis and cell death by creating an imbalance between the production of reactive oxygen species (ROS) and the antioxidant mechanisms (Figure 3). As a result, there is a direct injury to epithelial and endothelial cells via lipid peroxidation and up-regulation of pro-inflammatory cytokines [18, 20]. In the particular case of the liver, the oxidative damage of the tissue can be induced by Kupffer cells and neutrophils. Furthermore, an increased

oxidative stress drives to extensive hepatocellular necrosis and contributes to the development of hepatic fibrosis and cirrhosis [17].

From the therapeutic and pharmacodynamics standpoints, CeO_2NPs are a potential candidate to act as a buffer of ROS species in the inflamed tissue towards recovery of homeostasis. However, an oncoming question from the pharmacokinetics viewpoint arose in the process of this research. In particular, the effects of oxygen-dependent environment on the nanoceria integrity and its therapeutic activity were investigated. The correspondent answers are systematically analyzed in the *Results sections* of this Chapter.

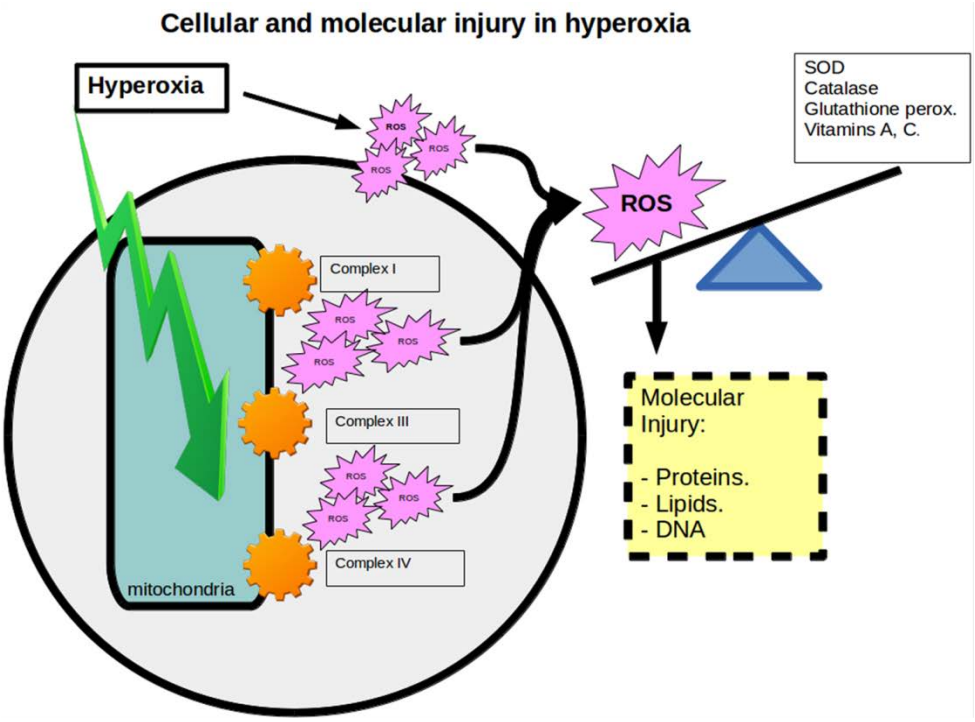

Figure 3. Cellular and molecular injury in hyperoxia. *Scheme taken from Prieto del Portillo, I. et al. (2014)* [20].

RESULTS AND DISCUSSIONS

1. The surface charge of CeO_2NPs in cell culture media (CCM)

As mentioned in the *Introductory section* of this Chapter, once the NPs are introduced to the bloodflow, a rapid interaction with serum proteins occurs and leads to formation of protein corona on the NP surface. Similar interactions may alter the surface charge, as well as the hydrodynamic diameter of the nanoparticles.

To experimentally corroborate these predictions, as-synthesized naked (surfactant-free) CeO_2NPs were incubated in a serum supplemented cell culture media (CCM). These experimental conditions served as a simplified imitation of the bloodflow and the obtained data confirmed a protein corona formation and changes in surface charge of NPs. Thus, the initial cationic charge of as synthesized NPs (Figure 5, red arrow) was rapidly reverted to anionic, after the NP dispersion in CCM (Figure 5, blue arrow). Moreover, a progressive decay of the surface charge suggests an enhancement (or hardening) of protein corona over time and a consequent increase of the NPs hydrodynamic diameter.

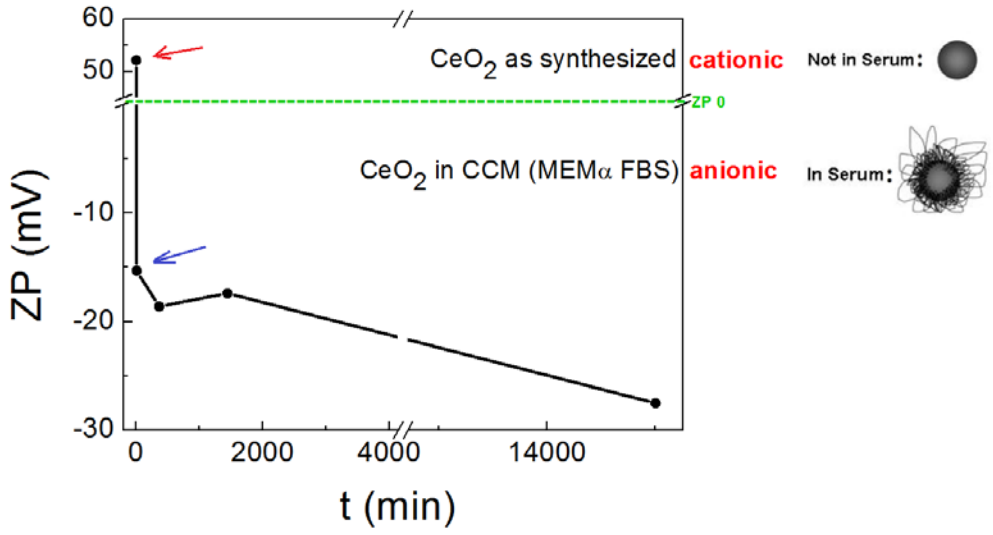

Figure 4. Zeta Potential (ZP) measurements of colloidal CeO_2NPs in solution (blue arrow) and in serum supplemented cell culture media (CCM: MEMα FBS). *As-synthesized surfactant-free nanoparticles display cationic surface charge (+52 mV). In CCM the NPs display a negative surface charge (-16 mV), red arrow. A gradual decrease of negative surface charge suggests hardening of protein corona on the NP surface. Samples of CCM incubated NPs were taken at 5min, 6h, 24h and 10 days.*

2. Oxygen-dependent behavior of CeO_2NPs surface under hypoxic, normoxic and hyperoxic conditions

As mentioned in the *Introductory section 3*, a question about the nanoceria surface behavior under oxygen-dependent environment was raised. For that aim, hyperoxic, normoxic and hypoxic conditions were imitated in solution of colloidal CeO_2NPs. Thus, as-synthesized colloidal nanoparticles were placed under a constant supply of nitrogen gas (N_2) in order to mimic the hypoxic conditions in aqueous solution. On the other hand, the opposite conditions were set by placing the NPs under continuous supply of oxygen gas (O_2) to mimic the hyperoxic conditions. A control aliquot of as-synthesized NPs was kept at room temperature without modifications as normoxic sample.

The following Figure 5 displays consequent behavior of CeO_2NPs during two weeks under the described conditions. Note that the NPs used in these experiments were not purified (the designed synthesis of nanoceria leads to an 80% yield reaction, where 20% of free cerium precursor remains in solution in Ce^{3+} state. This amount of remaining Ce^{3+} in solution was normalized to 1 and taken as initial point at time zero. This amount of free cerium serves as internal control to check whether additional oxidation occurs or not in oxygen-dependent environment).

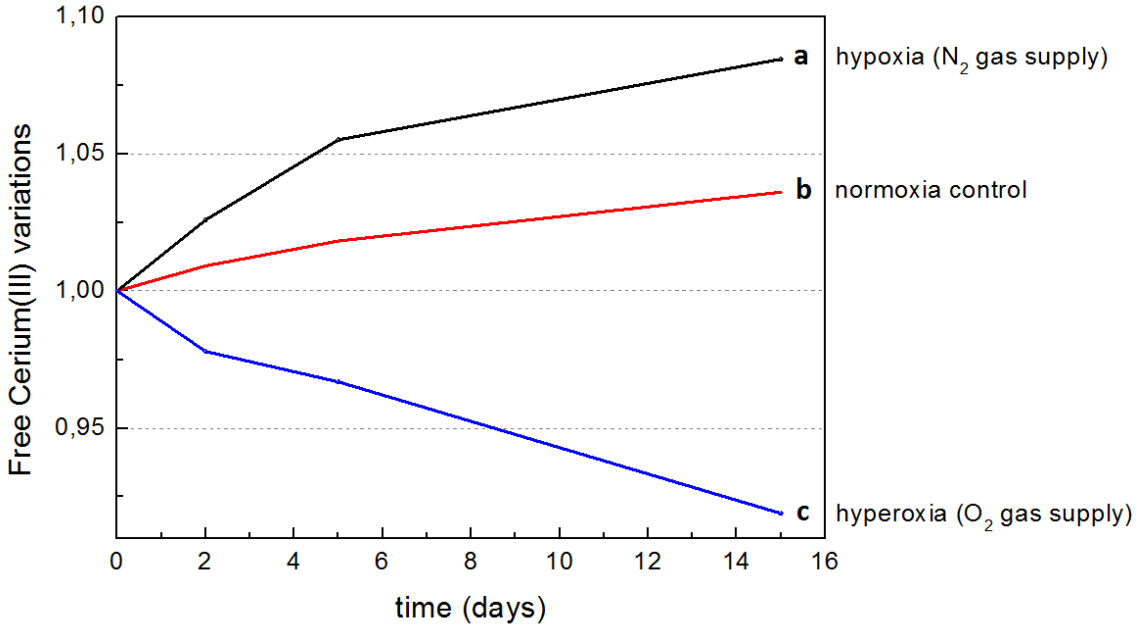

Figure 5. Time evolution of the chemical stability (dissolution) of PVP-coated 4nm CeO_2NPs under normoxic, hypoxic and hyperoxic conditions. *(a) The gradually increased black line corresponds to an increase of free cerium in solution, suggesting NPs dissolution under hypoxic conditions, provided by N_2 supply. (b) The control sample of colloidal CeO_2NPs shows tendency to dissolve within time when stored under normoxic conditions (red line). (c) A continuous supply of O_2 to a suspension of CeO_2NPs promotes a decrease of the initial levels of free Ce^{3+}. This data suggests that a highly oxidant (hyperoxic) environment keeps the NPs in their solid state (no dissolution). Moreover, a gradual decrease of free cerium levels (blue line) suggests the formation of more NPs through an oxidation of free Ce^{3+} precursor in solution under these conditions.*

Therefore, on one hand, in the inflamed tissue with heightened ROS levels (e.g. cirrhotic liver under hyperoxic conditions), the administered CeO_2NPs will tend to persist in a solid state, keeping their antioxidant activity and chemical stability, since no dissolution under hyperoxic conditions has been observed (Figure 5, c). This behavior of the nanoceria surface can be interpreted as highly desirable, since it is of high interest that a therapeutics remains in active state while the inflammation persists. The given data also displays a gradual consumption (oxidation) of the remaining levels of free cerium precursor. Another satisfactory result from a biomedical point of view is a natural tendency of nanoceria to dissolve (Figure 5, b). Considering the fact that a gradual elimination of the nanomaterial is preferable to its bioaccumulation, it can be concluded that under normoxic (physiological or healthy) conditions the nanoparticles will tend to dissolve and be excreted from the organism.

Finally, a tendency of CeO_2NPs to dissolve under hypoxic conditions (Figure 5, a) is an important observation that should be taken into account when dealing, for instance, with some types of cancer inflammation with hypoxic nature. In such conditions, the NPs would tend to dissolve more rapidly, thus a repeated administration of CeO_2NPs might be needed.

Note that this data corresponds to a chemical imitation of the oxygen-dependent environment. As known, a biological environment is a highly complex system, where many of factors are involved. Therefore, these chemical imitations make it possible to study the nature of the NPs surface without biological interferences such as proteins, ions, etc. However, once understood the behavior of nanoceria in solution, one of the future steps towards this line of research is an *in-vivo* experiment of its biodistribution, which is analyzed next.

3. Study of the in-vivo biodistribution and biopersistence of CeO_2NPs in fibrotic vs healthy rats

The following study is a fruit of collaboration with the Hospital Clinic of Barcelona that ended up into the article of Oró, D., Yudina, T. et al. (2016) [17]. Additionally to the article, this section gives a more detailed overview of the biodistribution and pharmacokinetics of CeO_2NPs. Briefly, an *in-vivo* model was carried out employing a total number of 32 rats, producing an amount of 420 samples. One half of the animals was subjected to a CCl4 treatment that induces hepatic damage, while the other half were healthy rats. All of the animals received repeated administration of biocompatible dose of CeO_2NPs (for more detailed information see the Methods section). Animals were sacrificed at 90min; 3, 6 and 8 weeks after the last administration of the NPs. The organs were dissected, acid digested and analyzed by ICP-MS spectroscopy to quantify the amount of cerium in organs (liver, spleen, lung, kidney, heart, brain). The following Figure 7 displays the percentage of cerium in the correspondent samples.

As displayed in Figure 6, the highest percentage of the administered CeO_2NPs was located in the liver (up to 90%) and spleen (up to 20%) in both groups of animals. The main difference between healthy and fibrotic rats was the next: an amount of cerium located in the heart and lung of healthy animals, sacrificed at larger times (Figure 6, greed circle). Second difference between the two groups was that the levels of cerium in healthy liver were slightly decreased with time.

The explanation of such differences is relied on the oxygen-dependent environment of both groups. In fibrotic rats, a highly oxidant environment with overproduction of ROS keeps the NPs surface in its solid (*ergo* active) state. In contrast, in healthy rats, the NPs tend to dissolve with time and, as a result, traces of free cerium are detected in heart and brain, while the same time the levels of hepatic cerium are slightly decreased. This

data is in agreement with the results in section 2 (Oxygen-dependent behavior of CeO_2NPs surface). Apparently, CeO_2NPs display an “smart behavior” which is attractive from therapeutic viewpoint, by keeping itself active in inflamed tissue with excessive ROS, and dissolving into ions within a healthy organism.

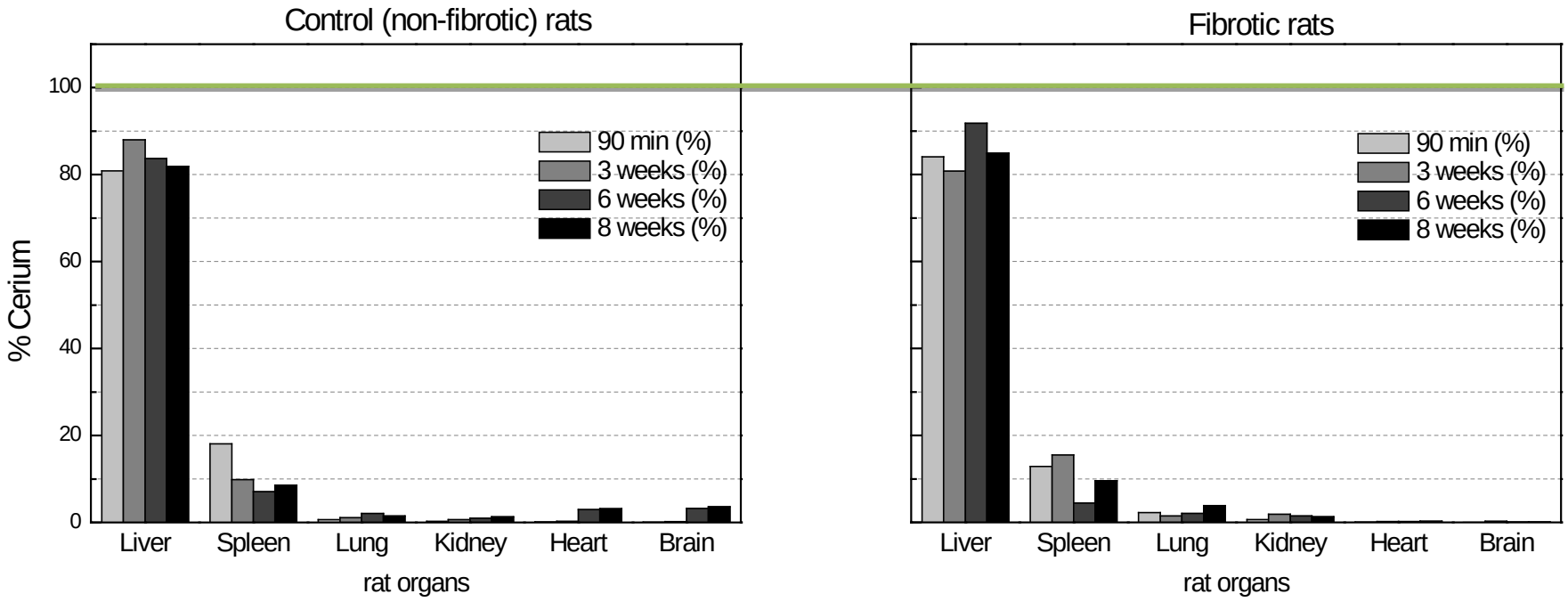

Figure 6. ICP-MS quantification of cerium biodistribution in healthy (non-fibrotic) and fibrotic rats. *Both groups of animals (non-fibrotic and fibrotic) were subjected to a treatment with CeO_2NPs. Here, a total amount of the administered CeO_2NPs is normalized to a 100% (green dot line). In case of healthy rats, the amount of cerium was increased in brain and heart at 6 and 8 weeks (green circle). The levels of cerium in healthy liver were slightly decreased within time, suggesting NPs elimination from the liver.*

4. Visualization of CeO_2NPs in rat liver tissue by Electron Microscopy

In addition to the previously described quantitative determination of cerium amount within the liver, a qualitative data was obtained using Electron Mictroscopy technique. Liver tissue slice was fixed on a TEM grid and analyzed by SEM-HAADF and EDX modes, as displayed in the following Figure 7.

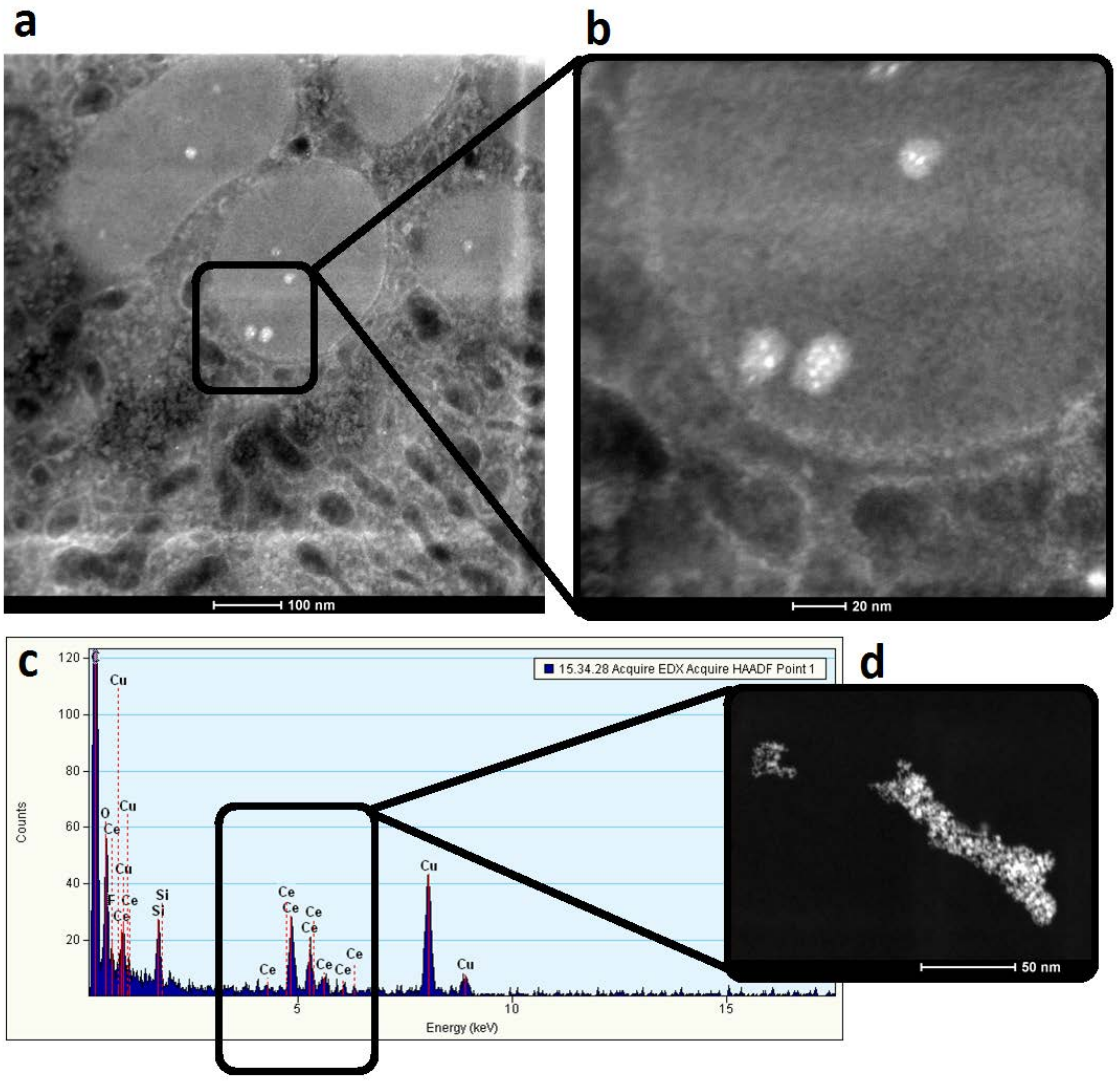

Figure 7. Electron microscopy imaging of the tissular localization of CeO_2NPs in liver tissue slices. *(a) STEM-HAADF micrograph of the liver tissue slice. The bright dots*

contrast elements with high density, suggesting a presence of CeO_2NPs uptaken by lysosomes. (b) Zoom-in image of the micrograph in (a): an enhanced magnification allows a better visualization of the accumulations with bright contrast. (c) EDX profile of the bright accumulations showed in (a, b and d) corroborates their chemical composition that corresponds to CeO_2NPs.

As known, the used doses of the administered NPs are biocompatible (*ergo* low). This fact complicated the NPs visualization and localization throughout the tissue. Therefore, one of the potential steps towards this line of investigation is specific labeling of nanoceria in order to facilitate the task of its visualization and (sub) cellular localization. One of the requirements of an optimal labeling is its biocompatibility. Thus, neither alterations nor toxicological side effects would be expected. During this Thesis research, one of the alternatives of nanoceria labeling has been explored. In particular, hybrids of magnetite and CeO_2NPs have been synthesized forming core-shell structures with magnetic properties. The understanding of the chemistry of the magnetite-nanoceria hybrids formation and the optimization of the reaction kinetics, are currently in a process of study as an additional line of future research.

5.Homogeneity of CeO_2NPs biodistribution throughout the rat liver

One of the most important requirements of any therapeutics is its successful arrival to the target (e.g. organ of interest). However, in living tissue the inflammation may be heterogeneously distributed, predominating in one of its regions.

In order to determine how homogeneous is the distribution of cerium (whether in form of NP or cerium (III) ions) within the rat liver, the following experiment of the *in-vivo* biodistribution was performed. After the NPs administration to a rat (see experimental details in the Methods section), the rat liver was divided in eight sections (Figure 8,

right image). The section 8 was arbitrarily named as the “central section”, since it corresponds to the central fork of blood irrigation, where the branches of portal, arterial and biliary drainage are branched away. All of the lobes (middle, left lateral and right lateral) were divided in two sections each. The aim of dividing the lobes in two parts is that one of the sections is the farthest from the center of irrigation, while the other is the clothest to it. Here, the correspondent “farthest” sections are: 1, 4 and 5. The correspondent “closest” sections are: 2, 3 and 6, respectively. The caudate lobe (section 7), as well as the central section 8, were analyzed entirely, due to a small size of both. The following Figure 6 illustrates the correspondent sections of the rat liver (right image) and the correspondent amount of cerium (left image). The data suggests a relatively homogeneous distribution of cerium (whether in form of NP or cerium (III) ions) along the organ, since an amount of detected cerium is similar between the “farthest” and the “closest” areas of the organ.

Note that the anatomy of the human liver differs from the rat liver; however these findings are useful to predict a correct biodistribution of cerium to the most distant sections of the liver. So that, from a therapeutical perspective, if the inflammation is located within the distant parts of any of the liver lobes, the NPs of cerium oxide could reach them through the blood supply in a correct way.

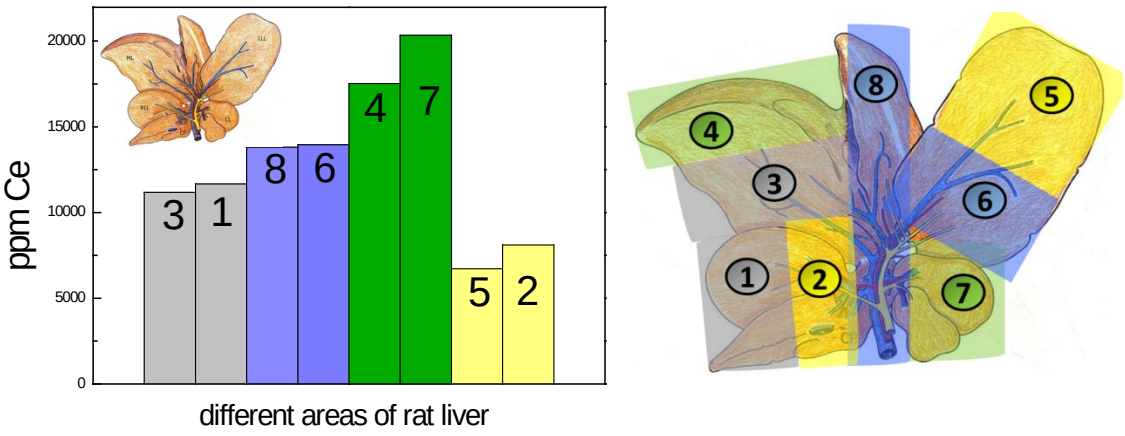

Figure 8. Biodistribution of cerium along the rat liver. *The rat liver was extracted and divided in eight sections (right image) after the administration of CeO_2NPs and their in-vivo biodistribution within the organism. All of the eight sections were similar in mass. The samples were acid digested and analyzed by ICP-MS spectroscopy. The section 8 was arbitrarily named as the "central section", since it corresponds to the central fork of blood irrigation, where the branches of portal, arterial and biliary drainage are branched away. The aim of dividing the lobes in two parts is that one of the sections is the farthest from the center of irrigation, while the other is the clothest to it. Here, the correspondent "farthest" sections are: 1, 4 and 5. The correspondent "closest" sections are: 2, 3 and 6, respectively. The caudate lobe (section 7), as well as the central section 8, were analyzed entirely, due to a small size of both. No significant differences in amount of cerium are detected by ICP-MS between the farthest and the closest sections from the irrigating center. This data suggests a relatively homogeneous biodistribution of cerium within rat liver. The liver was kindly provided by collaborators from the Hospital Clinic of Barcelona (Oró, D.) after the in-vivo administration of the NPs and the organ dissection.*

BIBLIOGRAPHY

[1] Casals, E., T. Pfaller, et al. (2010). "Time Evolution of the Nanoparticle Protein Corona." Acs Nano **4**(7): 3623-3632.

[2] Li, J. X., X. L. Chang, et al. (2014). "Toxicity of inorganic nanomaterials in biomedical imaging." Biotechnology Advances **32**(4): 727-743.

[3] Moss, D. M. and M. Siccardi (2014). "Optimizing nanomedicine pharmacokinetics using physiologically based pharmacokinetics modelling." British Journal of Pharmacology 171(17): 3963-3979.

[4] Arslan, Z., M. Ates, et al. (2011). "Probing metabolic stability of CdSe nanoparticles: Alkaline extraction of free cadmium from liver and kidney samples of rats exposed to CdSe nanoparticles." Journal of Hazardous Materials **192**(1): 192-199.

[5] Chan, W. C. W., D. J. Maxwell, et al. (2002). "Luminescent quantum dots for multiplexed biological detection and imaging." Current Opinion in Biotechnology **13**(1): 40-46.

[6] Morgan, N. Y., S. English, et al. (2005). "Real time in vivo non-invasive optical imaging using near-infrared fluorescent quantum dots." Academic Radiology **12**(3): 313-323.

[7] Klaassen, C. D. and J. Liu (1997). "Role of metallothionein in cadmium-induced hepatotoxicity and nephrotoxicity." Drug Metabolism Reviews **29**(1-2): 79-102.

[8] Vinceti, M., F. Bonvicini, et al. (2010). "Possible involvement of overexposure to environmental selenium in the etiology of amyotrophic lateral sclerosis: a short review." Annali Dell Istituto Superiore Di Sanita **46**(3): 279-283.

[9] Navarro, E., F. Piccapietra, et al. (2008). "Toxicity of Silver Nanoparticles to Chlamydomonas reinhardtii." Environmental Science & Technology **42**(23): 8959-8964.

[10] Vrc, V. I., Zuntar, I., et al. (2014). “mparison of In Vitro Toxicity of Silver Ions and Silver Nanoparticles on Human Hepatoma Cells.” Environmental Toxicology DOI 10.1002/tox

[11] Lasagna-Reeves, C., D. Gonzalez-Romero, et al. (2010). "Bioaccumulation and toxicity of gold nanoparticles after repeated administration in mice." Biochemical and Biophysical Research Communications **393**(4): 649-655.

[12] De Jong, W. H., W. I. Hagens, et al. (2008). "Particle size-dependent organ distribution of gold nanoparticles after intravenous administration." Biomaterials **29**(12): 1912-1919.

[13] Massernini, M. (2013). “Nanoparticles for Brain Drug Delivery.” ISRN Biochemistry.

[14] Silva-Dias, A., I. M. Miranda, et al. (2015). "In vitro antifungal activity and in vivo antibiofilm activity of cerium nitrate against Candida species." Journal of Antimicrobial Chemotherapy **70**(4): 1083-1093.

[15] Garner, J. P. and P. S. J. Heppe (2005). "Cerium nitrate in the management of burns." Burns **31**(5): 539-547.

[16] Burkes, S. and C. S. Mccleskey (1947). "The Bacteriostatic Activity of Cerium, Lanthanum, and Thallium." Journal of Bacteriology **54**(4): 417-424.

[17] Oro, D., T. Yudina, et al. (2016). "Cerium oxide nanoparticles reduce steatosis, portal hypertension and display anti-inflammatory properties in rats with liver fibrosis." Journal of Hepatology **64**(3): 691-698.

[18] Lee, S. H., S. I. Do, et al. (2014). "Hyperoxia accelerates progression of hepatic fibrosis by up-regulation of transforming growth factor-beta expression." World Journal of Gastroenterology **20**(11): 3011-3017.

[19] Moller, S., J. S. Iversen, et al. (2010). "Reduced baroreflex sensitivity and pulmonary dysfunction in alcoholic cirrhosis: effect of hyperoxia." American Journal of Physiology-Gastrointestinal and Liver Physiology **299**(3): G784-G790.

[20] Prieto del Portillo, I. et al. (2014). "Oxygen Therapy in Critical Care: A Double Edged Sword".

ANNEX 1

MATERIALS AND METHODS

MATERIALS AND METHODS CHAPTER 2

1. Characterization techniques

The understanding of the properties and peculiarities of nanomaterial becomes impossible without systematic characterizations of the samples by suitable equipment. Here, different techniques were used to characterize the nanoparticles and to monitor the studied processes and phenomena. Brief description of these measurements procedures are described next.

1.1 UV-Vis (Ultraviolet — Visible) spectroscopy

Among the techniques of nanoparticles characterization, one of the most commonly used in many fields of science and industry is UV-Vis spectroscopy. It is fast, easy to operate, sensitive, selective to NPs, with short time of measurement and do not require calibration. It gives information about the presence of (optically active) nanoparticles in solution, their aggregation state and a presence of (optically active) contaminants. Nanoparticles have optical properties that are very sensitive on size, shape, agglomeration and concentration changes. In particular, Cerium oxide possesses specific optical properties: it is quite transparent to visible light (no signal between 400-800 nm), but has excellent UV radiation absorption ability (showing a characteristic absorption peak of Ce^{4+} at 298 nm). Briefly, the light beam is sent from a Tungsten and D2 lamp, passed through the filter, monocromator, mirror and beam splitter, before arriving to the sample corvette and the blanc cuvette. The intensity of light that crosses the sample of colloidal dispersed CeO_2NPs is in the range between 260 to 800 nm. Once crossed the sample, the light is converted into current by photodiodes and the data is

represented as the absorbance of analyze in function of the wavelength of incident light.

Sample preparation and data processing: Aliquots of 1 – 1.5 ml of the samples were placed in optical polystyrene corvettes (Deltalab, Ref 303103) and UV-vis spectra acquired by Schimadzu UV-2400 spectrophotometer. Due to the detection limits of the equipment, water-based dilutions of NPs were needed in case of highly concentrated samples.

1.2 Zeta Potential (ZP) and Dynamic Light Scattering (DLS)

In order to understand the behavior of nanoparticles in one solvent or another, it is crucial to know which surface charge the nanoparticle displays in each case, since this parameter will determine the interaction between the NP and ions, proteins, molecules, etcetera. Therefore, Zeta Potential is a useful measurement of the surface activity of colloidal particles. Briefly, a double layer exists around each particle. If a particle is cationic, a thin anionic layer of contraions is formed around the particle, known as the Stern layer. Beyond the Stern layer, there is a wider layer of mostly opposite charge, known as Diffuse layer. The Slipping plane is a distance from particle surface where ions move with the particle. Thus, it is difference between the dispersing medium and the surface of hydrodynamic shear (Slipping plane). Zeta Potential depends on the pH, conductivity, temperature and a solvent. Besides, the absence of bubbles in sample is mandatory in order to avoid aberration data. The Isoelectric Point of the nanoparticles (PI that corresponds to a zero charge of the surface) is another important data to be measured in order to understand the aggregability and/or stability of the particles at different pH. This issue was detaily analyzed in case of CeO_2NPs and is developed in Chapter of *Stability and evolution*.

Another of the most commonly used technologies in sizing nanoparticles is Dynamic light scattering (DLS). The small molecules in solution, as well as the nanoparticles in

colloidal suspension, undergo the Brownian motion. Therefore the distance between the scatterers (molecules or nanoparticles) in the solution is constantly changing with time. When incident light hits small particles, it is scattered in all directions (Rayleigh scattering), as long as the particles are small compared to the wavelength (below 250 nm). The basis of this method is to use time variation of scattered light from motion to obtain their hydrodynamic size, size distribution and the polydispersity index (PdI) using Stokes-Einstein relationship.

Sample preparation and data processing: Aliquots of 1-1.5 ml of the colloidal suspension of NPs (synthesis solution) were placed in a sizing cuvette (Malvern Instruments) for ZP determination, or placed in optical polystyrene cuvette (Deltalab Ref 303103) for DLS determination. Both measurements were analyzed by Zetasizer Nano-ZS (Malvern Instruments). The measurements of each sample were displayed in triplicates by the equipment and represented in graphs using Origin software.

1.3 Electron Microscopy (HR-TEM, HAADF, EELS, EDX)

The engineered nanoparticles were numerously analyzed at the Electron Microscopy Division by the High-Resolution Transmission Electron Microscopy, Tecnai F20 HR(S)TEM 200 kV. (Please consult the Nomenclature appendix for the abbreviations, mentioned in this section). The Electron Microscopy offers a high variety of characterization techniques, essential for a better understanding of the material of interest, in particular of nanometer sized Cerium oxide. The ones that were used in this work are: (1) obtaining of sample images at high and low resolution by HR-TEM; (2) analysis of sample composition by EDX, EELS and HAADF-STEM modes and (3) structural determination of the samples by EELS. Briefly, the electrons are produced inside the Electron gun, accelerated towards an anode that accelerates the electron beam to a high potential and directs it to the sample grid, through the column. Working in vacuum minimizes contamination of samples with hydrocarbons and water, while

the electromagnetic lenses (condenser and objective) manipulate the trajectory of the beam to the sample. The incident beam interacts differently with the sample, giving the next information: the elastically scattered electrons by the sample correspond to HR-TEM and HAADF-STEM data; the inelastically scattered electrons to EELS and the emitted X-rays to EDX data.

Sample preparation and data processing: The ultrafine 200-mesh copped TEM grids (Ted-Pella, Inc.) were placed on a filter paper. Afterwards, 250µl of the colloidal suspension of NPs were deposited drop by drop over the grid and left to dry on air. The obtained images were analyzed by Image J, a Java-based image processing program. For each sample, the size of at least 150 nanoparticles was measured in order to determine the average size and the size-distribution.

1.4 X-ray diffraction (XRD)

X-ray powder diffraction is a non-destructive technique widely used for the characterization of crystalline materials. It determines the atomic order inside the crystal, nanoparticle size, crystalline purity and/or defects. Briefly, X-rays are generated in a cathode ray tube by heating a filament to produce electrons, accelerate them toward a target by applying a voltage and bombarding the sample with electrons. When electrons have enough energy to dislodge the inner shell electrons of the sample, characteristic X-ray spectra are produced, reflected towards a detector and recorded. The signal is converted to a count rate and output to a computer. Typically, the achieved pattern is compared with universal database standard patterns.

Sample preparation and data processing: A 10 ml aliquot of the synthesis solution was centrifuged twice (45 min at 15.000 rpm), in order to ensure a maximal precipitation of the nanoparticles. A supernatant was discarded and the precipitates were dried at room temperature for 2 days, to avoid further NP transformations. The data was collected on a PANalytical X-Pert PRO MPD diffractometer using a Cu Kα 1 radiation

source (λ = 1.541 Å). The 2Θ diffraction (Bragg) angles were measured by scanning the goniometer from 20º to 100º. The peak positions and their width at half maximum (FWHM) were determined by the X-Pert High Score program after the baseline correction. The particle size was determined by Scherer equation (1918) that relates the crystalline size to the broadening of peak in the diffraction pattern: $\tau = K \cdot \lambda / \beta \cdot \cos\theta$ (where τ is an average crystallite size; K is a Scherer constant, usually assumed as K= 0.9; λ is the wavelength of the radiation; β is the integral breadth of a reflection (in radians 2θ) located at 2θ; and θ is the Bragg angle).

1.5 ICP-MS (inductively coupled plasma mass spectroscopy)

The ICP-MS techniques has been an important tool to determine several parameters of interest during the performed synthesis and applications of CeO_2NPs, such as the reaction yield (the oxidation rate of cerium (III) precursor), the *in-vivo* biodistribution of CeO_2NPs in cirrhotic and healthy rats, as well as the pH-dependent degradation of nanoceria along time. Briefly, the liquid sample is transformed into an aerosol, which is then transported into plasma of very high temperature. Plasma ionizes the aliquot to positively charged ions that represent the elemental composition of the sample. Most ICP-MS detection systems use electron multipliers, which convert ion currents into electrical signals. The magnitude of the electrical signal is proportional to the number of analyte ions present in the sample.

Sample preparation and data processing: Aliquots of 1 ml of the synthesis solution were centrifuged to assure complete removal of nanoparticles from the supernatant (45 min at 15.000 rpm, by Allegra™ 64R Centrifuge, Beckman Coulter Inc). Ones centrifuged, the supernatant was carefully transferred to another eppendorf and centrifugation was repeated. The resultant supernatant was transferred to a clean eppendorf and analyzed by ICP-MS technique. The Induced Coupled Plasma-Mass Spectroscopy (ICP-MS, LEITAT Technological Center) was performed using an ICP-MS

Agilent instrument (Model: 7500cx) with a detection limit of 0.02386 ppb. Typically, NP samples were diluted to an optimal concentration for ICP-MS analysis. Ga was used as the internal standard and the integration time/point and time/mass were 0.1 sec and 0.3 sec, respectively with a 3x repetition. The results were displayed in µg/L (µg of Cerium per liter of sample). The performed dilutions were taken into account in order to get the real concentration of Cerium in ppm (parts per million).

2. Designed protocols of CeO_2NPs synthesis

2.1 Guideline about the LPS-free synthesis of CeO_2NPs

To obtain LPS-free CeO_2NPs, the synthesis was performed in fume hoods, replacing distilled water with pure milliQ water (18.2 MΩ conductivity and < 5 ppb TOC). Before the synthesis started, all the glass material and stirring bars were heat pretreated in an oven at 260ºC for 1h; naturally cooled down to room temperature and rinsed with milliQ water to remove calcined traces. The consistent use of gloves and sterile pipette tips is mandatory.

2.2 Synthesis of naked (surfactant-free) CeO_2 NPs

To prepare CeO_2NPs at 0.1 mg/ml with an average deameter around 5 nm (4.2 ±0.97 nm), an amount of 100ml of milliQ water was placed under vigorous stirring (500 rpm) in a glass bottle at room temperature. Then, 0.434 g of cerium (III) nitrate hexahydrate ($Ce(NO_3)_3 \cdot 6H_2O$, 99%, Sigma) were added, to give a 10 mM concentration of initial cerium (III) precursor. The solution was vigorously mixed during 15 minutes. Afterwards, 0.3 ml of an as-received TMAOH (Sigma, 1M) were gently added dropwise during half of a minute, approximately, to give an initial [OH-] concentration of 1 mM.

The solution suffered several changes in color from pale yellow to whitish, during the first two hours of reaction. 48h later, the CeO_2NPs were ready at 0.1 mg/ml concentration and stored at 4ºC until use.

To prepare CeO_2NPs at 1 mg/ml with an average deameter around 7 nm (7.13 ±2.7 nm), an amount of 100ml of milliQ water was placed under vigorous stirring (500 rpm) in a glass bottle at room temperature. Then, 0.434 g of cerium (III) nitrate hexahydrate ($Ce(NO_3)_3 \cdot 6H_2O$, 99%, Sigma) were added, to give a 10 mM concentration of initial cerium (III) precursor. The solution was vigorously mixed during 15 minutes. Afterwards, 2.2 ml of an as-received TMAOH (Sigma, 1M) were gently added dropwise during half of a minute, approximately, to give an initial [OH-] concentration of 10 mM. The solution suffered several changes in color from pale yellow to whitish, during the first two hours of reaction. 48h later, the CeO_2NPs were ready at 1 mg/ml concentration and stored at 4ºC until use.

2.3 Synthesis of PVP-coated CeO_2 NPs

An amount of 100ml of milliQ water was placed under vigorous stirring (500 rpm) in a glass bottle at room temperature. Then, 2.5g of Polyvinylpyrrolidone (PVP of 10kDa, Sigma Aldrich) was added, to give a 2.5mM concentration of PVP. The solution was left at room temperature under vigorous stirring (500 rpm) for 10min, until all the solid was homogeneously dissolved. Afterwards, 0.434 g of cerium (III) nitrate hexahydrate ($Ce(NO_3)_3 \cdot 6H_2O$, 99%, Sigma) were added, to give a 10 mM concentration of initial cerium (III) precursor. The solution was vigorously mixed during 15 minutes. Then, 2.2 ml of an as-received TMAOH (Sigma, 1M) was gently added dropwise during half of a minute, approximately, to give an initial [OH-] concentration of 10 mM. The solution suffered several changes in color, from pale yellow to whitish, during the first two

hours of reaction. 24h later, the PVP coated nanoparticles were ready at 1 mg/ml concentration to be used or stored at 4ºC for months.

2.4 Synthesis of BSA-coated CeO_2 NPs

Glass vial 1: an amount of 0.625 g of BSA (Sigma) was placed in a sterile glass vial and dissolved in 10 ml of PBS (Dulbecco´s phosphate buffered saline 10x, Sigma) without stirring, to give an homogeneous solution of BSA at 0.94 mM concentration.

Glass vial 2: in parallel, in another glass vial, 0.147 g of Cerium (III) Nitrate Hexahydrate ($Ce(NO_3)_3 \cdot 6H_2O$, 99%, Sigma) were dissolved in 40ml of milliQ water under vigorous stirring (500 rpm), to give a solution at 10 mM concentration of cerium (III) precursor. Following, a volume of 880 µl of an as-received TMAOH (Sigma, 1M) was gently added dropwise, during half of a minute approximately. The reaction was left under vigorous stirring during five minutes.

Afterwards, the solution from the vial 2 was gently added to the vial 1 (it is important to keep this order) under gentle stirring during. One hour later the BSA-coated nanoparticles were ready to be used or stored at 4ºC for a couple of hours.

MATERIALS AND METHODS CHAPTER 3

1. Europium Tetracycline — Hydrogen peroxide (EuTc — H_2O_2) fluorimetric assay

In order to quantify the antioxidant (catalase-like) activity of nanoceria, as well as the effect of the NP size and coating on its surface reactivity, a cell-free system was chosen. The advantage of cell-free reactions is that nothing, but the reagents of interest

constitute the sample. Therefore, neither cellular nor chemical interferents might mask or alter the measurements of surface reactivity of nanoceria.

Hydrogen peroxide (H_2O_2) is a reactive metabolic product that is a key regulator in a number of oxidative-stress-related states. For this reason, it has been used as a reagent to analyze the antioxidant capacity of CeO_2NPs. Thus, H_2O_2 (Sigma-Aldrich) was fluorescently-labeled in aqueous solution by a highly specific Europium-Tetracycline dye (EuTc, Sigma-Aldrich). The advantage of EuTc is its fast combination with free H_2O_2, forming a highly fluorescent H_2O_2-EuTc complex in aqueous solution and at pH 7. Another advantage of EuTc assay is its applicability for turbid samples. In particular, it is useful for samples of colloidal suspension of nanoparticles.

A protocol of measurements, indicated by commercial supplier of EuTc (http://www.sigmaaldrich.com/catalog/product/sigma/02816?lang=es&region=ES) was slightly modified in order to work with colloidal nanoparticles and in cuvette. The fluorimetric reactions of NPs activity were performed at room temperature. Briefly, the H_2O_2-EuTc complex was formed by 10 minutes incubation of H_2O_2 and EuTc. Then, CeO_2NPs were added and fluorescence kinetics measured at 406nm (absorption) and 617nm (emission), during 20 min. The following data sums up some examples of the correspondent concentrations and a calibration curve preparation.

2. Example of the calibration curve preparation

Solution A (EuTc working solution): the entire amount of the supplied EuTc (Sigma-Aldrich) reagent was dissolved in 10 ml of distilled water. The stability of EuTc working solution is of one month if kept at 4ºC in the dark.

H_2O_2 stock solution at 1 M: 500 µl of 30% H_2O_2 (9.8 M ≈ 10 M) were diluted in 50 ml distilled water and vigorously mixed. Note that H_2O_2 stock and standard solutions are stable for one month and EuTc working solution for 6 months, kept at 4ºC in the dark.

Solution B (H_2O_2 stock solution at 10 mM): 250 µl of H_2O_2 Stock solution at 1 M were diluted in 50 ml of distilled water and vigorously mixed.

Calibration graph for H_2O_2: to perform the calibration graph for H_2O_2 concentration, 5 dilutions of Solution B were prepared in 50 ml of distilled water each, at room temperature, see table below:

	1	**2**	**3**	**4**	**5**
H_2O_2 (µM)	500	1000	1500	2000	4000
Solution B (ml)	2.5	5	7.5	10	20
H_2O (ml)	47.5	45	42.5	40	30
Total volume	50 ml	50 ml	50 ml	50 ml	50 ml

Table 1. *Example of the calibration curve preparation.*

For duplicate measurements: 100 µl of the diluted solution, 100 µl of Solution A and 800 µl of distilled water were added into a cuvette, mixed by pipetting and immediately put into a fluorimeter (Spectra-Max M2^e). The kinetic determination of EuTc- H_2O_2 complex formation was performed by measuring the fluorescence for 10 min. The same was repeated for all the diluted solutions 1 – 5 of the table. The obtained calibration graph is represented next, labeling with a green arrow the optimal concentration of H_2O_2 for EuTc saturation.

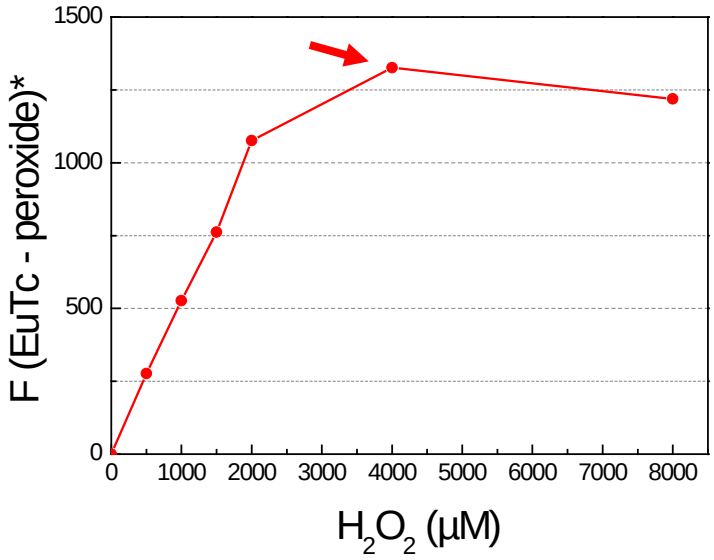

Figure 1. Example of the calibration curve for EuTc-H_2O_2 complex. *Blue pots represent the fluorescence intensity (F) of the complex at 10 min incubation. The red arrow indicates optimal H_2O_2 concentration to get complex saturation and, consequently, the maximal fluorescence intensity of the sample.*

According to the calibration curve, a complete saturation of 100 µl EuTc is achieved with 100 µl of 2000 µM of H_2O_2 (Figure 1, red arrow). However, one cannot assure that no free H_2O_2 rests unlabeled with EuTc. Therefore, one can choose working with 1000 µM H_2O_2 to make sure that all the added H_2O_2 is labelled.

3. Example of the determination of CeO_2NPs activity

To assay the catalase-like potency of CeO_2 NPs, in terms of EuTc-H_2O_2 complex degradation, the reaction mixes were prepared following the proportions indicated in the table 2. Briefly, For each new measurement, 100 µl of Solution A (EuTc dye) were mixed with 100 µl of H_2O_2 at 1000 µM concentration and incubated in dark for 10 min. Then, 800 µl of a sample, for instance, colloidal solution of as-synthesized naked CeO_2

NPs, were added, mixed by pipetting and immediately putted into the fluorimeter to measure the kinetics of EuTc-H_2O_2 complex degradation by the nanoparticles.

	Sample	**Blanc**	**Sample**	**Blanc**	**Sample**	**Blanc**
	Naked CeO_2 NPs	**$Ce(NO_3)_3$ 10mM**	**PVP-coated CeO_2NPs**	**PVP solution 2.5mM**	**BSA-coated CeO_2NPs**	**BSA solution 0.9mM**
Solution A (µl)	100	100	100	100	100	100
H_2O_2 (µl)	100	100	100	100	100	100
NPs sample (µl)	800	-	800	-	800	-
Blanc (µl)	-	800	-	800	-	800
Total volume	1 ml	1 ml	1 ml	1 ml	1 ml	1 ml

Table 2. *Example of the determination of CeO_2NPs activity.*

Note that in case of PVP or BSA-coated CeO_2 NPs, correspondent blancs and controls were analyzed. In case of the comparison between catalase-like potency of different samples, the nanoparticles were equalized by surface area or by number of nanoparticles per milliliter, in order to be comparable.

MATERIALS AND METHODS CHAPTER 4

1. Incubation of CeO_2NPs in serum-supplemented CCM

Briefly, right after synthesis, the NPs were purified and immediately diluted 1:10 in CCM (the usual dilution in studies using cell cultures). Since the collaborative studies of this project employed MEMα cell culture for hepatic cell line Hep G2 [HepG2] (ATCC®

77400™); the same cell culture was employed for these experiments. Thus, at different time points (5min, 6h, 24h and 10 days), NPs were purified again and the surface charge of NPs was measured by Zetasizer Nano-ZS (Malvern Instruments). For more detailed information about the fundamental basis of the ZP technique, consult the Materials and methods section of Chapter 2.

2. Titration curve for isoelectric point determination

To determine the Isoelectric point of as-synthesized CeO_2NPs, right after the synthesis the same amount of NPs solution (e.g. 3 ml) was placed in falcons and the pH of solution adjusted from acidic to alkaline, by nitric acid (HNO3 at 70%, Sigma-Aldrich) and sodium hydroxide (NaOH stock at 1-10mM, Sigma-Aldrich), respectively. The NPs were left under vigorous stirring for 1h and the correspondent surface charge was measured by Zetasizer Nano-ZS (Malvern Instruments). For more detailed information about the fundamental basis of the ZP technique, consult the Materials and methods section of Chapter 2.

3. Spectrophotometric detection of ionic Cerium in solution by Xylenol Orange

In order to quantify free Ce (III) ions in solution and in particular, to measure the tendency of CeO_2NPs to dissolve under certain conditions, the spectrophotometric quantification by Xylenol orange labeling of free cerium (III) resulted in a good alternative to conventional ICP-MS analysis. Xylenol Orange is a metallochromic indicator that forms a stoichiometric complex 1:1 with free cerium (III) in solution. In 1962 Tonosaki, K. and Otomo, M. evaluated the applicability of xylenol orange as spectrophotometric reagent for various metal cations, including cerium. The protocol

of Tonosaki, K. et al. was slightly modified in this work, in order to use smaller amounts of the samples, in particular, to carry on the reaction of cerium-xylenol labeling inside a 1.5ml cuvette for UV-Vis detection, instead of 25ml reservoir. To reproduce a calibration curve of Tonosaki, K. et al. several stock solutions are needed, such as xylenol stock at 10^{-3} M concentration; acetate buffer at pH 6; cerium (III) stock at 40 µg/ml concentration (e.g. cerium nitrate). The correspondent curves are displayed in Figure 1.

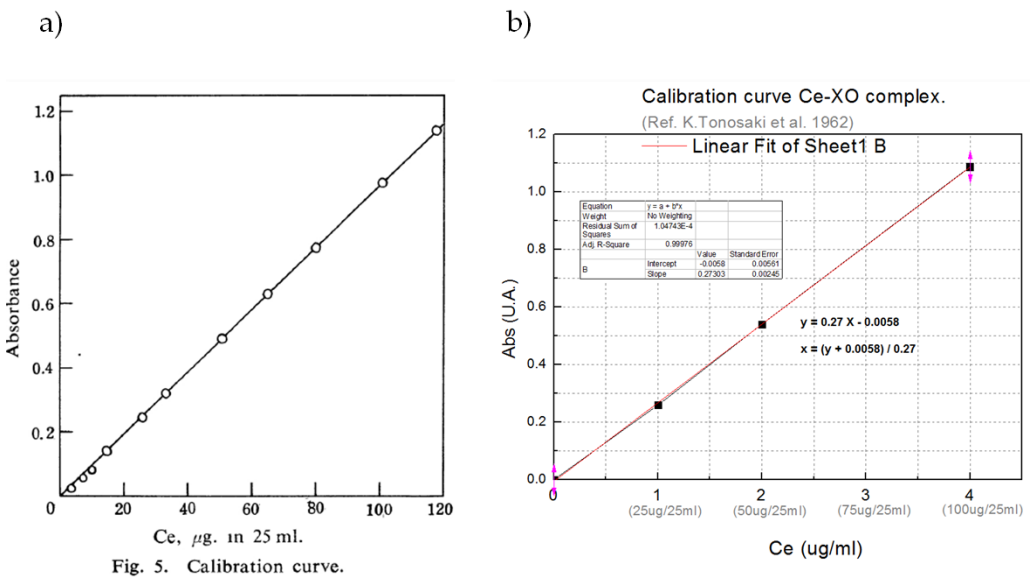

Figure 1. Example of calibration curves for Xylenol Orange-cerium (III) complex. *(a) a calibration curve of Tonosaki et al. (1692), (b) a reproduced calibration curve following the same conditions, where: y = 0.27 X – 0.0058 and X = (y + 0.0058) / 0.27 = concentration of Ce(III) in the sample.*

An example of the proportions of reagents, for a total volume of 1.5 ml of a cuvette, is displayed below and serves to perform measurements of free cerium (III) in samples of interest:

Sample of NPs (µl)	x	x	x	x
Xylenol stock (µl)	210	210	210	210
Acetate buffer (µl)	903.6	903.6	903.6	903.6
Water (ml)	(1.5 –x)	(1.5 –x)	(1.5 –x)	(1.5 –x)
Total volume (ml)	1.5	1.5	1.5	1.5

Table 1. Example of the proportions of reagents for cerium-xylenol reaction in a total volume of 1.5ml (equivalent to a UV-vis cuvette).

Note that for any type of the samples of interest, a correspondent blanc must be prepared to ensure that no interferences nor aberration data is obtained. For instance, in case of CeO_2NPs samples, the blanc of NPs did not show any interference in UV-vis measurements of xylenol-cerium (III) complex.

Once the sample of interest is prepared, the UV-visible absorbance profile is acquired by Schimadzu UV-2400 spectrophotometer. The measured absorbance is converted to concentration of cerium (III) using the equation of the calibration curve and resting the blanc spectrum.

4. Digestion of organs and biological fluids for the ICP-MS determination of cerium (in-vivo biodistribution study)

The dissection of the organs was performed by the collaborators from the Hospital Clinic of Barcelona. After having received representative amount of organs and fluids, the samples were stored at -80ºC until the digestion process started.

Previously to samples digestion, empty falcons were weighted (with the correspondent lids). Then, pieces of organs were placed in falcons, closed with the lids and weighted. The weight of each organ was calculated by difference. Afterwards, 5ml of nitric acid (HNO_3 70%, Sigma-Aldrich) was added to each falcon with organs. The falcons were left opened (without the lid) inside the fume hood overnight and at room temperature. The next day, the falcons were closed with correspondent lids and heated in a bain-marie at 50-55ºC during the day. Afterwards, the samples were naturally cooled down to room temperature and 5 ml of hydrochloric acid were added (HCl, Sigma-Aldrich). Again, the falcons were left opened (without lids) inside the fume hood overnight at room temperature. The next day the digested samples were diluted with water to a final volume of 30 ml and sent to ICP-MS analysis (http://leitat.org/english/). In case of liquid biological samples (e.g. urine and serum), an equal volume of the samples was acid digested (example: 0.35ml of serum in 3ml of HNO_3 70%; 3ml of urine in 5ml of HNO_3 70%). Heating of the samples in bain-marie was the same, as in case of organs. The urine samples were finally diluted to a volume of 30ml, while the serum up to 5ml. In order to calculate the amount of cerium in original samples in ppm units, all of the dilutions must be reverted and the weight of each organ considered.

For more detailed information about the fundamental basis of the ICP-MS technique, consult the Materials and methods section of Chapter 2.

MATERIALS AND METHODS OF ANNEX 2

1. Characterization techniques and LAL assay

The employed characterization techniques of the nanoparticles, such as UV-visible spectroscopy, Zeta Potential and Dynamic Light Scattering are described in the Materials and Methods section of Chapter 2. For detection and quantification of bacterial endotoxin in samples, a quantitative chromogenic test was employed, known as the Endpoint Chromogenic Limulus Amebocyte Lysate (LAL) Test, provided by Lonza. The preparation and measurements of the samples were performed following the protocol of the kit http://www.lonza.com/.

ANNEX 2

LPS-free synthesis of inorganic nanoparticles intended for biomedical applications.

INTRODUCTION

Endotoxins (LPS) are a subset of pyrogens that come from Gram-negative bacteria cell wall. They are toxic, very stable and present on all surfaces. In this Chapter, the biological effects of LPS and consequent importance of LPS-free synthesis of inorganic nanoparticles, intended for biomedical applications, will be analyzed, taking into account current knowledges, limitations and attainments, and proposing some strategies to deal with this issue.

1. Bacterial endotoxins: structure and biological effects

Nanotoxicology is an important branch of study that entails an understanding of the consequences of toxic exposure to nanoparticles in the health-care field and industrial uses. It also involves the treatment and prevention of nanoparticles-induced side effects in humans and the environment. Therefore, when designing nanoparticles for therapeutic applications, toxicological issues must be taken into account. As a consequence of that, the term "*safety-by-design"* of the nanoparticles has arisen and toxicity aspects are considered when designing the nanoparticles for *in-vitro* and *in-vivo* administration. Fortunately, the "neighboring field" of pharmacotoxicology is already extensively developed and all of the potential medicines that arise from the research area are strictly subjected to toxicological inspection previous to their clinical use. One of the most important standards is endotoxin-free nanocomposite. On that base, the newborn field of nanotoxicology can be piled on some of the well-established pharmacotoxicological standards, in order to design nanoformulations with acceptable endotoxin limits, suitable for biomedical applications.

Endotoxins or lipopolysaccharides (LPS) are toxic components of the cell wall of Gram-negative bacteria. It is an invariably characteristic component whether the microorganisms are pathogenic or not. Therefore, high levels of endotoxin are omnipresent in our living environment and exposure can induce a variety of biological effects when administered to animals and humans (from harmless fever to lethal septic shock). Unfortunately, the pyrogenic activity of endotoxins is much higher than that of most other pyrogenic substances. Moreover, killing the Gram-negative bacteria by sterilization procedures, does not assure elimination of endotoxins, since they are heat stable molecules. In particular, endotoxins are amphiphilic molecules with a hydrophilic hetero-polysaccharide chain of variable length (core), covalently bound to a hydrophobic fatty acid-containing tail (lipid A) (Figure 1, a) [1, 2, 3]. The polysaccharide component of LPS determines its antigenic nature (Antigen O). Once inside the body, natural defense cell like macrophages and monocytes recognize the bacterial endotoxin as foreign, experiencing toxicity and strong immunomodulatory response when exposed to LPS.

Specifically, at the cellular level, LPS binds to a co-receptor CD14 (along with the Toll like receptor TLR14 and MD-2) that is responsible for binding LPS and LPB (LPS binding protein) and induces cascades of signal transduction that lead to the release of proinflammatory cytokines (including IL-1β and IL-6), prostaglandins and tumor necrosis factor. In addition, the complement cascade, responsible for the enhancement of pathogens clearance from the organism, causes the release of histamine, a major effector for the allergic response. Aside from inflammation, overproduction of proinflammatory cytokines mediates the shock response: an organism responds with sepsis - a life-threatening condition that arises when the body's response to infection injures its own tissues and organs (Figure 1, b) [3, 6].

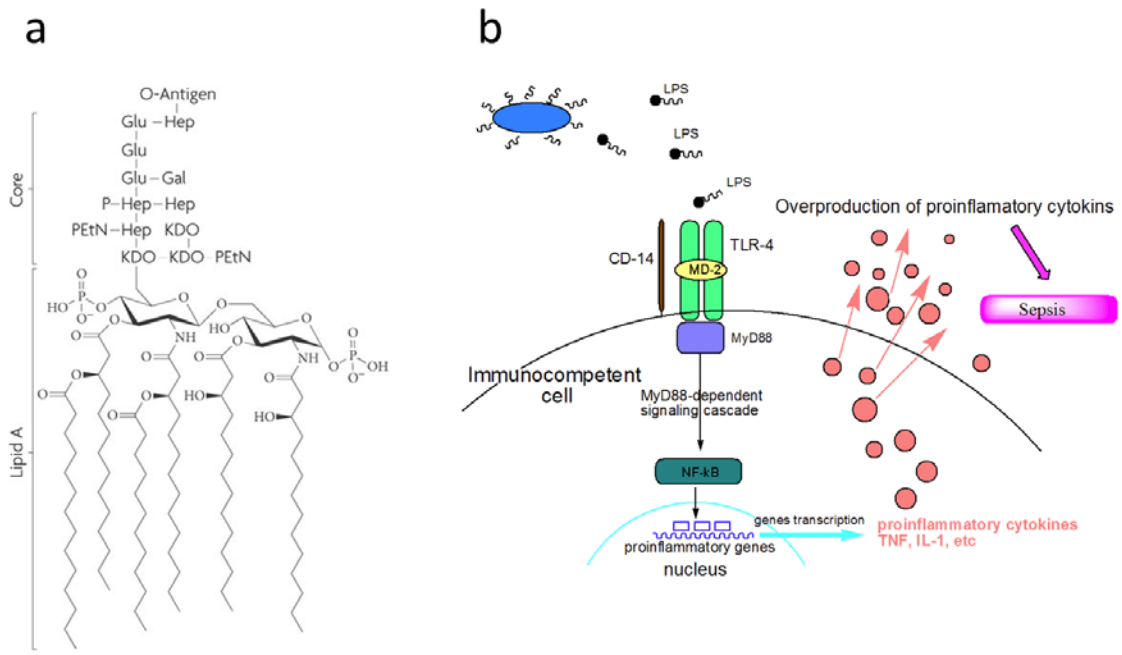

Figure 1. Structure and cellular effects of endotoxin. *(a) Chemical structure of endotoxin: antigen O, polysaccharide chain and Lipid A (image taken from reference [2]); (b) cellular effects of endotoxins: inflammation, allergic response, sepsis (image taken from reference [3]).*

2. Endotoxin Limit (EL)

Fortunately, animal and human body can tolerate small amounts of bacterial endotoxins. Since the severity of LPS-induced damage is proportional to its amount, a safe Endotoxin Limit (EL) has been established. Nowadays, the endotoxin testing is required for many sterile preparations. Note that the routes of the NPs administration are various (e.g. intravenous, intraperitoneal, intramuscular). One of the examples of EL determination is dispayed below (e.g. for intravenously administered products):

$$\underbrace{X\ EU/kg\text{-}h}_{\text{maximal recomended dose of product per kg of body weight and administered in 1h}} \cdot patient\ weight\ (kg) \cdot volume\ of\ product\ (ml) = EU/ml$$

If administered via IV (intravenous), the recommended dose is X = 0.2 EU/kg-h
Where EU = endotoxin Units

Since the EL is as a critical parameter for formulations, to be administered to humans, animals and different animal models, standard data for common injectables have been established by the USP (United States Pharmacopoeia) and is available in Appendix X.

Moreover, one of the most important considerations to keep in mind during biomedical applications of nanoparticles is that the correspondent Endotoxin Limits are different between the *in-vitro* cell cultures and the in-vivo models of humans and animal, due to differences in the correspondent immune systems. Thus, a well-tolerated LPS dose in rats might be lethal for monkeys, rabbits and humans [7] and a well-tolerated LPS dose in humans and animals might be lethal for a cell-culture or tissue and organ culture.

3. LPS-contaminated NPs vs intrinsically toxic NPs

Generally, in pharmaceutical and biological laboratories, where most of medicines are designed and tested, the sterility of material and an environment is strictly controlled, including control of the LPS levels. However, the inorganic nanoparticles use to be synthesized in chemical laboratories, where the levels of LPS are unknown and sterility aspects often neglected. The levels of LPS in chemical laboratories tend to be lower than in biological ones, due to high contents of chemicals and aggressive solvents, where microorganisms are not settled. Nevertheless, a probability to obtain LPS-contaminated nanoparticles is high. In an intralaboratory study in FNN (Future Nano Need) project, up to 70% of endotoxin-contaminated samples was observed (unublished data). As a result, the studies where the inorganic nanoparticles are used

for biomedical applications need to be aware of the LPS content in the nanocomposite (e.g. colloidal nanoparticles in a solvent), since resultant toxic effects may be due not to the nanoparticle itself, but to high levels of LPS either on the surface of the nanoparticle or dispersed in a solvent.

4. Current limitations in LPS removal and blockage

The LPS contamination of nanoparticles appeals for its removal or blockage. However, both strategies become useless due to the persistency of the endotoxin and the susceptibility of nanoparticles. This section is dedicated to a more detailed review of the current strategies of managing the LPS contamination.

In the case of LPS removal from a nanocomposite, two problems arise. On one hand, LPS is a highly stable molecule, pyrogenic (fever inducing), thermoresistant (up to 260ºC) and insensitive to pH changes. These peculiarities complicate its removal, especially from aqueous solutions and surfaces. On the other hand, conventional methods of sterilization may alter the unique properties of the nanoparticles of interest. For instance, methods such as filtration, autoclaving, formaldehyde and ethylene oxide treatments may induce changes in the NP integrity, shape or aggregation state [10].

This factors are especially important during the basic research and understanding of the nature of certain nanoparticles (e.g. surface properties, biocompatibility, toxicity), as well as in biomedical studies of their potential therapeutic effects; since the probability of aberrations in the NPs characterization and consequent biological responses is high.

Some of the conventional methods of purification:

- Filtration and ultrafiltration are useless. Even when the NPs size enables a use of ultrafilters, the whole bacteria may be successfully removed, but the endotoxin fragments will remain in the sample [4, 11]. However, often the size of the nanoparticles destined for biomedical purposes is low (the use of non-aggregated NPs, optimally of size between 6 to 20 nm is highly desirable for a better biodistribution and biocompatibility). Since the exclusion limit of conventional ultrafilters is of 25nm, filtration becomes useless.

- UV irradiation may modify the nanoparticles of interest. As to LPS removal by irradiation, it is important to consider that several inorganic NPs present photocatalytic properties. Besides, noble metal NPs have high optical absorption over a wide range of the light spectrum, including both, visible and UV light. As a result of UV irradiation during LPS removal, the photocatalytic NP is activated as a catalyst. Consequently, the UV treated nanomaterial suffers changes not only in its activity, but also in the redox state of the whole NP formulation.

- Blockage of LPS by polymyxin B induces additional toxicity. Taking into account a difficult removal of LPS, several studies reported a use of an antibiotic, polymyxin B, to block the endotoxin, instead of its removal. Polymyxin B is known for its high binding affinity to the part of lipid A of endotoxin (Figure 5.1). Since the given interactions result in neutralization of the toxic effects of LPS, polymyxin B has been widely used in *in-vitro* studies. However, its use in-*vivo* and in clinical practice has been numerously questioned due to the neuro-, nephro- and hepato-toxicity of the polymyxin B [12-14].

- Chromatography may remove charged NPs as well. Although, pharmaceutical industry makes use of chromatography for LPS removal. Even though, it may be inefficient depending on the characteristics of the formulation to be purified. In physiological condition, LPS usually carry negative charge for its electrostatic interaction with proteins and other biopolymers. Based on this principle, cation exchange columns like poly-lysine, as also the polymyxin B affinity columns, have been

applied in endotoxin removal. But, when the surface of the nanoparticles is charged, the exchange column may result inefficient, since it may interact with NPs and result in a sample loss. On the other side, small-sized NPs are characterized by their high surface reactivity and a tendency to aggregate in order to decrease their surface energy. Thus, any chromatographic treatment of the NP formulation may result in an aggregation of NPs. Such factors are unquantifiable and unpredictable; therefore, this particular purification method cannot be universally applicable for any type of inorganic NPs.

5. Detection of endotoxin (LPS tests)

In order to measure levels of LPS in a formulation of interest, several techniques were developed, such as a LAL test and a rabbit pyrogen test. According to the Committee for Medicinal Products for Human use (CHMP) of the European Medicines Agency, there are three pharmacopoeial references for the bacterial endotoxins test: European Pharmacopoeia (Ph. Eur.), Japanese Pharmacopoeia (JP) and United States Pharmacopeia (USP). As commented in previous section, the correspondent Pharmacopeias have set the bacterial endotoxin limits (EL) and, currently, the LAL test is the assay of choice for LPS determination in drugs, biological products and medical devices.

Generally, two types of LAL assays are used worldwide: gel clot techniques and photometric techniques (turbidimetric and chromogenic). All of them use an amoebocyte lysate from blood corpuscle extracts of horseshoe crab (Limulus Polyphemus or Tachypleus tridentatus). Nevertheless, several inconveniences have been reported as to LAL tests and their use in nanoformulations. On one hand, Dobrovolskaia, M. A. et al. alarmed about the ambiguities when using one test or another [8] and, on the other hand, some of the nanoparticles interfere in LPS measurements due to their physical and chemical properties [9]. These factors should be taken into account and contribute to develop improved versions for LPS quantification.

DISCUSSIONS

1. Prevention of LPS contamination during and after the NP synthesis

Since removal of endotoxin from contaminated NP formulations is extremely difficult and a generally applicable method is not available, it is important to avoid LPS contamination during synthesis and handling of the NPs.

Predominantly, among those who underline the importance of LPS-free synthesis of the NPs, only general precautions are briefly described. These are: use of fume hoods, LPS-free water and sterile material [15]. However, there are other possible sources of endotoxin contamination that should be considered and avoided during the synthesis and handling of the nanomaterial, before is applied in biomedical research or applications.

In our study, described in this Chapter, we go in-depth into the syntheses processes of inorganic NPs, speculating about the potential sources of LPS contamination and describing the correspondent precautions to follow; taking into account both, the physicochemical properties of the NPs, as well as the biological peculiarities of LPS.

2. Potential sources of nanoparticles contamination and guidelines for its prevention.

2.1. Considerations <u>before</u> the synthesis of nanoparticles started:

Glassware. Endotoxins are thermoresistant and are not destroyed by autoclaving. Endotoxicity is not necessarily lost with the loss of viability of microorganisms. Lipopolysaccharide is not destroyed to any significant extent by sterilization treatments, such as steam sterilization, gamma radiation, ethylene oxide, hydrogen peroxide, etc. Hence, before the synthesis started, all glass material and stirring bars should be cleaned with acetone, rinsed with deionized water and depyrogenated in an oven at 260 ºC, for at least 1h, naturally cooled down to room temperature and rinsed with milliQ water to remove calcined traces.

Magnetic stirring bars. Many of the inorganic NPs are synthesized by precipitation methods, where continuous stirring is crucial for successful formation of the NPs and their monodispersity. Therefore, the surface of the used magnetic stirring bars is another possible source of LPS contamination. Not all of the stirring bars may be placed under 260ºC for depyrogenation, so it is important to work with stirring bars with suitable thermoresistant coating. In this case, PTFE (Polytetrafluoroethylene) encapsulated stirring bars are the preferred ones, due to chemical and thermal properties of PTFE (-200°C to +260°C).

Solid reagents (handling and weighting). In most of the nanochemical syntheses, commercial powders are weighted and dissolved in aqueous or organic solvents. The commercial container of the powders must be opened and handled inside the fume hood only. All the spatulas must be cleaned with acetone, rinsed with deionized water and wiped inside the fume hood previous to use. To control the microbiological contamination of the used reagents, it is highly recommended to place a microbalance inside the fume hood, wipe it with 70-90% ethanol and pretreat under UV exposure for 15 minutes; in order to proceed with the weighting of the solid reagents under controlled environment (inside the fume hood with laminar flux).

Liquid solvents and reagents (handling and pipetting). It is advisable to use the individually wrapped measuring pipettes and sterile pipette tips for automatic hand-held pipettes. The hand-held pipettes should be wiped with 70-90% ethanol, introduced into the airflow hood and pretreated under UV exposure for 15 min previous to use. Endotoxins are generally insoluble in organic solvents. It should be taken into account that the strong organic acids, as also the strong organic primary and secondary bases, as hydrazine and 2, 2´- iminodiethanol, break down the LPS structure. Thus, if the given NPs are synthesized in one organic solvent or another, the endotoxin can be destroyed without any special precautions, but interacting with the solvent [23]. In contrast, endotoxins are soluble in water; therefore LPS-free water should be used if the synthesis is carried out in aqueous phase.

2.2. Considerations during and after the synthesis of NPs:

Conventionally, the reaction of the nanoparticles synthesis is accompanied with punctual characterizations of the samples, in order to control the effectiveness of the process and to monitor the quality of produced material (size, shape, concentration, aggregation, etc.). When the synthesis reaction is carried out under controlled LPS-free environment, it is still important to consider possible sources of the sample contamination during the mentioned characterization procedures. Each synthesis is different and may include one characterization techniques or another. However, since the majority of them are conventional worldwide, here some examples are considered.

pH measurements of nanocomposites. During the pH measurements, the microelectrode of the pH meter is constantly exposed to liquid samples with different composition and purity. In these cases, the surface of the microelectrode can act as a vector of transmission of LPS contamination between samples. Therefore, a small aliquot of the sample of interest must be taken to proceed with pH measurements and

to avoid a direct contact between the microelectrode and the sample. Ones the pH of the aliquot is measured, the aliquot is never poured back to the original sample, but thrown away or used for other measurements.

UV-vis, ZP, DLS measurements of nanocomposites. Many of the conventional techniques of nanoparticles characterization, such as UV-Visible spectroscopy, Zeta Potential and DLS, are located outside the fume hoods and mostly under non-sterile conditions. Thus, to perform such determinations, separate aliquots of the sample of interest have to be taken in cuvettes. Ones the parameter of interest is measured, the aliquot is never poured back to the original sample, but thrown away or used for other measurements.

Glow Boxes. In chemical laboratories, some of the reagents used in syntheses of nanoparticles are usually handled inside a Glove Box (e.g. cobalt carbonyl, iron pentacarbonyl, titanium tetrachloride, cerium nitrate hexahydrate, TOP, etc.). These sealed containers allow manipulating reactants in a separate atmosphere, in order to prevent alterations of their chemical composition, such as undesirable hydration, oxidation, and sublimation, between others. The Glove Boxes provide a controlled atmosphere where no aerobia bacteria life is possible. However, it does not protect from anaerobic bacteria that might be present.

Laminar airflow hoods. Unlike the Glove Boxes that are hermetic to external environment, to control the microbiological contamination of the Airflow Hoods, it is mandatory to wipe the inner surface of the hood with 70-90% ethanol previous to each introduction of material or hands of the operator. Pretreatment of the hood with UV light for 15 min before and after use is desirable.

Limitations in use of UV germicidal irradiation. In microbiology, one of the disinfection methods is a use of short-wavelength ultraviolet light to kill or inactivate microorganisms by destroying nucleic acids and disrupting their DNA, leaving them unable to perform vital cellular functions. This procedure is not enough to provide LPS-free environment, but is conventionally used in addition to another sterility procedures. However, some of the nanoparticles are sensitive to UV light due to their optical properties. Thus, nanoparticles made of certain metals, such as gold, silver or titanium; strongly interact with specific wavelengths of light. For instance, the illumination of a semiconductor photocatalyst with ultraviolet radiation activates the catalyst, altering a redox environment in the aqueous solution. Consequently, to avoid undesirable transformations of the properties of nanocomposite, the UV irradiation needs to be excluded when the nanoparticles are inside the airflow hood.

3. Current investigation and future perspectives

The evaluation of the effects of LPS contamination on the characterization of inorganic NPs is an attractive challenge and is currently under study, as another branch of this Thesis research. In particular, one of the questions to be resolved is whether the LPS contamination of the NPs surface (or the solvent) may be perceived numerically through such techniques of NP characterization as UV-visible spectroscopy, Zeta Potential and Dynamic Light Scattering. For instance, surface charge modifications or alterations of the NP monodispersity towards aggregation, could serve as an indirect tool to predict (by rapid and simple characterization of NPs and without need to perform LPS-tests) whether the samples of interest contain LPS or not. On the contrary, if the characterization techniques of NP will not detect any differences between the LPS-contaminated and LPS-free samples, it will be announced that the LPS-test of NPs destined for biomedical applications is a must, since NPs characterizations are not sensitive to a presence of LPS in the samples.

BIBLIOGRAPHY

[1] El-Moghazy, A. N. A. (2011). "Factors affecting endotoxin removal from aqueous solutions by ultrafiltration process." Journal of Scientific & Industrial Research **70**(1): 55-59.

[2] Ruiz, N., D. Kahne, et al. (2009). "TIMELINE Transport of lipopolysaccharide across the cell envelope: the long road of discovery." Nature Reviews Microbiology **7**(9): 677-683.

[3] Solov'eva, T., V. Davydova, et al. (2013). "Marine Compounds with Therapeutic Potential in Gram-Negative Sepsis." Marine Drugs **11**(6): 2216-2229.

[4] Sweadner, K. J., M. Forte, et al. (1977). "Filtration Removal of Endotoxin (Pyrogens) in Solution in Different States of Aggregation." Applied and Environmental Microbiology **34**(4): 382-385.

[5] Anspach, F. B. (2001). "Endotoxin removal by affinity sorbents." Journal of Biochemical and Biophysical Methods **49**(1-3): 665-681.

[6] Smulders, S., J. P. Kaiser, et al. (2012). "Contamination of nanoparticles by endotoxin: evaluation of different test methods." Particle and Fibre Toxicology **9**.

[7] Malyala, P. and M. Singh (2008). "Endotoxin limits in formulations for preclinical research." Journal of Pharmaceutical Sciences **97**(6): 2041-2044.

[8] Dobrovolskaia, M. A., B. W. Neun, et al. (2010). "Ambiguities in applying traditional Limulus Amebocyte Lysate tests to quantify endotoxin in nanoparticle formulations." Nanomedicine **5**(4): 555-562.

[9] Li, Y., P. Italiani, et al. (2015). "Optimising the use of commercial LAL assays for the analysis of endotoxin contamination in metal colloids and metal oxide nanoparticles." Nanotoxicology **9**(4): 462-473.

[10] Vetten, M. A., C. S. Yah, et al. (2014). "Challenges facing sterilization and depyrogenation of nanoparticles: Effects on structural stability and biomedical applications'." Nanomedicine-Nanotechnology Biology and Medicine **10**(7): 1391-1399.

[12] Danner, R. L., K. A. Joiner, et al. (1989). "Purification, Toxicity, and Antiendotoxin Activity of Polymyxin-B Nonapeptide." Antimicrobial Agents and Chemotherapy **33**(9): 1428-1434.

[13] Cooperst.Ms (1974). "Inactivation of Endotoxin by Polymyxin-B." Antimicrobial Agents and Chemotherapy **6**(4): 422-425.

[14] Falagas, M. E. and S. K. Kasiakou (2006). "Toxicity of polymyxins: a systematic review of the evidence from old and recent studies." Critical Care **10**(1).

[15] Vallhov, H., et al., The importance of an endotoxin-free environment during the production of NPs used in medical applications. Nano Letters, 2006. **6**(8): p. 1682-1686.

[16] Cafun, J. D., K. O. Kvashnina, et al. (2013). "Absence of Ce3+ Sites in Chemically Active Colloidal Ceria Nanoparticles." Acs Nano **7**(12): 10726-10732.

[17] Bastus, N. G., J. Comenge, et al. (2011). "Kinetically Controlled Seeded Growth Synthesis of Citrate-Stabilized Gold Nanoparticles of up to 200 nm: Size Focusing versus Ostwald Ripening." Langmuir **27**(17): 11098-11105.

[18] Pottier, A. S., S. Cassaignon, et al. (2003). "Size tailoring of TiO_2 anatase nanoparticles in aqueous medium and synthesis of nanocomposites. Characterization by Raman spectroscopy." Journal of Materials Chemistry **13**(4): 877-882.

[19] Carp, O., C. L. Huisman, et al. (2004). "Photoinduced reactivity of titanium dioxide." Progress in Solid State Chemistry **32**(1-2): 33-177.

[20] Foster, H. A., I. B. Ditta, et al. (2011). "Photocatalytic disinfection using titanium dioxide: spectrum and mechanism of antimicrobial activity." Applied Microbiology and Biotechnology **90**(6): 1847-1868.

[21] Visai, L., L. De Nardo, et al. (2011). "Titanium oxide antibacterial surfaces in biomedical devices." International Journal of Artificial Organs **34**(9): 929-946.).

[22] Sarina, S., E. R. Waclawik, et al. (2013). "Photocatalysis on supported gold and silver nanoparticles under ultraviolet and visible light irradiation." Green Chemistry **15**(7): 1814-1833.

[23] Perrine, T. D., J. Kyle, et al. (1969). "Solubility of Endotoxin and Stability of Its Biological Activity in Organic Liquids." Biotechnology and Bioengineering **11**(5): 1037.

ANNEX 3

Collaborative article (Journal of Hepatology)

`Cerium oxide nanoparticles reduce steatosis, portal hypertension and display anti-inflammatory properties in rats with liver fibrosis.` Oro, D., Yudina, T., et al. (2016). J Hepatology. 64(3):691-8.

NOMENCLATURE

AuNPs	*Gold Nanoparticles*
BSA	*Bovine Serum Albumin*
CCM	*Cell Culture Medium*
DLS	*Dynamic Light Scattering*
DMEM	*Dulbecco´s Modified Eagle Medium*
EELS	*Electron Energy Loss Spectroscopy*
EDX	*Energy-Dispersive X-ray Spectroscopy*
EL	*Endotoxin Limit*
FBS	*Fetal Bovine Serum*
FWHM	*Full Width at Half Maximum*
HAADF	*High Angle Annular Dark Field*
HR-TEM	*High Resolution-Transmission Electron Microscopy*
ICP-MS	*Inductively Coupled Plasma Mass Spectroscopy*
LAL	*Limulus Amoebocyte Lysate assay*
LPS	*Lipopolysaccharides (endotoxin)*
NPs	*Nanoparticles*
PC	*Protein Corona*
PI	*Isoelectric Point*
ROS	*Reactive Oxygen Species*
STEM	*Scanning Transmission Electron Microscopy*
TEM	*Transmission Electron Microscopy*
TGA	*Thermogravymetric analysis*
TNF	*Tumor Necrosis Factor*
UV-Vis	*Ultra Violet-Visible Spectroscopy*
XRD	*X-Ray Diffraction*
ZP	*Zeta-potential*

LIST OF CONTRIBUTIONS

1. ARTICLES IN PEER-REVIEWED JOURNALS

Oró, D., Yudina, T., Fernández-Varo, G., Casals, E., Reichenbach, V., Casals, G., González de la Presa, B., Sandalinas, S., Carvajal, S., Puntes, V., Jiménez, W. *"Cerium oxide nanoparticles reduce steatosis, portal hypertension and display anti-inflammatory properties in rats with liver fibrosis." Journal of Hepatology (2016).*

Oró, D., Yudina, T., Ribera, J., Marfà, S., Fernández-Varo, G., Puntes, V., Jiménez, W. "*Cerium oxide nanoparticles (CeO_2NPs) normalize the cell viability, reduce overexpression of proinflammatory cytokines and protect the in-vitro human hepatic cells from oxidative stress." (in preparation)*

Arce-Cerezo, A., Ribera, J., Pauta, M., Casals, G., Fernández-Varo, G., Yudina, T., Puntes, V., Morales-Ruiz, M., Jiménez, W. *"The treatment with cerium oxide nanoparticles (CeO_2NPs) increases hepatic regeneration after partial hepatectomy (PHx) in rats." (in preparation)*

Yudina, T., Casals, E., Arbiol, J., Gomez-Bastús, N., Puntes, V. *"Synthesis and properties engineering of highly biocompatible and active CeO_2 nanoparticles for biomedical applications." (in preparation)*

Yudina, T., Puntes, V. "The safety by design aspects for synthesis of nanoceria for medical applications. Review." (in preparation)

Yudina, T., Puntes, V. *"LPS-free synthesis of inorganic nanoparticles intended for biomedical applications." (in preparation)*

2. CONFERENCE CONTRIBUTIONS

Poster (Austria) NaNaX 6, Nanoscience with Nanocrystals 2014. "LPS-free synthesis of inorganic nanoparticles."

Talk (Spain) NanoBio&Med 2014. "Nanoceria in biomedicine."

Poster (Spain) Nanobioapp 2015. "Antioxidant CeO2 nanoparticles for biomedical applications."